University of Verona

Graduate School in Translational Biomedicine

PhD Course in *Molecular and Cellular Biology and Pathology*

Generating a Pancreatic Cancer Mouse Model: from Cancer Stem Cells to *In Vivo* Imaging Strategies

Coordinator: Prof. Fumagalli Guido

Tutor: Sorio Claudio

PhD student: Ritelli Rossana

A.A 2009-2010

Contents

IV. RESULTS

Abstract

Background: Pancreatic cancer remains a highly aggressive and not curable cancer in spite of the ample research in the last decades. Since conventional treatment approaches have not satisfactory effects because they don't result in a significant improvement of the disease outcome, an effective research system is still strongly needed, in order to accurately predict the clinical efficacy of novel compounds developed for pancreatic cancer treatment.

Aim: the aim of the current study is to contribute to the generation of a complete and straightforward system useful for the identification and pre-clinic screening of novel drug for the treatment pancreatic cancer. This system should provide the techniques, the protocols and a pancreatic cancer model suitable firstly for *in vitro* high-throughput compounds screening and then for *in vivo* validation of the selected molecules.

Results: findings previously obtained in our laboratory have already demonstrate potential stem-like behavior of Panc-1 cells growing as 3-dimensional spheres (Panc1-spheres), isolated from adherent Panc-1 cell line. In this study we continued with the *in vivo* characterization of Panc-1 spheres because we used them as pancreatic cancer cell line model in the compounds screening system we are generating. So, we performed subcutaneus and orthotopical injections in nude mice with adherent Panc1 and Panc1-spheres cells. Tumor growths were followed using MRI. In order to deepen the characterization of Panc1-spheres, we also studied EMT on tumors derived from this experiment such as *in vitro* in both cell lines. Moreover, we observed that an improvement of imaging strategies was actually needed, in order to better control above all the formation of small masses as metastasis and early primary tumors, since MRI was not sufficient when used alone. For this reason, we also decided to focus our attention to the most important non-invasive small animal-imaging modalities available today, in particular MRI, Micro-Ultrasound (US) and In Vivo Optical Imaging. Then, we correlated these techniques, arriving to the point to have an "imaging protocol", able to offset some of the limitation of each modality when used alone, to be used in the compounds screening system we would like to generate.

Conclusion: Our findings have demonstrated that the pancreatic cancer spheres are more than just cancer stem-like cells. Our mouse model, established with Sphere-growing cells, may be used for the testing of novel compounds specifically designed to target this stem-like compartment, resistant to standard chemotherapies. A combined imaging approach, with combine MRI, Optical imaging and US, in this contest become extremely important, in order to follow primary tumor sizes and metastasis detection before and after the treatment with novel compounds.

Abstract (italiano)

Presupposti: nonostante gli enormi sforzi della ricerca per lo studio del carcinoma del pancreas, a tutt'oggi questo tumore aggressivo rimane incurabile e necessita di terapie mirate che garantiscano un miglioramento concreto della qualità della vita dei pazienti. Pertanto, è forte il bisogno di creare un sistema efficace e mirato all'identificazione di nuovi composti per la cura del cancro del pancreas.

Scopo: lo scopo di questo lavoro è quello di contribuire alla generazione di un sistema che porti selezione di nuovi composti per il trattamento del carcinoma pancreatico. Questo sistema include tecniche, protocolli e un modello cellulare e animale di tumore del pancreas indispensabili per testare *in vitro* un alto numero di composti e per la successiva validazione *in vivo* dei composti selezionati.

Risultati: nel corso di questo lavoro, abbiamo innanzitutto completato la caratterizzazione delle Panc1-sfere, che sono cellule tumorali presentanti caratteristiche di staminalità, precedentemente isolate nel nostro laboratorio dalla linea cellulare Panc1. Tali cellule coincidono con la subpopolazione cellulare più chemoresistente a numerosi composti già in uso clinico, pertanto sono ritenute essere il modello cellulare più indicato per la selezione di nuovi farmaci sia *in vitro* che *in vivo*. Al fine di studiare il comportamento *in vivo* delle Panc1-sfere, dapprima abbiamo inoculato queste cellule in sede orto topica in topi immunodeficienti e seguito la crescita tumorale ortotopici tramite Risonanza Magnetica (RMI). I nostri risultati hanno dimostrato che le Panc1-sfere rappresentano la subpopolazione più aggressiva perché crescono più velocemente rispetto alla controparte aderente, metastatizzano con maggiore frequenza e sono positive ai *markers* mesenchimali. Inoltre, abbiamo osservato che la RMI non è in grado di rilevare masse che poi sono state trovate nel corso delle necropsie, pertanto abbiamo effettuato un secondo esperimento, utilizzando due tecniche di *Imaging* in più: l'ecografia e l'*Imaging* Ottico. I risultati dimostrano che l'utilizzo contemporaneo di più tecniche di *Imaging* è estremamente utile perché fornisce informazioni complementari garantendo una maggiore precisione soprattutto per seguire *in vivo* gli effetti dei composti che saranno selezionati dallo screening *in vitro*.

Conclusione: i nostri risultati dimostrano che il tumore ortotopico generato inoculando le Panc1-sfere è un buon modello che può essere usato nello validazione *in vivo* di nuovi composti potenzialmente in grado di curare questa malattia. Inoltre, proponiamo un protocollo combinato delle tre metodiche di *Imaging* che, considerando i limiti e i vantaggi di ciascuna, garantisce di monitorare la crescita tumorale in ogni sua fase, sempre nelle migliori condizioni.

Abbreviations

BLI= Bioluminescence Imaging

BSA= Bovine Serum Albumine

CSC=Cancer Stem Cells

CSM= Cancer Stem Cell Medium: DMEM+F-12 (1:1), 1X B27, Fungizone 1% Penicillin/Streptomycin, 5 mg/ml Heparin supplemented with 20 ng/ml EGF and FGF

DM= Differentiation Medium: DMEM+F-12 (1:1)+1X B27, Fungizone, 1% Penicillin/Streptomycin, 1% FBS

D-PBS= Dulbecco's Phosphate Buffered Saline solution without Ca++ and Mg++

EMT=Epithelial to Mesenchymal Transition

GEM= Gemcitabine

GR= Gemcitabine-resistence

HGF= Hepatocyte Growth Factor

IPMN= intraductal pancreatic mucinous neoplasm

MCN= mucinous cystic neoplasm

MET= Mesenchymal to Epithelial Transition

Micro-CT= micro-computer tomography

Micro-PET=micro-positron emission tomography

Micro-SPECT= Single photon emission computed tomography

Micro-MRI=micro-magnetic resonance imaging

PanIN = pancreatic intraductal neoplasia

PCSC= Pancreatic Cancer Stem Cells

PDAC= Pancreatic ductal adenocarcinoma

SDF1= Stromal Derived Factor 1 alpha

SM= Standard Medium: RPMI+10%FBS+1% Penicillin/Streptomycin

WST-1= (4-[3-(4-Iodophenyl)-2-(4-nitrophenyl)-2H-5-tetrazolio]-1,3-Benzene disulfonate

I. Introduction

Pancreatic cancer is one of the most lethal human cancers with an overall survival rate of 3-5% and a median survival of less than 6 months. The short median survival is explained by the absence of early symptoms and lack of appropriate diagnostic tools for early detection. The cancer's lethal nature results from its propensity to rapidly disseminate to the lymphatic system and distant organs, occurring in more than 80% of cases. Metastasis to loco-regional lymph nodes or distant organ are one of the major features of pancreatic cancer and are typically already present at the time of diagnosis. This aggressive biology and resistance to conventional and targeted therapeutic agents leads to a typical clinical presentation of incurable disease at the time of diagnosis still today. Many efforts have been made in the past years, but conventional treatment approaches have little impact on the course of this aggressive neoplasm [1].

1.1 ***Pancreas anatomy and physiology***

The pancreas, an organ of endodermal derivation, is the key regulator of protein and carbohydrate digestion and glucose homeostasis (Fig. 1). The exocrine pancreas represents the 80% of the tissue mass of the organ; it is composed of a network of acinar and duct cells for the production and digestive zymogens into the gastrointestinal tract. The acinar cells, organized in functional units along the duct network, synthesize and secrete zymogens into the ductal lumen. Within the acinar units near the ducts there are the centroacinar cells. The endocrine pancreas regulates metabolism and glucose homeostasis through the secretion of hormones into the bloodstream and; it is composed of four specialized endocrine cell types organized together into clusters called Islets of Langherhans [2].

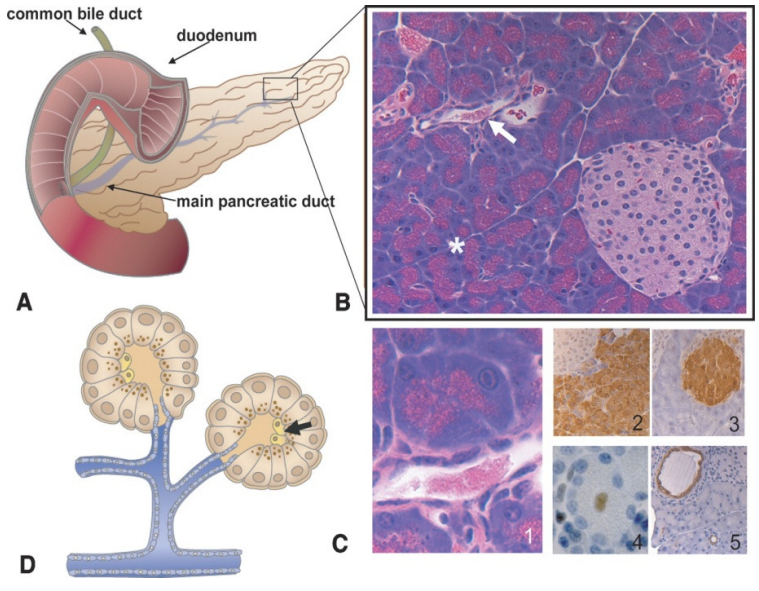

Figure 1. *Anatomy of the pancreas.*
(A) Anatomy of the pancreas
(B) The major components of the pancreatic parenchyma on a histological level. At lower right is an islet of Langherhans, The asterisk is placed among acini, which are involved in secreting various digestive enzymes into the ducts (indicated by the solid arrow).
(C)H&E- and immunohistochemical-stained sections of pancreatic tissue. (Panel 1) An acinar unit in relationship to the duct. (Panel 2) Acinar units. (Panel 3) Islet of Langerhans. (Panel 4) A centroacinar cell. (Panel 5) Ductal cells.
(D) Representation of an acinar unit.

The pancreas arises from dorsal and ventral buds in the anterior endoderm, and during embryonic specialization a critical event is the repression of Sonic Hedgehog (Shh). This event results in the expression of the pancreatic homeobox transcriptor factor Pdx1 in the nascent pancreatic bud. Multipotent Pdx1+ cells are maintained in an undifferentiated state by Notch signaling (Fig. 2). Following Notch repression, Pdx1 progenitor cells are capable of differentiating into distinct pancreatic lineage, the three functional compartments of the pancreas, acinar, ductal and endocrine.

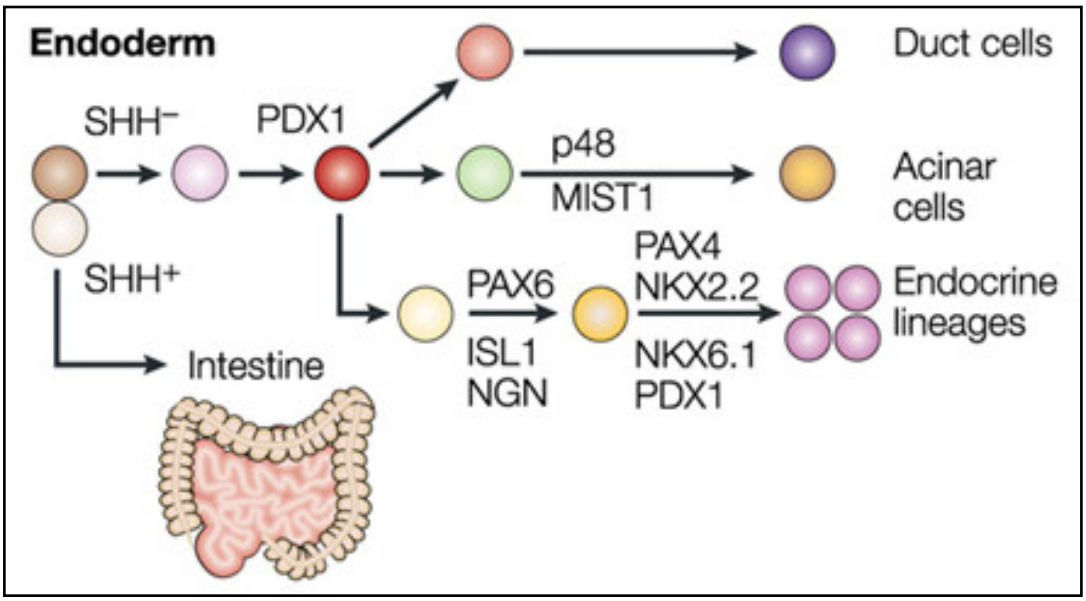

Figure 2. *Cell differentiation program in the pancreas*

There is a spectrum of distinct pancreatic malignancies with histological and molecular features that resemble the characteristics of the various normal cellular constituents. These multiple tumor types and hallmark features are summarized in Table 1.

Table 1. *Pancreatic tumors and associated genetic alterations*

Pancreatic neoplasm	Histological features	Common genetic alterations
Ductal adenocarcinoma	Ductal morphology; desmoplasia	*K-RAS, p16^{INK4a}, TP53, SMAD4*
Variants of ductal adenocarcinoma		
a. Medullary carcinoma	Poorly differentiated; intratumoral lymphocytes	*hMLH1, hMSH2*
b. Colloid (mucinous noncystic) carcinoma	Mucin pools	*MUC2 overexpression*
Acinar cell carcinoma	Zymogen granules	*APC/β-catenin*
Pancreatoblastoma	Squamoid nests, multilineage differentiation	*APC/β-catenin*
Solid pseudopapillary neoplasm	"Pseudo" papillae, solid and cystic areas, hyaline globules	*APC/β-catenin*, CD10 expression
Serous cystadenoma	Multilocular cysts; glycogen-rich epithelium	*VHL*
Pancreatic endocrine tumors	Hormone production	*MEN1*

(Hezel et al, 2006, Genes and Devel.)

Metastatic pancreatic tumors are characterized by highly chemoresistance, in fact response rate to multiple classes of agents including antimetabolites is less than 20%. Gemcitabine is the standard treatment for metastatic pancreatic cancer, replacing 5-Fluorouracil thanks to its clinical

improvements of diminishing the common debilitating symptoms. However, Gemcitabine, given alone or in combination with other chemotherapeutic agents (Table 2), opens the possibility of 6-month in median survival; for this reason, the research of a effective treatment is the most important challenge and aim in clinical oncology up to now.

Table 2. *Therapeutic approach for pancreatic cancer*

Mechanisms or categories	Agents	Therapeutic approaches
Antimetabolite	Gemcitabine	Neoadjuvant chemotherapy: combined with other chemotherapeutic agents Locally advanced disease: combined with radiation, other chemotherapeutic agents Metastatic disease: single agent (standard); combined with 5-fluorouracil, topoisomerase I inhibitors, platinums, taxanes, or molecularly targeted agents
	Capecitabine	Locally advanced or metastatic disease: combined with chemotherapeutic agents and radiation
	5-Fluorouracil	Adjuvant therapy: single agent or in combination with other chemotherapeutic agents Locally advanced disease: combined with radiation Metastatic disease: single agent or combined with gemcitabine
	Tegafur-uracil (UFT)	Resected pancreatic cancer: combined with gemcitabine
	Leucovorin	Adjuvant therapy: combined with other chemotherapy
	Pemetrexed	Metastatic disease: combined with gemcitabine
Platinums	Cisplatin	Neoadjuvant chemotherapy: combined with gemcitabine; Adjuvant therapy: combined with other chemotherapy Metastatic disease: combined with gemcitabine
	Oxaliplatin	Metastatic disease: combined with gemcitabine; second line for advanced disease
Antibiotics	Doxorubicin	Adjuvant therapy: combined with other chemotherapy
	Mitomycin C	Adjuvant therapy: combined with other chemotherapy
Topo-I inhibitor	Irinotecan	Metastatic disease: combined with gemcitabine
	Exatecan	Metastatic disease: single agent or combined with gemcitabine
Antiangiogenesis	Cetuximab	Locally advanced or metastatic disease: combined with gemcitabine
	Bevacizumab	Advanced disease: combined with gemcitabine; Metastatic disease: combined with gemcitabine and erlotinib
	Erlotinib	Advanced disease: combined with gemcitabine
	Gefitinib	Metastatic disease: combined with gemcitabine
	Sorafenib	Advanced disease: combined with gemcitabine

(Hezel et al, 2006, Genes and Devel.)

1.2 ***Morphological characteristics of Pancreatic ductal adenocarcinoma***.

Pancreatic ductal adenocarcinoma (PDAC), so called because of its histological resemblance to normal ducts. PDAC commonly arises in the head of the pancreas with infiltration into surrounding tissues including lymphatics, spleen, and peritoneal cavity, and with metastasis to the liver and lungs. The disease is characterized by the presence of a dense stroma of fibroblasts and inflammatory cells, termed desmoplasia. Moreover, pancreatic stellate cells, a subpopulation of

cells in the normal pancreas with fibroblast characteristics, have been observed in experimental models to respond to pancreatic injury and may contribute to the desmoplastic response in the setting of cancer [3]. PDAC primarily exhibits a glandular pattern with duct-like structures and varying degrees of cellular atypia and differentiation. Less common subtypes of PDAC include colloid, adenosquamous, or sarcomatoid histology.

The three known precursor lesions are pancreatic intraductal neoplasia (PanIN), intraductal pancreatic mucinous neoplasm (IPMN), and mucinous cystic neoplasm (MCN).

Of these precursor lesions, the most common and extensively studied is PanIN, which is found in the smaller-caliber pancreatic ducts. Summarizing, PanINs are microscopic lesions in the smaller (less than 5 mm) pancreatic ducts; it is characterized by a spectrum of divergent morphological alterations localized into normal ducts showing graded stages of increasingly dysplastic growth [4]. PanINs are graded from stages I to III: the earliest one is characterized by the appearance of a columnar, mucinous epithelium and with increasing architectural disorganization and nuclear atypia through stages II and III (Fig. 3). PanIN I (divided in I-A and I-B) shows flat epithelial lesions composed of tall columnar cells with basally located nuclei and abundant supranuclear mucin. The nuclei appear small and round to oval in shape and ductal hyperplasia emerges. The high-grade PanINs ultimately transform into frank PDAC and is characterized by evidence of areas of invasion beyond the basement membrane. Mitosis are abnormal.

Several molecular profiling studies have subsequently reinforced the PanIN-to-PDAC progression model through documentation of an increasing number of gene alterations in higher grade PanIN (see Section 1.3).

Less common precursor lesions are MCNs and IPMNs. MCNs are large mucin-producing epithelial cystic lesions that harbor a distinctive ovarian-type stroma with a variable degree of epithelial dysplasia and focal regions of invasion. IPMNs resemble PanINs at the cellular level but grow into larger cystic structures. Of interest, two subtypes of invasive cancer have been found in association with IPMNs; typical PDAC, and a colloid type characterized by copious mucin production.

Among IPMNs and MCNs, both common and distinct molecular events in comparison with PanINs have been described, suggesting that each precursor lesion may reflect variations on a common theme of malignant transformation of the duct.

Expression profiling has revealed several up-regulated genes commonly associated with PanINs, IPMNs, and PDAC; however, how these PDAC precursor lesions relate to each other, their common or separate cellular origins, and whether each type leads to distinct molecular and biological PDAC subtypes remain to be fully explored.

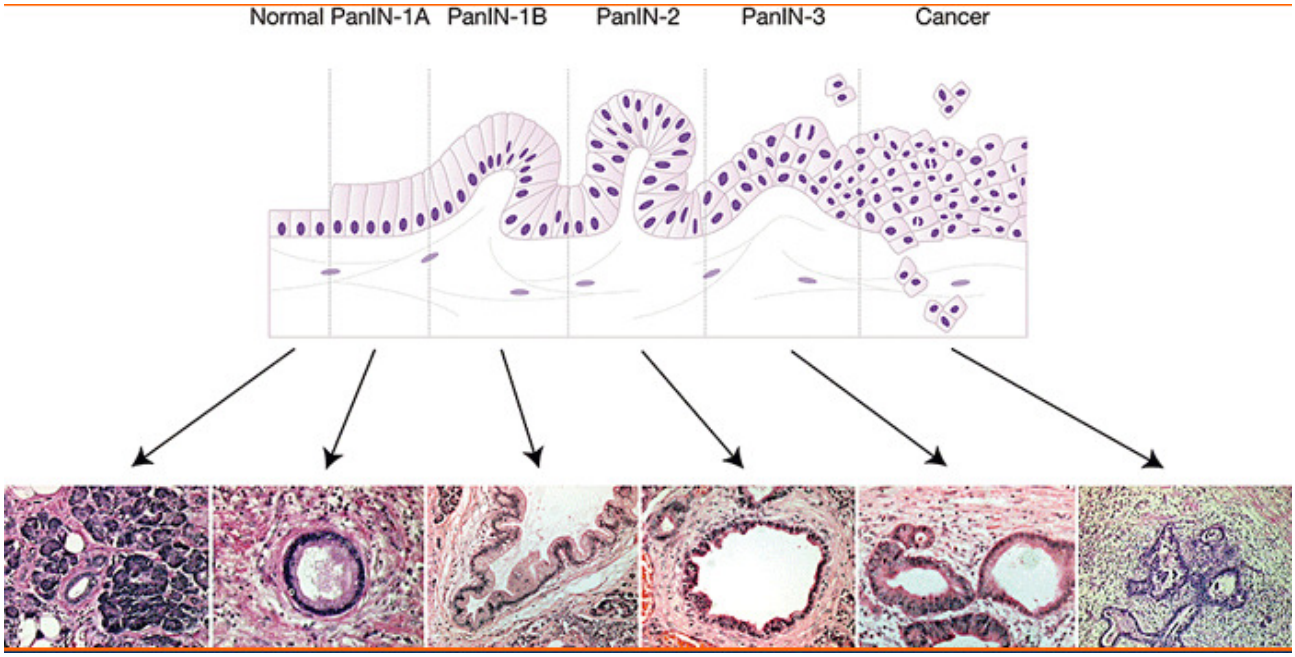

Figure 3. *Progression model for pancreatic cancer. The majority of pancreatic cancer is thought to develop through a series of hyperplastic and dysplastic ductal lesions termed pancreatic intraepithelial neoplasia (PanIN).*

1.3 ***Molecular genetics of PDAC***

Analyzing evolution of PDAC, a defined set of genetic lesions have been provided, often implicating known cancer genes and classical cancer signaling pathways. These molecular events have been linked with defined histopathologic stages of PDAC progression (Fig. 3). Pancreatic cancer is associated with a high rate of inactivation of three tumor suppressor genes: TP53, $p16^{INK4A}$, and SMAD4. The p53 nuclear protein activates transcription of a cyclin kinase inhibitor $p21^{WAF1/CIP1}$. Following genomic stress, inappropriate growth factor stimulation or expression of oncogenic *ras* [5] increased expression of p53, and thus $p21^{WAF1/CIP1}$ resulted in inactivation of specific CDK/cyclin complexes and braking or termination of the cell cycle so that DNA repair or apoptosis can occur. Loss of these functions by inactivation or alteration of the p53 gene have been reported in more than 50% of pancreatic cancers.

The $p16^{INK4A}$/$p14^{ARF}$ (also known as CDKN2A) locus on chromosome 9q21 encodes these two tumor suppressor genes. Loss of function by mutation, deletion or promoter hypermethylation occurs in 80% to 95% of sporadic cancers [6]. The $p16^{INK4A}$ gene regulates cell cycle progression by inhibition of cyclin D/CDK4/6 complexes and thus inhibition of Rb phosphorylation. The interaction of $p14^{ARF}$ with MDM2 leads to p53 activation. In pancreatic-cancer development, inactivation of $p16^{INK4A}$ seems to be of greater importance than inactivation of $p14^{ARF}$ since

germline and sporadic mutations have been identified that target $p16^{INK4A}$ and leave $p14^{ARF}$ intact. Recent studies indicates that inactivation of p16 leads to overexpression of pRB that is linked with chemoresistance [7].

SMAD4 (also known as DPC4) is deleted or mutated in more than 50% of pancreatic carcinomas [8]. The gene product is an intracellular mediator of the transforming growth factor beta (TGF-β) pathway that inhibits cell growth by inducing G_1 arrest, but it also may have a role in angiogenesis. TGF-β is the prototypic member of a superfamily of secreted proteins, whose other members include the Bone Morphogenic Proteins (BMPs) and Activins. These growth factors signal through serine/threonine kinase receptor complexes that, upon ligand binding, phosphorylate receptor-regulated Smad proteins (SMAD2, SMAD3, and the obligate binding partner SMAD4) regulating a variety of cellular functions including proliferation, differentiation, migration, and apoptosis.
The importance of TGF-β signaling in pancreatic cancer is illustrated by the fact that 90% of tumors show loss of heterozygosity (LOH) at the SMAD4 locus, with 50% of PDAC having either homozygous deletion or mutational inactivation of the second allele.
The loss of *SMAD4* in PDAC may have a primary role in modulating the interaction of the tumor with the microenvironment rather than in growth control of the tumor cells themselves.

K-RAS, a member of the RAS family of GTP-binding proteins, mediates a wide variety of cellular functions such as proliferation, differentiation, and survival. Although RAS is a GTPase, its intrinsic activity is inefficient and requires GTPase activating proteins (GAPs) to promote GTP hydrolysis and attenuate downstream signaling. Activating *K-RAS* point mutations at codon 12 (from GGT to GAT or GTT, and more rarely CGT) results in substitution of glycine with aspartate, valine, or arginine. These mutations are the first known genetic alterations, occurring sporadically in normal pancreas tissue, and are detected in ~30% of early neoplasms with the frequency rising to nearly 100% in advanced PDAC (Fig. 4).
Consistent with a central pathogenic role of the $K\text{-}RAS^{G12D}$ mutation, many mice engineered with pancreas-specific expression of this activated *K-RAS* allele sustain classical PanIN lesions that can progress to PDAC in the appropriate tumor suppressor background.

Focusing the attention to the connections between development and cancer, the cross roles of the Hedgehog and Notch signaling pathways in PDAC pathogenesis have recently been investigated. The mammalian Hedgehog family of secreted signaling proteins comprised of Sonic, Indian, and Desert Hedgehog (SHH, IHH, and DHH, respectively) regulates the growth and patterning of many

organs, including the pancreas, during embryogenesis [9]. The Hedgehog pathway is negatively regulated by the Patched (PTC) tumor suppressor protein, which inactivates the Smoothed protein (SMO). Hedgehog ligands engage the PTC transmembrane protein and disrupt inhibition of Smo, activating the Gli family of transcriptional regulators. Alterations that activate this pathway, including loss of *PTC,* activating mutations in *SMO,* and overexpression of GLI and HH proteins, have been implicated in a variety cancers, including pancreatic adenocarcinoma. Activation of the Hedgehog pathway has been implicated in both the initiation of pancreatic ductal neoplasia and in the maintenance of advanced cancers. SHH is absent from the normal adult pancreas, but is activated in PanINs, exhibiting a graded increase in progressively later-stage lesions and carcinomas; moreover, its signaling seems to be necessary for tumor maintenance [9, 10].

The role of SHH in pancreatic cancer development is one of the investigation this study is based on (see Section 1.5).

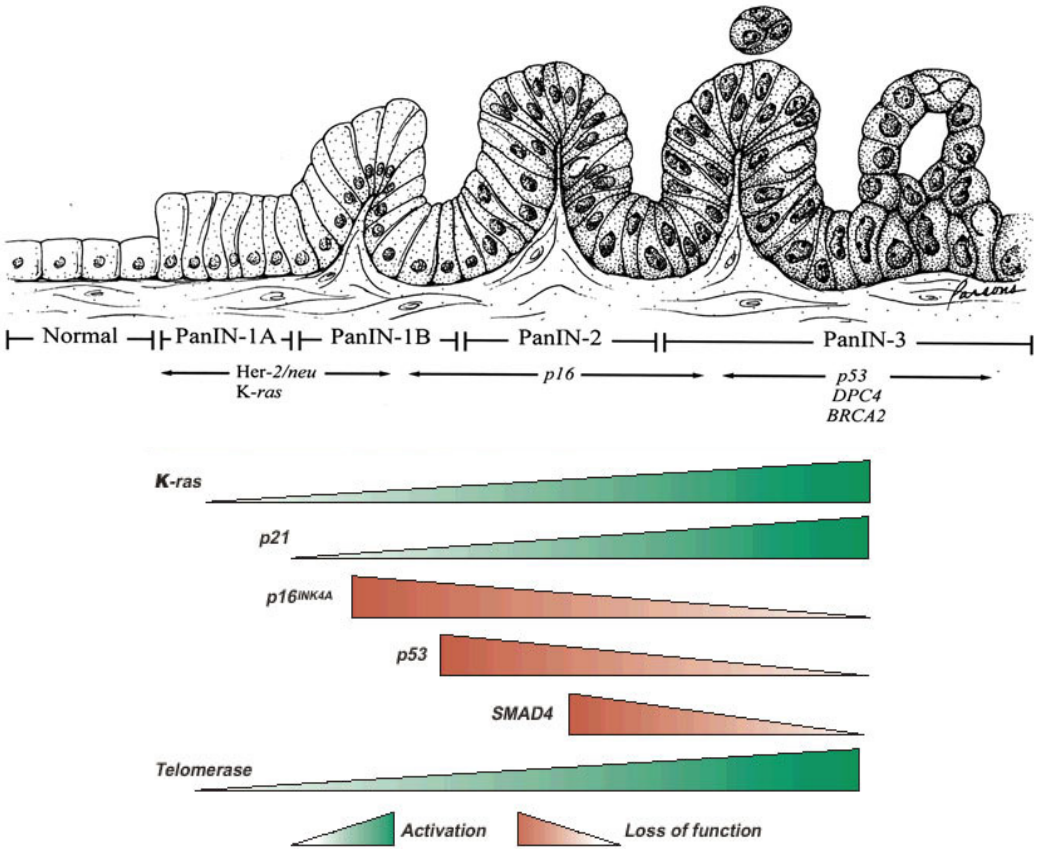

Figure 4. *Histologic-genetic progression model for pancreatic cancer.*

1.4 Cancer Stem Cells.

Cells with stem cell characteristics have been identified in several solid tumors, like breast, colon or pancreas [1] and have been named 'cancer stem cells'.

This term first referred to a cancer cell able to produce tumors when injected into SCID mice, demostrating self-renewal properties and giving rise to other cell types in the tumor were xenografted into immunodeficient mice. This small population of undifferentiated cells with stem cell characteristics can perform asymmetrical division to replicate themselves, but also to create a committed progenitor cell at the same time, like normal stem cell population.

Two general models to explain heterogeneity present in solid cancer cells have been suggested up to now. The first of them supposes that cancer cells of many different phenotypes have the same potential to proliferate extensively.

Instead, according to the second cancer stem cells hypothesis, most cancer cells have only limited proliferative potential, but a subset of cancer cells, the cancer stem cells, consistently proliferate extensively in clonogenic assays and can form new tumors on transplantation. Like their normal stem-cell counterparts, they are able to self-renewal and produce more differentiated cells without stem cells properties contemporaneously (Fig. 5). This last model shown underlines that just a distinct subset of cells is enriched for the ability to form new tumors, whereas most cells don't possess this ability.

This could be the reason why existing therapeutic approaches, thought largely on the first model, failure; so, the second hypothesis is consider to be more accurate.

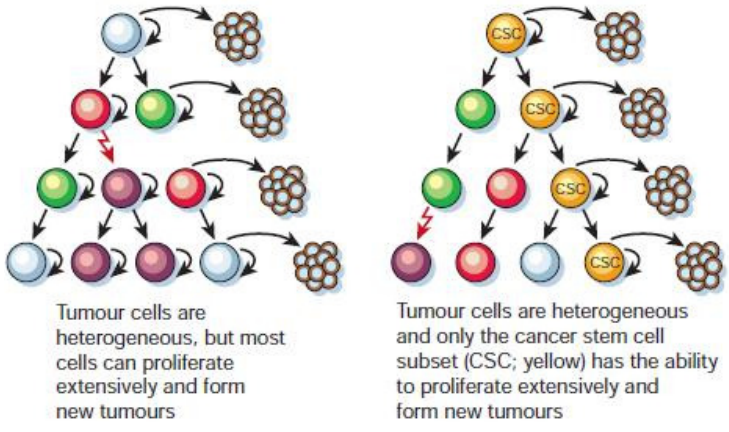

Figure 5. *The cancer stem cells hypothesis.*

Conventional therapies kill mainly cells with limited proliferative potential. If the putative cancer stem cells are less sensitive to these therapies, then they will remain viable after therapy and can re-establish the tumor. By contrast, if therapies can be specifically targeted against cancer stem cells, they might more effectively kill the cancer stem cells, rendering the tumors unable to maintain themselves or grow again (Fig. 6).

Cancer stem cells may be responsible for tumor initiation, metastasis, and resistance to treatments; so, they are the cells to target to cure a cancer.

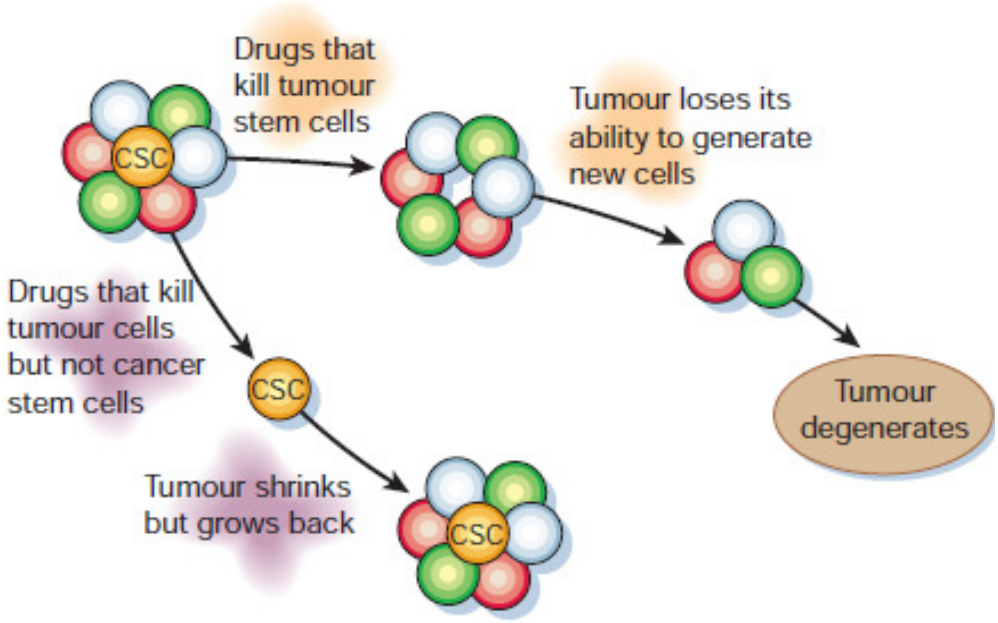

Figure 6. *Drugs and cancer stem cells*

- ***1.4.1 Pancreatic Cancer Stem cells***

Cancer stem cells were first identified in acute myelogenous leukemia by Dick and collegous, which isolated CD34+/CD38- leukemic stem cells from human acute myelogenous leukemia [11]. Subsequently, Li et al [12] investigated the relationship between cancer stem cells and pancreatic cancer progression. In that study, a subpopulation of highly tumorigenic cancer cells were identified, analyzing the expression on the cells surface of CD44, CD24 and epithelial-Specific antigen ESA, on the basis of prior work on breast cancer stem cells in which ESA+ CD24-CD44+ cells, capable to generate tumors histologically similar to primary breast cancer, were found [13]. Pancreatic cancer stem cells resulted triple-positive for the markers CD24, CD44, ESA, showing features typical of adult stem cells, such as ability to self-renew and activation of developmental pathway like Sonic Hedgehog pathway. Li and collegous performed also FACS-sorted cells from human pancreatic adenocarcinoma xenografts: cells were suspended in a Matrigel mixture and subcutaneously injected into immunocompromised NOD/SCID mice. Interestingly, pancreatic cancer cells with the CD44+ CD24+ ESA+ phenotype (which represented only 0.2–0.8% of pancreatic cancer cells) had a 100-fold increased tumorigenic potential compared to non-tumorigenic cancer cells negative for the same markers. Moreover, the treatment with the

chemotherapeutic agent gemcitabine on these pancreatic tumor xenografts involved in enrichment of the CD44+ CD24+ ESA+ cell population.

Thanks to characterization studies of cell surface markers associated with solid tumor stem cells, the stem cell markers' list is long today. CD133, also known as prominin-1, has also been used to identify putative cancer stem cells in breast, brain, liver, colon, prostate, and pancreatic tumors [14]. It was first discovered as a marker of normal hematopoietic stem cells and later was found to mark stem/progenitor cells from a variety of tissues. Evidence for existence of CD133+ pancreatic cancer stem cells was first reported by Hermann et al. [15]: similar to Li et al., FACS approach was chosen to prospectively isolate and characterize CD133+ cells from primary pancreatic cancer patient tissue samples and tumor cell lines. They found that in the majority of patient's samples, the capacity of cells to form primary tumors following orthotopic implantation in nude mice was limited to a subpopulation of CD133+ cells that were exclusively tumorigenic and highly resistant to standard chemotherapy (Gemcitabine). The CD133+ cells were serially passed, demonstrating self-renewal capacity and were able to generate tumor heterogeneity, producing differentiated non-tumorigenic progeny.

Primary pancreatic tumors comprised a higher fraction of $CXCR4^+$ cells that displayed increased migratory activity *in vitro* and, furthermore, correlated with metastatic disease in pancreatic cancer patients. CXCR4 is the receptor of the stromal cell-derived factor 1 (SDF-1), an important mediator in cell migration; for this reason, the positivity to CXCR4 is often investigated.

Data produced by Hermann and collegous demonstrated that depletion of the CXCR4 subset of all CD133+ cells isolated from cells lines, such as highly metastatic human pancreatic cancer cell line L3.6pl or the cell line MiaPaca, completely inhibited the formation of spontaneous liver metastases, without affecting their tumorigenic potential. SDF-1 appeares to be the strongest inducer of migration for CD133+ cancer cells in vitro and this data correlated well with what was found in metastasis' patients. In these cell selected for their CD133+/ CXCR4+, the authors observed also the loss of cytokeratin, one of the first steps of the epithelial to mesenchymal transition (EMT) program (see Section 1.6). Authors defined a distinct subset of $CD133^+/CXCR4^+$ cells that localized to the invasive edge of pancreatic carcinomas and exhibited significantly stronger migratory activity *in vitro* than $CD133^+CXCR4^-$ cells. Only $CD133^+CXCR4^+$ cells demonstrated *in vivo* metastatic activity to the liver. Moreover, pharmacological depletion of $CD133^+CXCR4^+$ cells by inhibition of the CXCR4 receptor profoundly reduced the metastatic potential of pancreatic tumors without altering their tumorigenic potential. These findings have important therapeutic implications, as the design of drugs that target the metastatic CSC would be envisaged to have a profound effect on patient survival.

As discussed previously, in Section 1.1, therapies specifically targeting pancreatic cancer stem cells will likely be needed to result in total tumor eradication and prevention of metastasis. Because cancer stem cells possess many of the features of normal stem/progenitor cells, it will be important to determine if novel strategies may be effective in targeting cancer stem cells without interfering the activity of normal stem/progenitor compartment. Novel screens specifically designed to target cancer stem cells are available today; examples are DNA and tissue microarray analyses of tumors, that are widely used to identify cancer subtypes trying to improve diagnosis and treatment. The use of sphere formation assays *in vitro* as well as implantation and serial transplantation assays *in vivo* might be actually useful in the identification of agents that selectively kill cancer stem cells, improving the drug discovery in this field.

An example of *in vitro* screening using selected cancer stem cells requires the use of a steroid-like compound cyclopamine that binds to and inhibits the SMO protein (G-protein-coupled receptor family protein of hedgehog signaling); it inhibits the growth of cells and tumors with activated Hedgehog signaling, even if cyclopamine alone is not capable of effectively diminishing the CSC pool until undetectable levels *in vitro* and *in vivo* [16]. Using an orthotopic xenograft model, Feldmann et al. demonstrated that cyclopamine (in particular, the orally bioavailable small-molecule Hedgehog inhibitor, IPI-269609) profoundly inhibited metastatic spread in combination with gemcitabine, significantly reduceding the size of primary tumors at the same time [17].

Moreover, in pancreatic cancer cell lines, inhibition of Hedgehog with cyclopamine has been shown to result in the downregulation of Snail and upregulation of E-cadherin [18]. This was consistent with the inhibition of epithelial-to-mesenchymal transition (EMT) and was mirrored by a reduction of *in vitro* invasive capacity of tumor cells.

These findings suggest that, targeting the Hedgehog signaling, growth of cancer stem cells can be reduce strongly.

- ***1.4.2 Cancer Stem cells and epithelial-mesenchymal transition***.

Metastasis is the predominant cause of lethality in cancer patients. However, looking to the cancer stem cells hypothesis discussed before and currently accepted, not every cell in a tumor has the ability to metastasize to other organs. Metastatic potential depends on multiple factors that determine overall tumor cell growth, survival, angiogenesis and invasion and only a sub-set of tumor cells show these characteristics. The epithelial-mesenchymal transition (EMT) is considered to be a crucial event in the metastatic process, because the disruption of epithelial cell homeostasis and the acquisition of a migratory mesenchymal phenotype are required for distal tumor masses formation (see also section 1.6) [19]. To date, the classical view on the metastatic cascade follows

these steps: 1. EMT occurring in a subpopulation of tumor cells; 2. dissociation of tumor cells from primary tumor; 3. invasion of neighboring tissue; 4. intravasation; 5. transport through vessels surviving to *anoikis*; 6. extravasation from vessels; 7. establishment of migratory cells at a secondary anatomical site, probably in a state of "dormance" for a prolungate period of time; 8. growth of the mass.

In many epithelial tumors, an EMT or loss of differentiation is frequently evident at the invading edge of the tumor and is probable to mediate cellular detachment in a limited number of cells. The EMT appears to be controlled by crucial pathways such as the Wnt and transforming growth factor β pathways, both of which can be aberrantly activated during neoplasia. Recent reports suggest that there may be a direct link between the EMT and acquisition of stem cell properties. Cells undergoing an EMT could conceivably be the precursors to metastatic cancer cells, perhaps even metastatic CSCs. CSCs may also have a role in the creation of a particular niche for metastasis probably because they often undergo to EMT program. Recently, the link between highly tumorigenic behavior, CSCs and EMT is strongly studied; it is possible that CD133+ cells, about which we discussed before, have undergone EMT explaing at the same time their highly metastatic phenotype. Several pathways that mediated stem cell self-renewal, like WNT, Shh and NOTCH, also play a role in EMT induction.

Important findings by Shah and collegous [20] demonstrate the correlation between EMT and gemcitabine-resistant (GR) cells: they obtained resistant cells by culturing the pancreatic cancer cell lines L3.6pl and AsPC-1 in serially increasing concentrations of gemcitabine. Gemcitabine-resistant cells underwent distinct morphological changes, including spindle-shaped morphology, appearance of pseudopodia, and reduced adhesion characteristic of transformed fibroblasts. Moreover, these cells were more invasive and migratory. GR cells were increased in vimentin and decreased in E-cadherin expression. Immunofluorescence and immunoblotting experiments revealed increased nuclear localization of total beta-catenin. These alterations point out the epithelial-to-mesenchymal transition (EMT) in gemcitabine-resistent cells, which could coincide with CSCs. Infact, resistant cells were activated in the receptor protein tyrosine kinase, c-Met and increased in expression of the stem cell markers CD (cluster of differentiation) 24, CD44, and epithelial-specific antigen (ESA). Then, these emerging lines of evidence suggest the molecular and phenotypic association that occur between the acquisition of EMT, chemoresistence and crucial role of CSCs in metastatic behavior in cancer. The Notch Pathway is involved, as we have already said, in EMT during tumor development and is particularly associated in the switch of cells from polarized to motile invasive cells. The increased activation of members of this pathway (such as Notch-2 and Jagged-1) in GR cells reinforces this knowledge, and data coming from Shah and collegous underline also that the

down-regulation of Notch signaling induces reversal of EMT to MET in GR cells [20] (see Section 1.6).

1.5 ***Characterization of Pancreatic Cancer Stem Cells: preliminary data of our laboratory.***

As descrive in section 1.4, it has become increasingly clear that many tumours contain a very small (2-5%) subpopulation of cells, called cancer stem-like cells (CSCs). Summarizing, CSCs stem cells' properties were hypothesized to be more aggressively growing, are chemoresistant to a lot of molecules and present tumour metastatic capacity.

CSCs are usually recognized by expression of their membrane protein expression profile (CD133, CD44, CD24 and ESA particularly). Moreover, previous observations have clearly demonstrated that CSCs have the ability to grow as cellular aggregates with spheroidal shape, called spheres (sph), in contrast to the adherent counterpart (adh). We capitalized this property, instead of separating stem marker-positive cells from negative ones, to obtain CSCs.

To generate spheres, a panel of 8 well-established pancreatic cancer cell lines which grow like adherent cells were thus subjected to culture in CSCs medium (CSM), a serum-free medium supplemented with growth factors (EGF and FGF). It was previously been demonstrated that this colture conditions promote sphere-growing of cells. The 8 cell lines subjected to culture with CSM were: Panc-1, Psn-1, and Panc-2 (PancTu1) coming from primary tumors; CFPAC, Suit-2 Im, Suit-2 Io, S2CP9 coming from liver metastasis, and T3M4 coming from Lymph node metastasis. The cells started to change their typical epithelial morphology within 24-36 hours from the incubation with CSM. Six cell lines, with the exception of PancTu1 and T3M4, developed spheres.

The difference in behavior of spheres versus adherent cells was investigated in a panel of *in vitro* phenotypic assays and, in the current study, in a orthotopic mouse model.

The results of the preliminary data confirmed the hypothesis that sphere growing cells not only display stem cell characteristics but can be considered as the aggressive subpopulation of pancreatic tumors. Preliminary data generated in our laboratory demonstrated the link between aggressiveness and stemness in sphere growing pancreatic tumor cells.

Figure 7. *Pictures of Panc-1 spheres obtained from established adherent cells line cultured in CSM for four weeks*

The cells typically lost their rhomboidal epithelial shape and became floating cells or cell clusters. After 1 week, the floating spheroids were collected without disturbing the remaining adherent cells and were grown until they reached a sufficient density to be transferred to a 75 cm2 flask. After four weeks, a clear distinction between the cell lines that had the capability to form spheres and the ones that had not could be made. Six of the eight adherent cell lines (Panc-1, Psn1, CFPAC, Suit-2 Im, Suit-2 Io and S2CP9) were classified as 'capable to form spheres' (Fig. 7).

All works were focused on the characterization of Panc-1 cells. The most important characteristic of this cell line about its genetic profile are: mutation of Kras and p53 genes (+), deletion of p16 gene, DPC4/Smad, DCC and BRCA2 are wild type. The expression of the complete panel of stemness markers (CD24, CD44, ESA, CD133) was assessed in Panc-1 spheres and adherent cells both at the gene and protein levels using qRT-PCR and FACS technology, respectively. CD24 gene expression in Panc-1 spheres is 25-fold higher than in adherent cells.

In order to assess whether pancreatic spheres were enriched in dedifferentiated cells, CK19 labeling, a ductal marker routinely used as a differentiation marker in the diagnosis of pancreatic cancer, was performed on both sphere growing and adherent cells. CK19 was absent in spheres whereas 80–90% of the Panc-1 adherent cells showed CK19 positivity.

To verify that PANC-1 sphere growing cells also display characteristic stem cell properties, typical stem cell functionalities such as self-renewal and multipotentiality was assessed.

For self-renewal assay, Panc-1 spheres were dissociated into single cells and plated in a 96-well plate as a single cell per well. After seven to ten days only 16% of the single cells were able to produce second generation spheres; moreover, the newly formed spheres were morphologically more regular than the initial spheres. These observations confirmed that Panc-1 spheres contain a stem-enriched subpopulation of cells, potentially responsible for a more aggressive tumor behavior.

The multipotentiality test was aimed at demonstrating that Panc-1 spheres when subjected to differentiating conditions results in an increase of Panc-1 differentiation markers from different cell

lineages. Cells were grown in chamber slides at a density of 100 cells/well in DM or in SM. After 10 days, dissociated spheres were completely attached to the plastic slides and, compared to the Panc-1 adherent cells; they assumed mixed morphological shapes. For instance, some elongated cells were morphologically comparable to fibroblasts, whereas others were more epithelial-like. Specific markers of pancreatic development were selected in order to track the differentiation profile of Panc-1 spheres in differentiating conditions. As already described in Section 1.1, embryonic pancreatic epithelium gives rise to the three pancreatic cell types (endocrine, acinar and ductal cells); in both rodents and humans. In order to evaluate the multipotentiality, CK19, Pdx1 and Isl-1 were chosen as markers of the different cell types. The observation that PANC-1 adherent cells are more differentiated than Panc-1 spheres was confirmed by the fact that the expression of both PDX1 (an early pancreatic progenitor cell marker) and Isl-1 (beta cell precursor marker) are inversely related to differentiation [22].

Panc-1 spheres are CK19 negative; 19 days after differentiation in DM, 30% of the cells became CK19 positive. In particular CK-19 positive cells were found to be fibroblast-like with epithelial shape. Since the adherent cells displayed even a higher CK19 positivity (up to 80-90%), these results may indicate that the adherent cells are more differentiated than Panc-1 spheres.

The gene expressions of CXCR4, Osteopontin and Hedgehog signaling pathway components (e.g., Shh, Gli1, Ptc1), were analyzed both in Panc- 1 spheres and adherent cells. In fact, it has been demonstrated that there is a clear correlation between increased pancreas cancer metastatic potential and increased expression of proteins such as the chemokine receptor CXCR4 [15] and Osteopontin [23].

CXCR4 is a chemokine receptor (GPCR). Upon binding of its natural ligand SDF-1, CXCR4 has been reported to be involved in cell migration, angiogenesis, proliferation and metastasis. Osteopontin (OPN), the natural ligand of CD44, was also reported to be involved in pancreatic metastasis.

Spheres in comparison to adherent Panc-1 showed a 9 fold higher mRNA expression of CXCR4 and 350-fold increase in osteopontin mRNA. The mRNA levels of the Hedgehog pathway components Shh, Gli1 and Ptch were investigated in spheres vs adherent cells in order to assess hedgehog pathway activation at the receptor level (Shh) and downstream the receptor activation (Gli1 and Ptch). FACS analysis demonstrated that Panc-1 spheres also displayed an increased membrane expression of CXCR4 when compared to their adherent counterpart Indeed, the percentage of membrane CXCR4 expression increased from 6,20 % in adherent cells to 19,40% in cells derived from spheres.

In order to assess the growth rate of Panc-1 spheres compared to the adherent cells, the WST-1 proliferation assay was performed. The adherent cells were grown in 10% FBS and 1% FBS whereas the spheres were grown in CSM. Although the growth rate during the first seven days of the experiment was the same in all three conditions, after more than 7 days the Panc-1 spheres started to grow significantly faster than the adherent cells.

The chemoresistance of the Panc-1 sphere-growing vs adherent cells was assessed by incubating the cells for 7 days with increasing concentrations of GEM. Subsequently the growth reducing capacity of GEM was quantified using WST-1 proliferation assay.

As depicted in Figure 8, at 10 µM of GEM (red arrow), all adherent cells were killed, whereas 10% of the sphere population survived to Gemcitabine up to 200 µM. Preliminary results obtained in our laboratory confirmed the observation of Gou et al. who reported that Panc- 1 spheres contain a chemoresistant, side population of 15%.

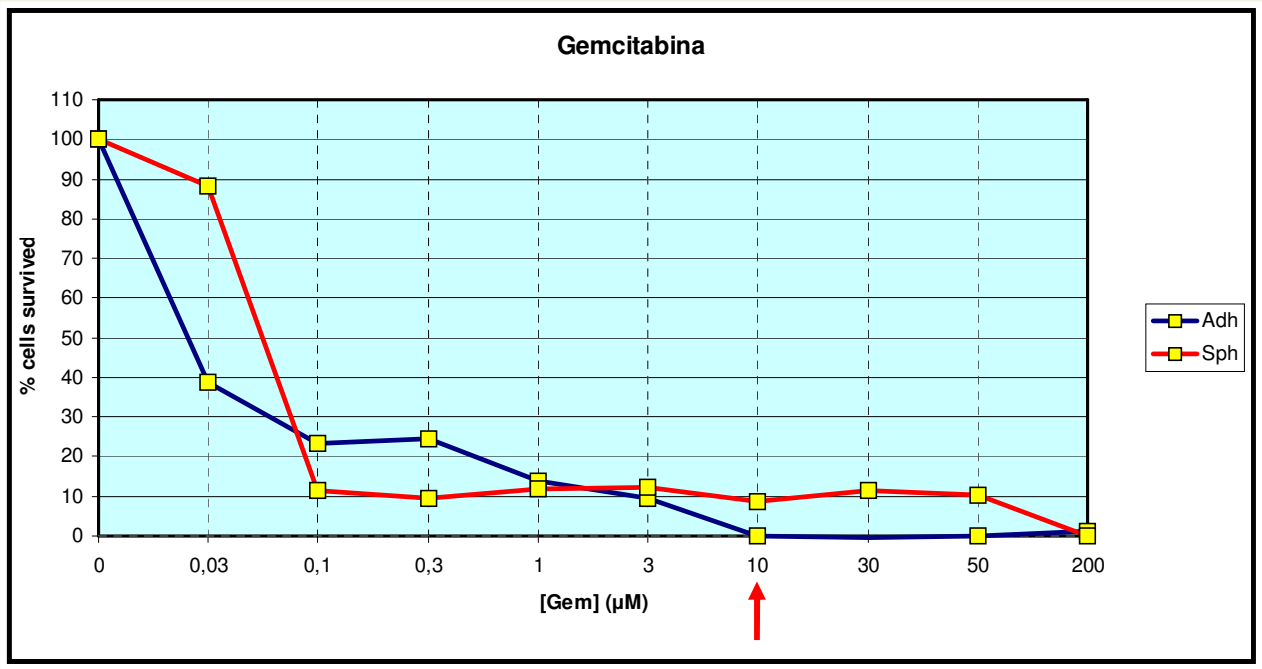

Figure 8. *Proliferation profile (WST-1) of sphere-growing vs adherent Panc-1 upon incubation with increasing concentrations of GEM (Figure kindly provided by Dr. Dandrea M.C.P.)*

To validate the Panc-1 sphere model the pancreatic tumour standard of care treatment Gemcitabine, was used. 50 female athymic mice were divided in two groups: 25 mice were injected with 10^7 Panc-1 adherent cells and 25 mice with the same number of Panc-1 spheres. One week after the injection, tumour growth was monitored. Mice injected with Panc-1 spheres showed a bigger tumour mass than adherent cells: the average tumour mass of spheres was 177 mm3 compared to the tumour mass derived from adherent cells which was 77 mm3. This observation can be

considered as a clear indication that Panc-1 spheres are enriched in tumour-initiating cells and confirms the in vitro observation that Panc- 1 spheres grow faster. Only when the tumors of all groups reached a similar tumour mass (range of 150-200 mm^3), randomization was performed (two groups of 10 mice each with a comparable tumour size) and GEM treatment was started. Gemcitabine was administered by IP to 10 mice at the dose of 100 mg/kg following a scheduling treatment which had been previously published (day 7, 10, 13, 16, 19, 22, 25, 28). The corresponding control mice were treated with the vehicle only (physiologic solution) . Tumour volume and body weight were monitored twice a week. A minor decrease in body weight loss (10%) due to GEM treatment was observed.

GEM demonstrated a significant tumour growth reduction after 22 days. Moreover, the in vivo data endorse the in vitro as well as the clinical data, demonstrating that GEM does not lead to a complete eradication of the tumour.

After establishing the difference in stemness markers and CXCR4 expression between spheres and adherent cells, a transwell migration assay was performed in order to assess the migrating capability of spheres vs adherent cells. Only SDF-1, the ligand of CXCR4, induced a significant difference in the migration capacity between spheres and adherent cells while had no noticeable effect on the migration of adherent cells.

Finally, findings obtained in our laboratory demonstrated that we have at our disposal a new pancreatic cancer model system that definitely better mimics certain clinical features both *in vitro* and *in vivo* settings.

1.6 ***Epithelial-mesenchymal transition (EMT).***

The metastatic mechanism is a multistep process. Resistance to *anoikis* has been shown to promote metastasis, since tumor cells can enter and disseminate into the bloodstream and can survive even losing their cell-cell contacts. *Anoikis* suppression is an important prerequisite for tumor cells to metastasize to distal sites. Different integrin complexes are linked with member of ECM ; integrin activation protect from *anoikis* in that way. To allow these change to be done, cells must be able to detach from the junctions that connect them to the neighboring ones, change their shape and polarity, delaminate and migrate. The event responsible for such profound modifications is the Epithelial–mesenchymal transition (EMT); it occurs in 90% of human tumor and could be first identified like a change in cell morphology. Epithelial cells are characterized by a highly baso-apical polarization essential for their biological role, such as vesicle transport or protective barrier.

The epithelial cell basolateral surface are closely associated with neighboring cells thanks to membrane-associated specialized junctions [19].

Mesenchymal cells display loss of baso-apical polarization and are characterized by front-rear polarization necessary for cell migration. Moreover, a distinct organization of actin cytoskeleton enhances communication with the extracellular matrix; so, in contrast with ephitelial, mesenchymal cells become flat and spindle-shaped, showing growth factors production in collaboration with surrounding stroma.

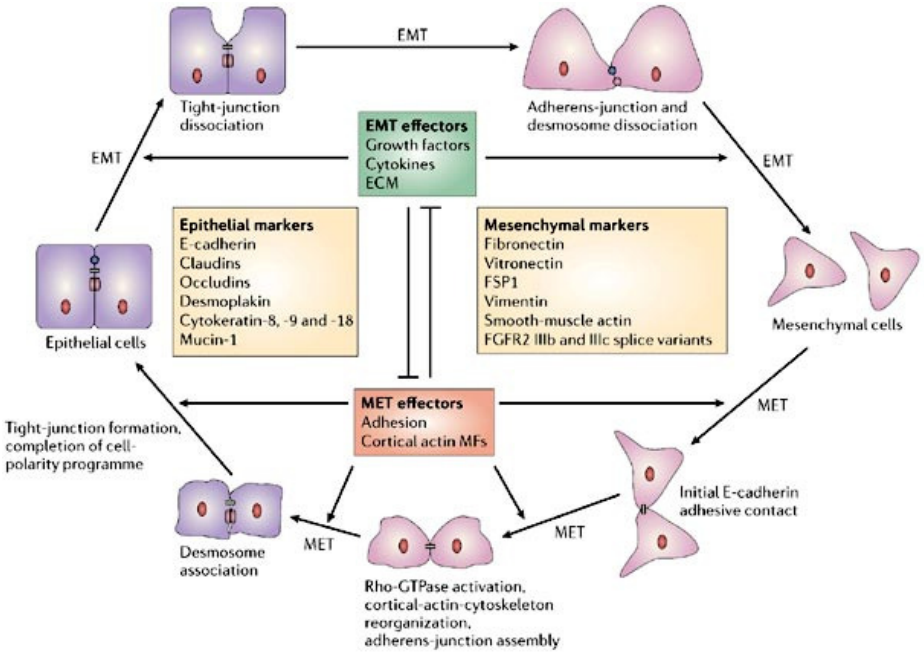

Figure 9. *From Epithelial to Mesenchymal cells and back to ephitelial phenotype (MET): main steps.*

While the main type of adhesion system in epithelia is E-cadherin mediated cell-cell interaction that stabilises the multicellular architecture, the adhesion system in mesenchymal cells comprises dynamic integrin-mediated cell-matrix interactions that allow the motility of single elements.

E-cadherin is a transmembrane glycoprotein with an extracellular domain that interacts with the E-cadherin molecule on adjacent cells, and an intracellular domain associated with a multiprotein complex comprising α-, β- and p120 catenin.

β-catenin binds to the cytoplasmic domain of E-cadherin and, through α-catenin, to the actin microfilament network of the cytoskeleton, connecting cell-cell adhesion with the intracellular mechanism involved in cell shape and migration regulation. Due to the functional link between E-cadherin complexes and cytoskeletal components, a change in the E-cadherin mediated adhesiveness leads to rearrangement of the cytoskeleton and, and at the same time, factors that

interfere with the latter will also affect the former. The binding of E-cadherin with catenins and actin cytoskeleton is essential for the formation of strong cell-cell adhesion and any event that perturbs the cadherin/catenin/cytoskeleton complex leads to destabilisation of cell-cell adhesion and reorganization of the actin cytoskeleton. E-cadherin based junctional complexes keep epithelial cells in a stationary, non-motile state and, therefore, disruption of cell-cell adhesion is of major importance in tumor invasion. E-cadherin acts as a tumor suppressor against invasion and metastasis, and its function is abolished during the malignant progression of most carcinomas by a variety of mechanisms. In this regard, it is noteworthy that one of the main changes occurring in both normal embryonic and pathological EMTs is the down-regulation of E-cadherin that leads to disorganization of the epithelial architecture and allows dissociation of single cells from their neighbours. A complete list of markers for detecting EMT is shown in Table 3.

Table 3. *Epithelial-Mesenchymal Transition markers*

Potential marker	Characteristics	Cellular localization
Mesenchymal markers; up-regulated during EMT		
FSP1/S100A4	Fibroblast calcium-binding protein	Nucleus and/or cytoplasm
Vimentin	Mesenchymal intermediate filament	Mainly cytoplasm
SLUG (SNAI2)	Snail homolog 2 (*Drosophila*); zinc finger transcriptional repressor	Nucleus
Twist	Up-regulated in mesenchymal	Nucleus
Epithelial markers; down-regulated during EMT		
E-cadherin	Type-1 transmembrane glycoprotein in adherent junctions	Membrane
Cytokeratin	Intermediate filament keratins found in the intracytoplasmic cytoskeleton	cytoplasm
Others		
Beta-catenin	Subunit of the cadherin protein complex. Armadillo family of proteins.	Normal epithelium: membrane. Mesenchymal cells after EMT mainly nuclear:

Another major protein involved in the change of the epithelial phenotype is the fibroblast-specific protein Fsp-1, also called S100A4; this protein is extensively linked to the mesenchymal phenotype and is considered as a marker of EMT. It is a cytoplasmic protein interacting with the cytoskeleton which seems to associate with mesenchymal-type cell morphology and to contribute strongly in motile events.

S100A4 is also expressed in metastatic carcinoma cells indicating that the mechanism underlying metastatic progression could involve EMT.

Wnt, TGF-β, hedgehog, Notch and nuclear factor-Kb signaling pathway have been found to be critical for EMT induction. In vivo, a reversion from mesenchymal cancer cells to more differentiated ephitelial cells, the reverse process called mesenchymal-epithelial transition (MET), has been shown in metastatic sites of human colonrectal adenocarcinomas, suggesting that the dedifferentiated mesenchymal phenotype is dynamic and reversible, as shown in Fig.ure 8 [24].

E-cadherin is regarded as a 'master' regulator of the epithelial/mesenchymal phenotype switch, as its repression can be sufficient to both induce and complete EMT and, on the other hand, its re-activation can result in MET.

1.7 ***Small animal imaging: an important tool in the pre-clinical research.***

The use of animal models in preclinical and basic studies makes possible to test diagnostic markers and drugs offering data that are more predictive of the distribution and efficacy of a compound. In recent years, new technologies have become available for imaging small animals. Noninvasive imaging in small living animal models has increasing importance in preclinical research becoming an independent speciality today [25]. Six are the most important imaging systems used for imaging small animals today. In succession, descriptions of these systems and their mail characteristics are reviewed below.

1.7.1 Imaging optico

Different devices are commercially available today because progress in the field of optics has revived interest in optical imaging as a powerful preclinical application.

Biomedical optical imaging includes bioluminescence and fluorescence imaging. Bioluminescence consists in the enzymatic generation of visible light by a living organism; it's a naturally occurring phenomenon in many non-mammalian species. Luciferases are enzymes that catalyze the oxidation of a substrate to release photons of light; the firefly Luciferase gene (*luc*) and the Renilla Luciferase gene (*ruc*) are the mainly used. *In vivo* bioluminescent imaging (BLI) needs genetic-engineered

cells containing an expression cassette in which bioluminescent report gene is constitutively expressed under the control of a selected gene promoter [25]. Mammalian tissue do not emit light naturally, so BLI is esteemed to be believable because imaging are generated with very little background and there is not autofluorescence to disturb the signal (Fig. 10). Moreover, because bioluminescence does not need stimulation of external light source, the problem of the excitation beam penetrating the tissue does not exist.

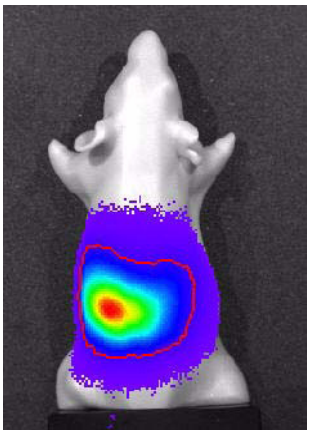

Figure 10. *Example measurement Region of Interest (ROI, red cycle) for planar spectral analysis. Pseudo-color image overlaid on a gray-scale photograph.*

1.7.2 Micro-RM

It's a powerful tool for imaging study in small animals. Thanks to micro-Magnetic Resonance (micro-MR), with a resolution of 10-100 µm, it's possible to obtain both anatomical and metabolic images; it's performed using horizontal-bore devices with static field ranging from 4.7 to 9.4 Tesla putting anesthetized animal on 20 to 40 cm tray [26]. Liquid cooling systems are used to obtain low temperature required for superconductivity for high-field magnets based on cryomagnets. T1 and T2 relaxation times are dependent on the magnetic field. To date, hybrid systems are being developed, such as MRI/PET, in order to increase complete information from a single device.

1.7.3 Micro-CT

Micro-Computed Tomography (Micro-CT) is the miniaturization of CT, a technique commonly used in clinical diagnostic imaging. It's able to supply very high resolution anatomical images, up to 9 µm, with three-dimensional views [25]. The use of specific contrast agents can further improve examination of soft tissue allowing studies of heart, angiogenesis and tumor growth; moreover, this technique is actually useful for studying pulmonary diseases, such as asthma and chronic obstructive pulmonary diseases. Most systems use a cone-beam X-ray source together with a solid-state detector that rotates around animals; in this way it's possible imaging the entire animal in a single scan. Second-generation micro-CT systems are based on the technology used in clinical

practice, including for example arrays with smaller detector elements and more powerful X-ray tubes, which allow faster scan (0.8 sec for the entire animal) and the possibility of performing perfusion studies, as well as the use of contrast agents. In fact, the use of iodinated contrast agents has improved image contrast so that it is possible to visualize 20 µm small-diameter vessels. Micro-CT systems have traditionally been used to study bone taking advantage of the favorable contrast between bone and soft tissue. It's really useful for studying soft-tissue and in characteristic anatomical phenotypes in transgenic animals [27].

1.7.4 Micro-PET

Positron Emission Tomography (PET) produces images of a biochemical function or process of the body on the bases of the activity of a positron-emitting radiotracer. The use of this technology is in expansion, although it is limited by the availability of a cyclotron and a radiopharmacy for the synthesis of the radiopharmaceuticals, determinant factors for the successful use of the technique. Fluorodeoxyglucose (FDG) labeled with the isotope 18F is the most commonly used. Micro-PET is specific, due to the possibility to mark a given molecule with a radioisotope without disturbing its biological function; it's sensitive, between 10 and 100 time greater than CT and MR; it can quantify the tissue concentration of the tracer. On the other hand, this technique lacks of anatomical information and the radioactive compounds are characterized by a very short half-life. Micro-PET is useful to provide a variety of metabolic data, such as functional and oncological imaging with FDG, studies of novel radiopharmaceutical or ligand receptors and, in recent years, it finds its utility in the study of the gene expression.

1.7.5 Micro-SPECT

Single photon emission computed tomography (SPECT, or less commonly, SPET) is a nuclear medicine tomographic imaging technique using gamma rays. In contrast with micro-PET, this system uses radioisotopes (xenon-133, iodine-123, for example) with long half-life, which don't needs a cyclotron to be produced [25]. Moreover, these radioisotopes are more available that those used in PET. In clinical practice, system used for studying large regions of the patient have a collimator with parallel holes not able to do enlargements. On the contrary, this technique applied for imaging small-animal requires must higher spatial resolution for imaging small objects. So, collimators capable to produce spatial resolution <1 mm are necessary. Limitation of Micro-SPECT are linked to the signal loss due to the collimator-induced attenuation of many incident photons and the decline of the photons signal when they go through the tissue ; moreover, in order to produce an adequate signal for image formation, elevated activity of the radiopharmaceutical is needed.

This technique can be used to monitor physiological function, metabolic processes, specially in brain activity, and quantify receptors density.

1.7.6 Micro-US

Micro- Ultrasound (Micro-US) is based on the use of sound waves specially for imaging soft tissue, it's relatively inexpensive but it's limited by the tissue depth or artifacts caused by bone or air between soft tissue. Even if faster and less referral than all the other technique described on top, is not as widespread as other imaging modalities, with the exception of the study of accessible biological structures such as the urinary bladder and blood vessels [28]. This technique can be used to a faster monitoring of tumor growth, just in order to see the presence of the masses.

1.8 *In vivo Bioluminescence Imaging (BLI)*

BLI is a no-radioactive imaging modality, in contrast o the other modalities such as PET, SPECT or CT, described before. On the other hand, BLI is not an absolutely quantitative imaging approach like PET or SPECT. This technique allows longitudinal monitoring of tumor growth, spread, and response to treatment in preclinical cancer models within the same individual, with no requirement to euthanize. This is of significant benefit as each animal comprises its own control; therefore fewer animals are needed per study, which reduces overall costs and labor.

Bioluminescence regards the enzymatic generation of visible light by living organism, a capacity typical of many lower organism including species of bacteria, marine creatures and insects such as firefly beetle. In nature, Luciferase genes encode proteins that act on substrates including D-Luciferin, the most commonly used in animal tumor models, or the coelenterazine for *Renilla* Luciferase (*ruc*). The choice of the reporter is dependent on the goals of the research, but coelenterazine substrate is less stable than the other one so that this kind of biochemical obstacles limit its use in research.

The firefly Luciferase (*luc*) is a molecule of 61 kDa, while *Renilla* Luciferase is smaller (36 kDa). Firefly Luciferase needs the presence of ATP, oxygen and magnesium in order to work, whereas no cofactors are required by *Renilla* Luciferase (Fig. 11). Light emission from the firefly Luciferase-catalyzed Luciferin reaction is broad-band (530–640 nm), peaks at 562 nm and its signal is stronger and persists more than *ruc*; *Renilla* Luciferase emits blue light al 482 nm, less quantity is necessary in comparison with the other one, but it's not efficient as Luciferin, even if no cofactors are required for the reaction. Since separate signal are distinguishable, it is possible to use both Luciferase in the same animal [29].

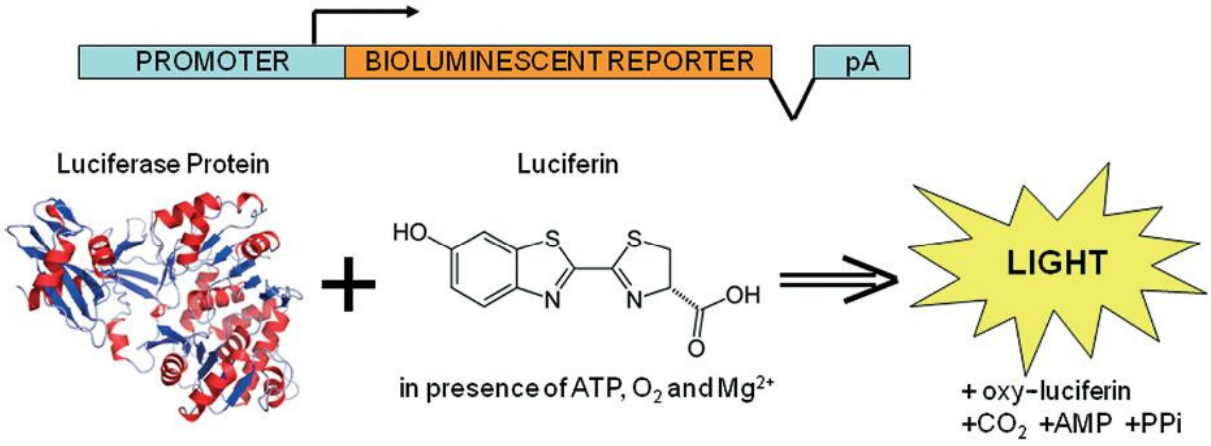

Figure 11. *Bioluminescence reporter cassette and Firefly Luciferase-Luciferin reaction*

The light emitted by Luciferase penetrates tissue depths of several millimeters to centimeters, however photons intensity decreases 10-fold for each centimeter of tissue depth. Sensitive light-detecting instruments must be used to detect bioluminescence in vivo in order to measure the number of photons emitted per unit area. Several commercially available systems are capable of detecting low levels of light. In general, these systems include a light-tight imaging chamber into with the animal is placed. Above this chamber sits a sensitive a *charge-coupled device* camera (CCD) that detect bioluminescence and converts photon flux detected into electrons. The CCD camera is cooled to -90° C in order to reduce thermal noise. In this way, the ability to detect low level of light is increased [30]. The data is measured in photons but the pseudo-color graphic allows rapid visual interpretation. Scientific image data is a two-dimensional array of numbers. Each element of the array or *pixel* contains a number that is proportional to the light intensity on that element. The CCD camera used for scientific imaging is essentially an array of photosensitive pixels and each pixel collects photons during an image exposure.

A subsequent electronic readout provides a photon intensity number associated with each pixel. In a bright area of the image, more photons are detected and the photon intensity number is greater than that in a dimmer area of the image. Images acquisition is typically ranging between 1 e 180 sec and is controlled by software for final image analysis. It's really useful to have the Luciferase image superimposed with other type of image, provided in Magnetic Resonance for example, in order to anatomically allocate the emission signal.

In vivo studies assessing tumor burden relative to bioluminescent signal have shown strong correlations between viable cells and bioluminescence. Dead or necrotic regions within a tumor, potentially indicative of a positive drug response, contribute to volume; therefore the ability to solely measure viable cells soon after treatment is advantageous for rapidly assessing drug efficacy over traditional volumetric-based measurements. BLI may therefore be useful in 'prevention trials'

for drugs specifically targeting the early stages of tumor development. As the whole animal is imaged, unpredictable sites of metastasis are evident and can be rapidly identified. Firstly, the efficiency of bioluminescent light transmission through an animal from its origin depends largely on the type and depth of overlying tissue as well as its scattering properties.

Haemoglobin absorbs light; therefore highly vascularized organs tend to have lower levels of light transmission compared with skin or muscle. Secondly, BLI traditionally has provided two-dimensional (2D) planar images with limited spatial and depth resolution. Recent advances have enabled the translation of BLI data into 3D tomographic imaging, thereby theoretically providing better quantification and signal localization.

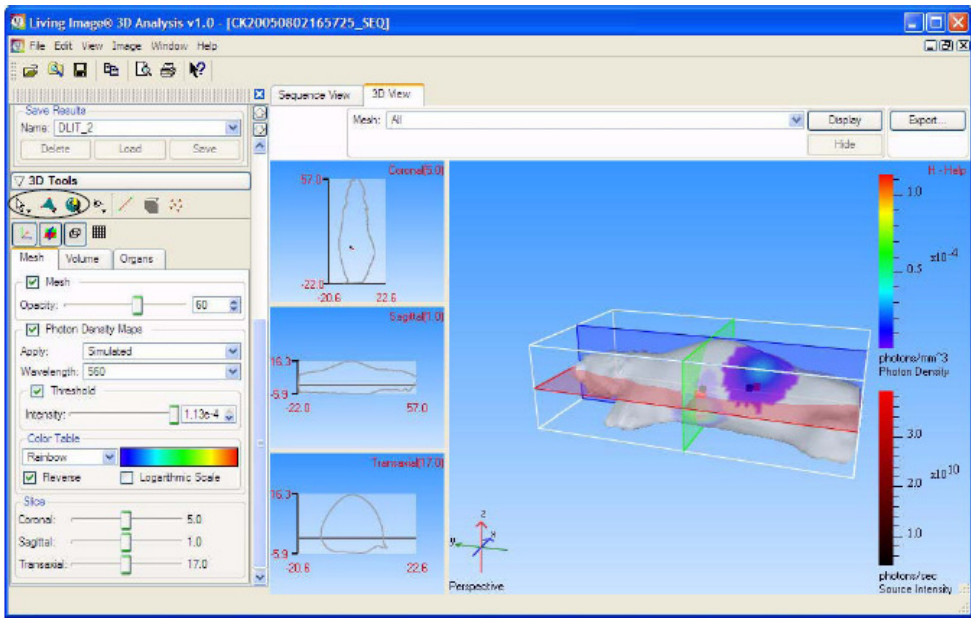

Figure 12. *3D tools in the 3D view window*

BLI does not provide anatomical information, software has been developed in order to superimpose virtual murine organs within a 3D bioluminescent image, a sort of “mouse atlas” that can help to predict the internal origin of bioluminescent signal when used in combination with 3D BLI protocols. Signal depth can be estimated by measuring the ratio of red to green emitted light on the surface of the animal from multiple aspects and computing its likely origin. Hypoxic regions within tumors may also affect signal intensity [31]. Bioluminescence is dependent on oxygen and a number of studies have found that the amount of light emitted from Luciferase- labeled cells is reduced as the oxygen concentration decreases. Oxygen tension limits for BLI are still not fully defined, however, and the HIF-1 (hypoxiainducible factor 1) promoter has been successfully used to express Luciferase and to report hypoxia *in vivo*. Similar to PET, the spatial resolution of BLI is relatively low (1–2 mm), due to the scattering and diffraction of light through tissue [32]. This can

make the precise localization of the signal source difficult to ascertain and a detailed assessment of primary tumor anatomy is often limited. Comparisons between different animal subjects may also be complicated by the variable depth of tumors in each, as the light signal will be variably attenuated. Although this problem may be overcome by using each animal as its own control, it is important to ensure that the animal is accurately and reproducibly positioned each time an image is acquired. Table 4 summarizes BLI applications in pre-clinical research.

Table 4. *BLI in pre-clinical research.*

Application	Example
Animal models	Xenograft, orthotopic, and GEM models of human cancer have been developed which express luciferase
Drug development	BLI allows therapeutic efficacy of cancer drugs to be established
Monitoring of genes	Luciferase-labelled cells may be used to monitor gene delivery and gene expression in vivo Genetic screening has also been performed using BLI, allowing identification of specific oncogenes
Tumor development	BLI may be used to study processes such as angiogenesis, apoptosis, and adhesion in cancer cells
Metastasis	High sensitivity of BLI allows the imaging of metastasis and minimal residual disease states in cancer models
Protein interactions	BLI has been used to image protein–protein interactions *in vivo*

II. AIMS OF THE STUDY AND DESIGN OF THE PROJECT

Pancreatic cancer remains one of the most lethal malignancies. Despite the efforts made in the past 50 years, conventional treatment approaches have little impact on the course of this aggressive neoplasm and the final resolution doesn't seems imminent yet. Moreover, to date an effective system is also still strongly needed, which accurately predict the clinical efficacy of new compounds developed in oncology for pancreatic cancer treatment.

The aim of the current study is to contribute to the generation of a complete and straightforward system useful for the identification of novel drug for pancreatic cancer treatment. This system should provide the techniques, the protocols and a pancreatic cancer model suitable for in vitro high-throughput compounds screening first and in vivo validation of the selected molecules then.

It has become increasingly clear that many tumors contain a very small subpopulation of cancer stem-like cells (CSCs) which are hypothesized to be the more aggressively growing and the more chemoresistant cell population of a tumour. For these reasons a well established CSCs cell line is considered the most interesting cancer model on which novel therapies can be in vitro and in vivo tested. CSCs, finally, offer the opportunities to develop therapies which actually enhance survival rate and life quality

The first goal of the current study was to complete the characterization of spheres growing pancreatic CSCs (Panc1-spheres),previously obtained in our lab from Panc-1 adherent cell line. We are going to use Panc1-spheres as pancreatic cancer model in our generating compounds screening system.

To *in vivo* confirming the aggressiveness, in term of growth rate and invasion capacity, already demonstrated by sphere growing cells in *in vitro* assays, we performed subcutaneous and orthotopical injections in nude mice with Panc1 and Panc1-sph cells. Tumor growths were followed using MRI. In order to underline the most malignant phenotype of Panc1-sph vs adherent Panc1 we also studied EMT on tumors derived from this experiment and on cytospinned cells.

Moreover, looking to troubles we encountered during Magnetic Resonance Imaging (MRI) acquisitions, we observed that an improvement of imaging strategies was actually needed, in order to better control above all the formation of small masses as metastasis and early primary tumors. Mirroring the importance of these mouse models in the pre-clinical testing, we decided to focus our attention to the most important non-invasive small animal-imaging modalities available today, in particular MRI, Micro-Ultrasound (US) and In Vivo Bioluminescence Imaging, tracing disadvantages and advantages of each one.

Then, the second goal was to correlate these techniques and arrive to the point to have an "imaging protocol", able to offset some of the limitation of each modality when used alone, to be used in our generating compounds screening system.

III. Materials & Methods

3.1 Cells lines and culture conditions

Human pancreatic cancer cell lines Panc-1 were grown in RPMI (Cambrex Bioscience, Milan, Italy) supplemented with 10% fetal bovine serum (FBS, Cambrex Bioscience, Milan, Italy), 100 U ml-1 penicillin and 0,1 mg ml-1 streptomycin. Adherent cells were maintained in standard conditions for a few passages at 37°C with 5% of CO2 and detached using Trypsin-EDTA solution (trypsin, 0,25%, EDTA 0,02%).

To generate suspension cells, and separate stem-like cells, adherent cells were washed twice in D-PBS 1X (Cambrex Bioscience, Milan, Italy) and then cultured in DMEM+F-12 (1:1) +1X B27+ 250 mg/ml Fungizone+ 1% penicillin/ streptomycin (Gibco, Invitrogen) + 5 mg/ml Heparin (Sigma, Inc), supplemented with 20 ng/ml EGF and FGF (Peprotech, Inc). The medium was further referred to as 'Cancer Stem Cell medium' (CSM). Adherent cells were left in CSM for at least 3-4 weeks or until the appearance of floating cell aggregates, further referred to as pancreatic cancer spheres. Spheres were then collected without disturbing the adherent cells and sub-cultured in CSM for at least four passages before initiating the *in vitro* and *in vivo* characterization experiments.

Human pancreatic cancer cell lines Panc-1 Luc+ were kindly provided by Dr. Scott Kern (Departments of Surgery, Pathology, and Oncology, The Johns Hopkins Medical Institutions, Baltimore, Maryland, USA) and maintained under G418 selection. We tested the bioluminescence activity of Panc-1-Luc+ cells before their injection in vivo in our mouse model such as their capability to grow in an in vivo system inoculating them in the flank of 5 mice.

3.2 Subcutaneous Pancreatic Cancer Xenografts

All animal experiments have been carried according to the ethical standards of the Verona University Review Board, and the animals were maintained in accordance with the institutional guidelines.

At first, $2x10^6$ adherent and sphere-growing pancreatic cancer cells in a final volume of 100 µl were injected into the right flank of female athymic CD1 mice (4 weeks old, Charles River).

Animals were monitored for tumor growth for an overall period of 30 days.

Tumor volumes and body weight were recorded twice weekly for the complete period.

Tumor volumes were calculated using the formula

$$\mathbf{V=(a * b2)/2}$$

Where where *a* is the biggest and *b* the smallest orthogonal tumor diameter.

3.3 Generation of orthotopic human pancreatic xenografts in immunodeficient mice.

All animal experiments have been carried according to the ethical standards of the Verona University Review Board, and the animals were maintained in accordance with the institutional guidelines.

At first, $5*10^5$ adherent and $5*10^5$ spheres cells in a volume of 30 µl of PBS were injected into the pancreas of female athymic CD1 mice (4 weeks old, Charles River). We divided the animals into two groups: five of them received 500.000 spheres cells, the other one received 500.000 adherent cells. For all successive experiments, the amount of $5*10^6$ (Gruoup one) and $2*10^6$ (Group two) adherent Panc1-Luc cells in a total of 60 µl of PBS containing 1% serum-free Matrigel (vol/vol) has been applied. The syringes containing the cells suspension were put into ice during all the time of surgery.

Animals were anesthetized using Ketamine/xylazine cocktail at a ratio of 100 mg kg^{-1} : 20 mg kg^{-1} placing the mice under a heat lamp. Once anesthetized, the mouse was placed on its right side painting the left side from the base of the neck to the tail with 70% (vol/vol) ethanol. The abdominal skin was picked up with forceps and a 1-cm incision with sterile micro-scissors was made slightly medial to the splenic silhouette. A second 1-cm incision was extended on the abdominal cavity without injury to the underlying organs. Using a pair of blunt-nose forceps, gently the tip of the pancreatic tail was grasped and the pancreas/spleen externalized in the lateral direction, exposing the entire pancreatic body and spleen. While gently retracting the pancreas laterally, we inserted the needle into the tail of the pancreas and passed in the pancreatic head region; slowly the cells solution was injected while withdrawing the needle to the mid-body of the pancreas forming a fluid-filled region within the pancreas parenchyma. When Matrigel was used, the pancreas was left externalized and untouched for 2 minutes waiting for the Matrigel solidification.

Then, the pancreas/spleen were internalized with blunt forceps and the abdominal muscle layer closed with continuous 4-0 suture, while the overlying skin was closed with a second set of interrupted 3-0 silk suture. The negative control group was constituted by five mice which received only Matrigel (60 µl).

All the mice were recovered from the effects of the anesthetic, continuing to monitor the temperature, skin color and respiratory rate under a heat lamp.

Mice were recovered from the procedure once they were in the sterna position, responded to the external stimuli and freely moved about inside the cage.

3.4 Optical imaging

We used VivoVision Systems, IVIS® 200 Series, Imaging System for small laboratory animals, Xenogen (Xenogen Corporation, Alameda USA), an advanced optical imaging system designed to improve quantitative outcomes of in vivo imaging. It's constituted by a camera sensor back thinned, back illuminated grade CCD 1 (2.7 x 2.7cm, -90° C), with a minimal image pixel resolution of 20µm (pixel dimension 13.5µm, imaging pixels 2048 x 2048), quantum efficiency >85% between 500 and 700nm, and > 30% between 400 and 900nm, and a 150W Quartz halogen 3250° Kelvin lamp. The stage of the instrument is heated to 37° C. IVIS 200 Series can work in two different modalities: fluorescence and bioluminescence modality. It is equipped with a set of excitation and emission filters: GFP (445-490nm), GFP background (410-440nm) DsRed (500-550nm), DsRed background (460-490nm) Cy5.5 (615-665nm), Cy5.5 background (580-610nm), ICG (710-760nm and ICG background (665-695nm). For bioluminescent spectral imaging applications, it have a specific filters set to characterize Luciferase-Luciferin system emission (560-580-600-620-640-660 nm) and it has a laser scanner that provides 3D surface topography for single-view diffuse tomographic reconstructions of internal sources.

Images were acquired and analyzed with Living Image 2.6 software and Living Image 3D (Xenogen Corporation, Alameda USA). The animals were placed in the Xenogen's induction chamber and anesthetized using 2.5-3.5% isofluorane. When the mice were in a moderately deep plane of aesthesia, breathing rhythmically, they were removed from the induction chamber and transferred in the imaging chamber putting their heads in the nose cone of the anesthesia manifold.

The tube that supplies the anesthesia to the box is split so that the same concentration of anesthesia is plumbed to the anesthesia manifold located inside the imaging chamber. The animals can be manipulated while they are in the chamber as long as their heads remains in the nose cone.

They were injected in the lower left abdominal quadrant with Luciferin (15 mg/mL or 30 mg/kg, in PBS, dose of 150 mg/kg, D-Luciferin, Firefly, potassium salt, 1.0 g/vial, Caliper Life Sciences) given intraperitoneally for firefly Luciferase.

We Prepared a fresh stock solution of Luciferin at 15 mg/mL in DPBSfor each imaging session. The fresh solution was filter sterilized through a 0.2 um filter.

We performed the acquisition protocol using these parameters: Total Time of acq. 300 seconds; Binning = 8; f/stop (diaphragm opening) =1 and 2; excitation filters =block; emission filters = open; photographic parameters: time=0.2seconds, binning = 4, f/stop=8; field of view = 12.8cm; high of sample =1.5cm. Two Region of Interest (ROI) were selected for each animal: one refers to total abdomen cavity, and one draws only around primary tumors sources emission.

3.5 Ultrasound

All the Ultrasound (US) examinations were performed on a Technos (Esaote, Milan, Italy) with harmonic imaging setting at low acoustic ultrasound pressure (CnTI, 16 MHz; MI < 0.1; DP 15 kPS).

The mice were placed on a table in supine position. An axial scan of the abdomen was taken, in order to locate the spleen and the pancreas, as point of references for the localization of the implanted tumor.

After the localization, three measures of each tumor were taken, in order to evaluate the approximately volume.

3.6 Magnetic Resonance Imaging

Mice were anesthetized by inhalation of a mixture of air and O_2 containing 0.5–1% isofluorane and placed in prone position into a 3.5 cm i.d. transmitter-receiver birdcage coil. Images were acquired using a Biospec Tomograph (Bruker, Karlsruhe, Germany) equipped with a 4.7 T, 33-cm bore horizontal magnet (Oxford Ltd., Oxford, United Kingdom); respiration rate were monitored**.** All mice were put in a supine position and fixed with tape on all extremities and the tail. The imaging planes were coronal and trasverse. The MR sequence parameters used in this study are summarising in Table 5.

Parameter	**Coronal T2 SE with fat-suppression (RARE)**	**Trasverse T2 SE with fat-suppression (RARE)**	**RARE T1 e T1 evo**
TR	5000 ms	5000 ms	
TE 1	67,2 ms	56 ms	
TE 2	67,2 ms	56 ms	
Average	2		
Field of view	5,30 cm	5 cm	3 cm
Matrix size	256 x 256	256 x 128	256 x 128
Repetition time	4398,6 ms		
Echos	1		
Interslice	1 mm	1 mm	0,75 mm

Slices	15	20	12 and 22 respectively
Slice thickness	1 mm	1 mm	0,75 mm

After T2-weighted images were acquired, for the last imaging session before sacrifice, all animals received Gadolinium (Gd)-DTPA (10 µl/10gr), 1:5, BW, Magnevist ™, Schering, Berlin, Germany), injected in the vein of the tail 15 min prior to imaging to enhance the contrast of the pancreas to the surrounding tissue in order to better delineate the tumor.

3.7 Cytospin

We used $4*10^5$ cells washed in cold PBS twice and diluted in 500 µl of cold PBS. All samples were put on ice.

Slides and filters were placed into appropriate slots in the cytospin with the cardboard filters facing the center of the cytospin; quickly 500 µl of each sample were aliquoted into the appropriate wells of the cytospin and spinned at maximum speed for 5 minutes.

3.8 Histological and Immunohistochemical analysis of tumor xenografts

Necropsies were performed by cervical dislocation of anaesthetized animals. Tumor samples were formalin-fixed, embedded in paraffin, sectioned and deparaffinized using xylene, and hydrated by series of decreasing ethanol washes. Hematoxylin/Eosin was performed for each samples. Ki-67 (clone, MM1 Novocastra), p53 (Novocastra), CK7 (Biogenex), E-Cadherin (Dako), S100A4 (Rabbit mAb, Dako) and Slug (C19G7, Rabbit mAb, Cell Signaling) were diluted respectively 1:50, 1:20, 1:500, 1:20, 1:500 and 1:50; antigen retrievals were performed at 95° for 15 min in buffer citrate pH=6. Vimentin (Biogenex) was diluted 1:500; CXCR4 (Abcam, rabbit mAb) was diluted 1:100 and antigen retrieval was performed at 95° for 15 min in buffer citrate pH=6, while Twist (Santa Cruz) was diluted 1:80 and antigen retrieval was performed at 95° for 15 min in buffer citrate pH=8.

Histology was performed with H&E staining.

All slides were acquired using Aperio Scan-Scope XT system.

IV. RESULTS

4.1 Panc-1 spheres show higher proliferation rate than adherent cells in vivo: subcutaneous mouse model

To assess the tumorigenicity properties of Panc-1 adherent cells and spheres, cells were subcutaneously injected in nude mice.

In this experiment, $2*10^6$ Panc-1 adherent or Panc-1 sphere growing cells were injected in the flanks of nude mice. The tumor growth was monitored for 30 days twice a week with a caliper. Tumor volume was calculated as reported in section 3.2.

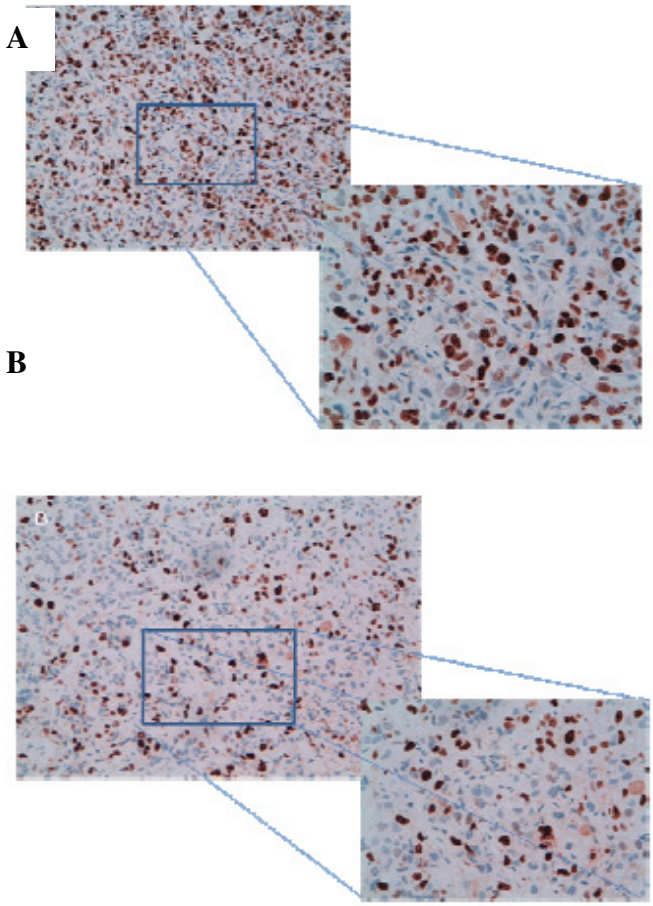

Figure 13. *Representative images of the Ki-67 staining of Panc-1 spheres (A) and Panc-1 adherent cells (B). Images were acquired at 20X. The inserts are 40X.*

The proliferation index of both adherent cell and sphere-derived tumors was determined by Ki67 immunostaining on paraffin-embedded tumor sections. As depicted in Figure 13, sphere-derived tumors demonstrate a significantly higher proliferation rate (70-80% positivity) when compared to adherent cell-derived tumors (40% positivity) (Fig.13).

4.2 Morphological analysis of the Panc-1 spheres vs adherent cells in the Subcutaneous Pancreatic Cancer Xenografts.

The morphology of tumors derived from Panc-1 spheres and adherent cells were investigated in a xenograft mice model. Therefore, $2x10^6$ cells of each cell type were injected subcutaneously in athymic female mice.

After 35 days, mice were sacrificed; tumors were resected from skin, and processed using formalin-embedded paraffin technology. H&E staining (Fig. 14) demonstrated that sphere growing tumors established in nude mice showed more irregular mitotic figures than adherent cell-derived tumors.

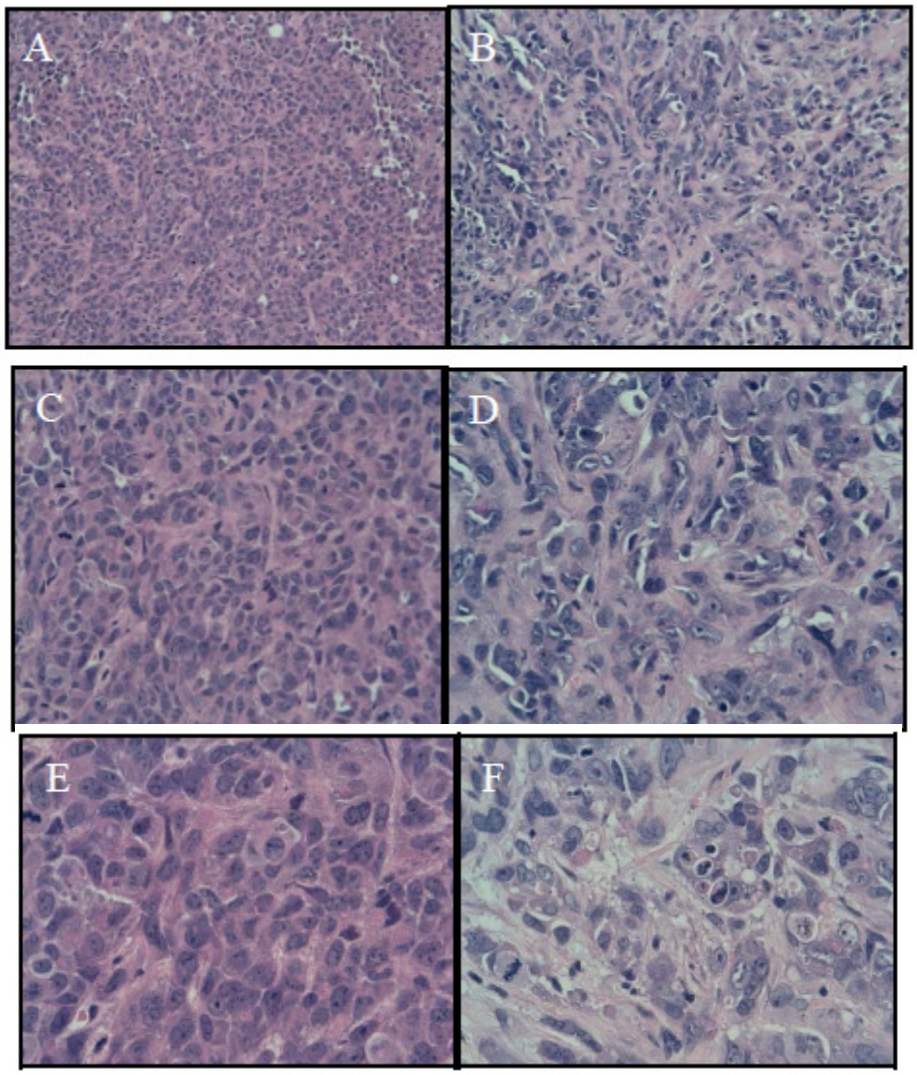

Figure 14. *H&E staining: comparison at different magnifications in tumors generated from Panc-1 adherent at A) 20X, C) 40X, E)63X, and from Panc-1 spheres at B) 20X, D) 40X, and F) 60X.*

Moreover, adherent cells demonstrated a more organized architecture whereas the spheres generated a more dysplastic tumor structure. Spheres were less organized; they contained more apoptotic

bodies and more mitotic figures (Fig. 15 B) and had a higher stromal reaction, (Fig. 15 B, arrows). They also demonstrated cancer cell infiltration in the perineural tissue (Fig. 15 C, D, arrows).

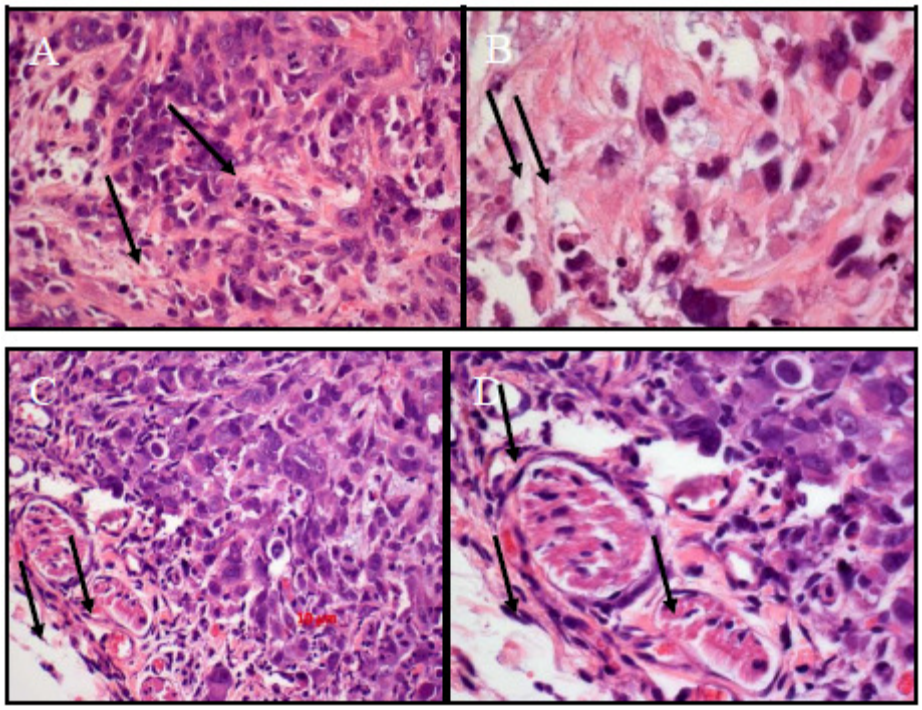

Figure 15. *Stromal reaction of tumors generated from Panc-1 spheres A) 200X and B) 400X. Sphere-derived tumors infiltrated in perineural tissue C) 200X and D) 400X.*

4.3 Panc-1 spheres grow faster and are more aggressive than adherent cells in vivo: the orthotopic mouse model.

In order to assess growth rate and aggressiveness of Panc-1-growing spheres respect to adherent Panc-1 cells, we performed orthotopic injections with both kind of cells using nude mice. We repeated this experiment twice (see section 2.3). In both cases, we divided the animals into two groups: five of them received $5*10^5$ spheres growing cells and the other one received $5*10^5$ adherent cells, both suspended in 30 µl PBS.

We followed tumor growth in MRI, setting the first control one month after surgery.

All tumors grew both in the first than in the second experiment. We observed that mice injected with Panc-1 spheres growing cells developed tumor faster than mice injected with Panc-1 adherent cells: in mice receiving Panc-1 spheres growing cells , small masses were detectable in MRI 6 week after surgery (Fig. 16), whereas no tumors were seen at the same time-point in mice receiving adherent cells . The latter needed other 2 weeks to develop detectable tumors (Fig. 17).

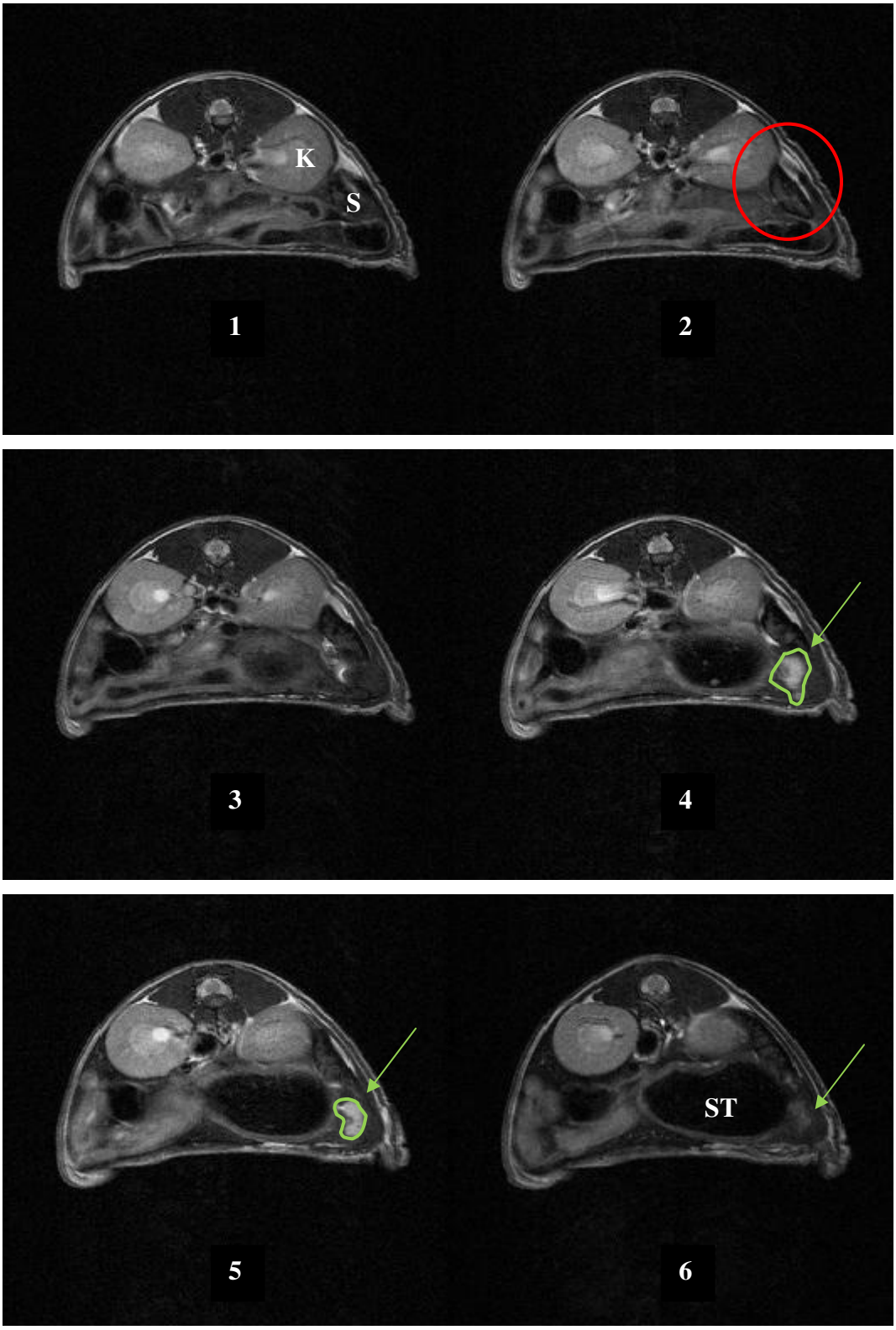

Figure 16. *MRI T2-weight sequences (1 to 6) of a mouse orthotopically injected with spheres growing Panc-1 cells, 6 weeks after surgery. Animal is lying face down. A tumor mass are detectable. The red ring indicates the anatomical area in with tumor should be grow (In picture 5: K= left kidney; S= Spleen; ST= stomach). Arrows indicates the developed tumor mass.*

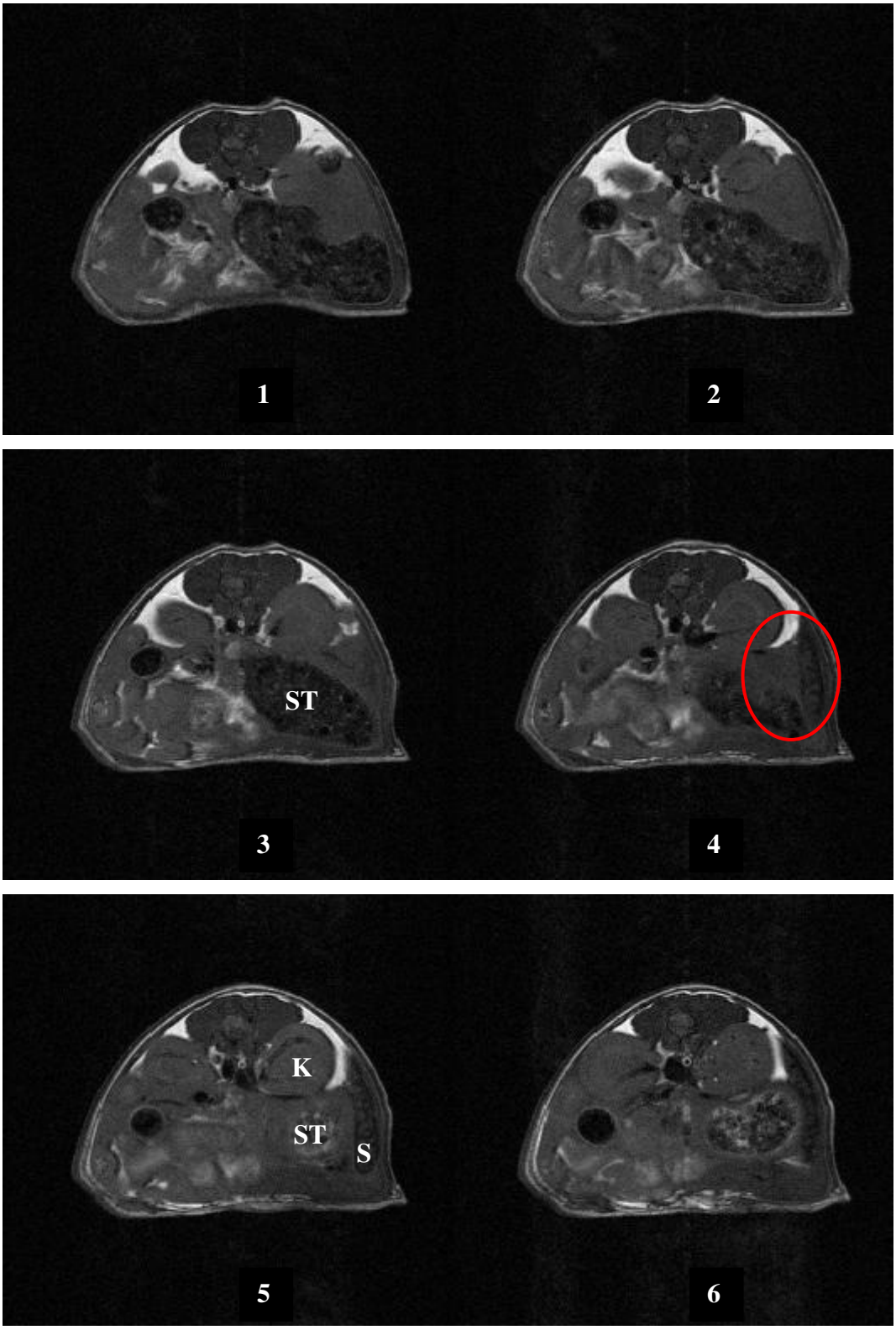

Figure 17. *MRI T2-weight sequences (1 to 6) of a mouse orthotopically injected with adherent Panc-1, 6 weeks after surgery. Animal is lying face down. No tumor masses are detectable. The red ring indicates the anatomical area in which tumor should grow. (In picture 5: K= left kidney; S= Spleen; ST= stomach).*

We observed tumor infiltration in the spleen, a phenomena already know in literature as "infiltration *ad continuum"* (Fig. 18) in one mouse injected with adherent cells and in two injected with spheres. Moreover, in 4/5 mice injected with spheres, putative metastasis were detected during necropsy (Fig. 19), in the liver, stomach and intestine. No metastasis were found in mice injected with adherent Panc-1 cells.

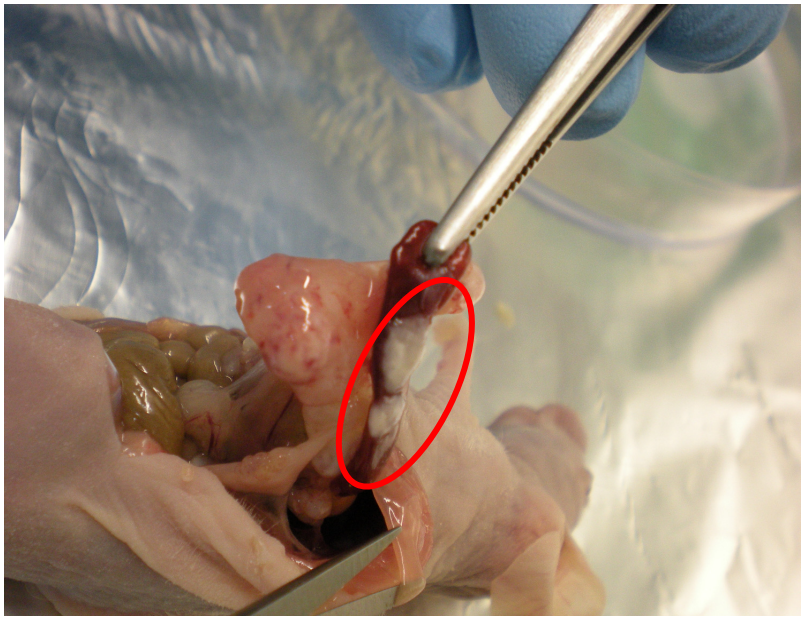

Figure 18. *First orthotopic experiment: tumor infiltration in the spleen, "infiltration ad continuum"(red ring) , derived from spheres growing*

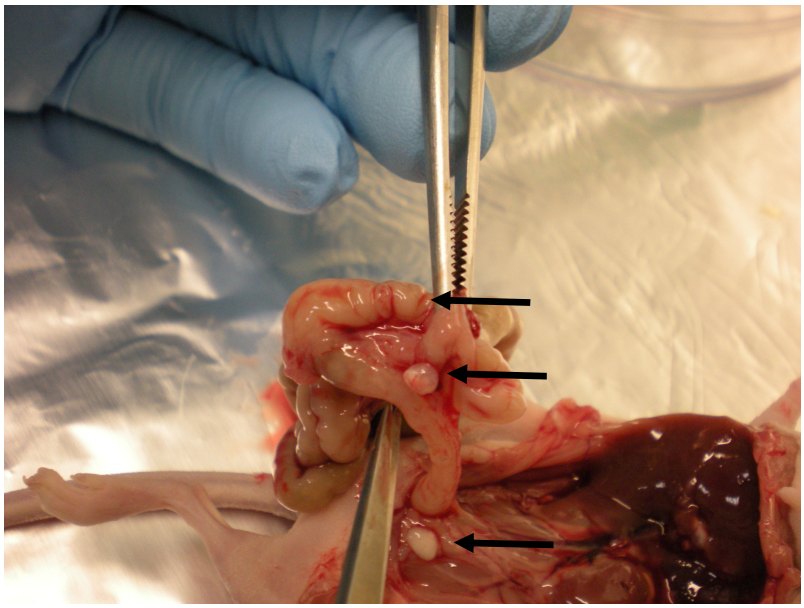

Figure 19. *First orthotopic experiment: putative metastasis (black arrows), derived from spheres growing cells.*

In the second experiment, as already seen in the first one, mice inoculated with spheres developed tumors faster that those inoculated with adherent cells (data not show).

Putative metastasis were found in 5/5 animals injected with spheres, in which we identified the presence of small masses in the gut and tumor spots on the liver, as shown in the Fig. 20 and 21. One mouse injected with adherent cells showed metastasis in the intestine (data not shown).

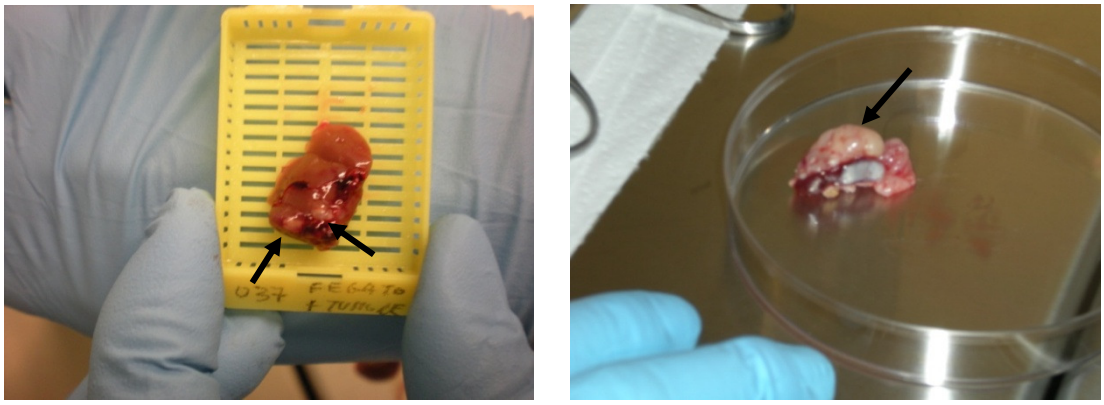

Figure 20. *Second orthotopic experiment: arrows indicate putative metastasis in the liver (picture on the left) and tumor mass attached to the spleen (picture on the right).*

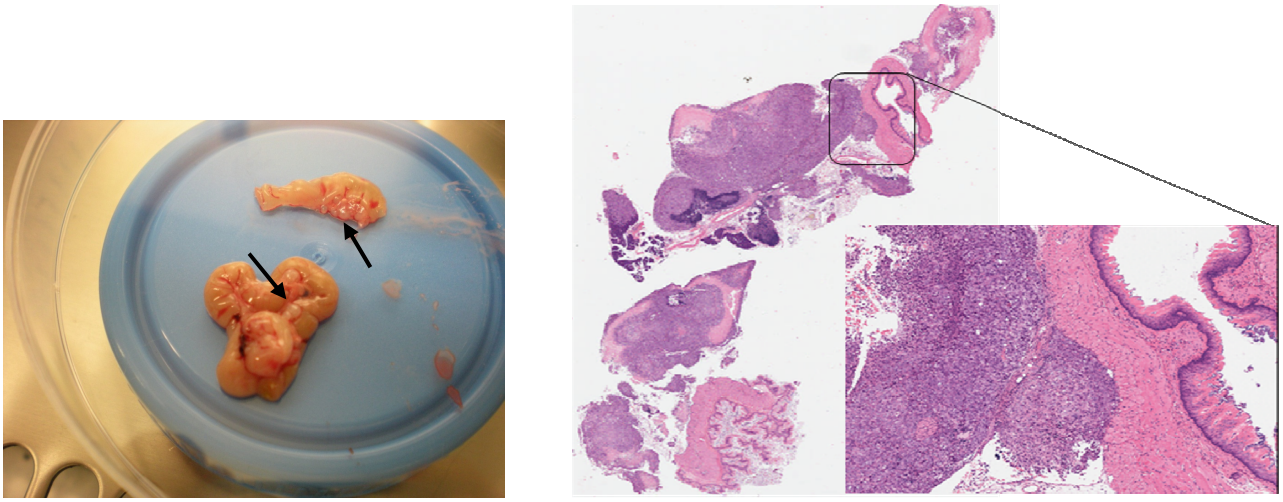

Figure 21. *Second orthotopic experiment: arrows indicate small putative tumor masses found in the intestine, from primary tumor derived spheres growing cells (picture on the left);H&E staining of the small tumor masses collected from the small intestine (picture on the right).*

It have to be underlined that supplementary small masses attached to the small intestine were never identified during MRI analysis. The images below refer to the mouse shown in Fig. 19. It's a MRI T2-weight sequence performed one week before necropsy; the primary tumor mass is clearly detectable (spotlight in green perimeter, Fig. 22). Images are clear and no breath artifacts are present. Even if all the conditions are favorable, no masses within the small intestine were found during MRI session, on contrary to what necropsy disclosed.

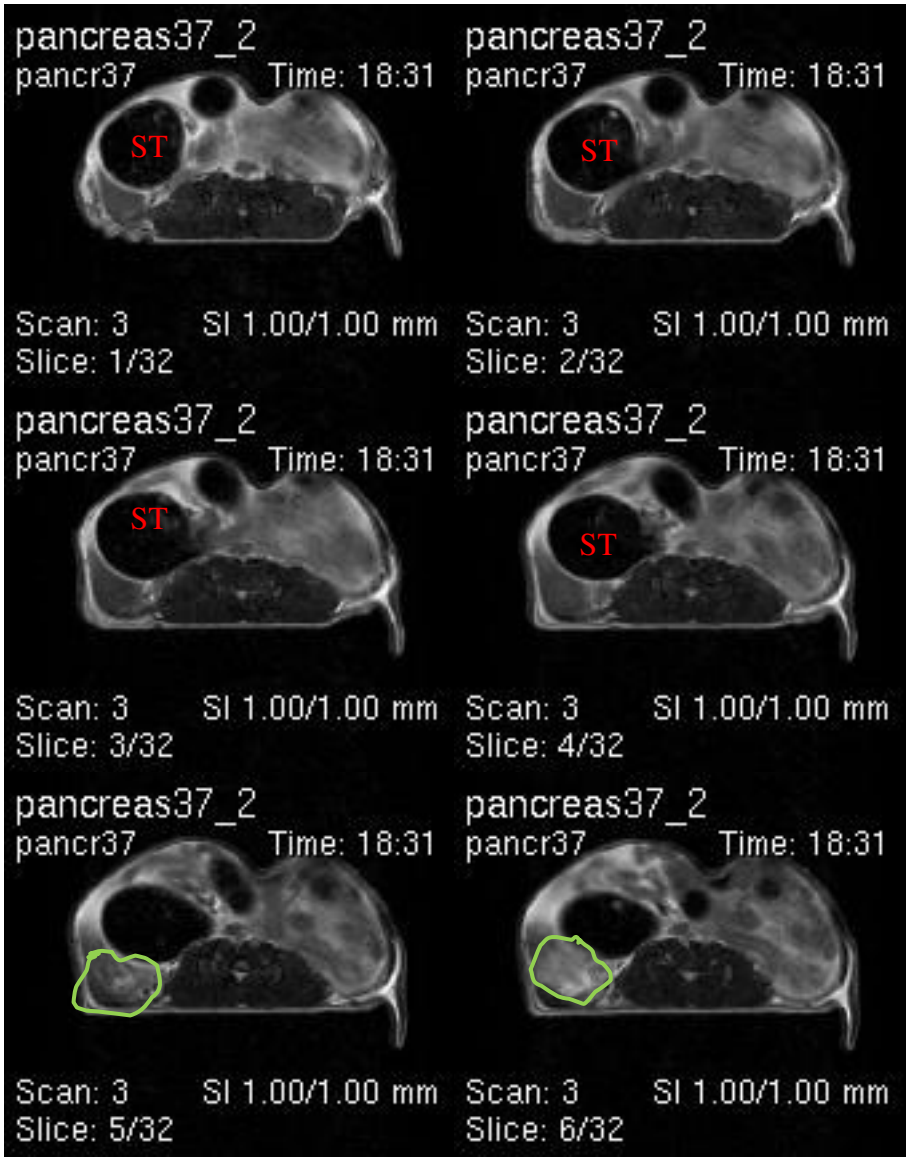

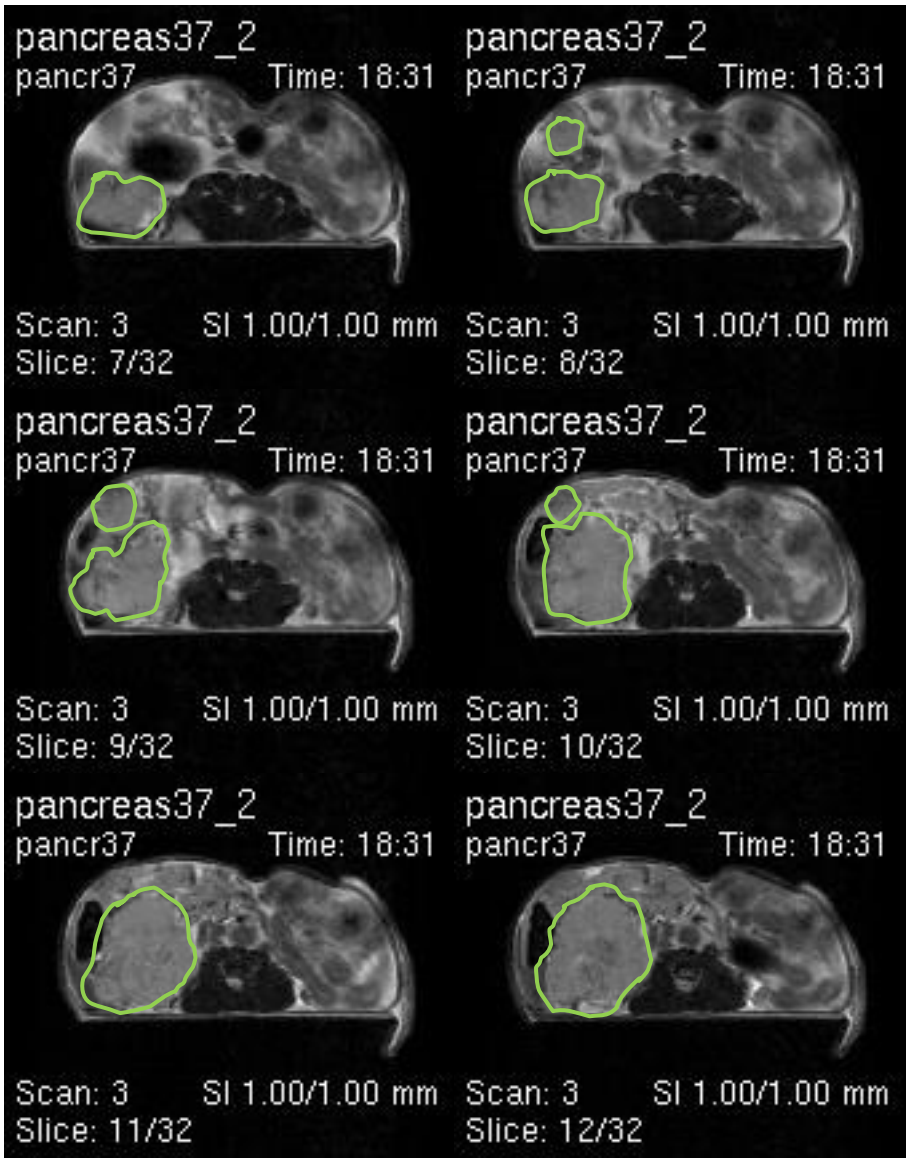
pancreas37_2
pancr37
Time: 18:31
Scan: 3
SI 1.00/1.00 mm
Slice: 7/32
pancreas37_2
pancr37
Time: 18:31
Scan: 3
SI 1.00/1.00 mm
Slice: 8/32
pancreas37_2
pancr37
Time: 18:31
Scan: 3
SI 1.00/1.00 mm
Slice: 9/32
pancreas37_2
pancr37
Time: 18:31
Scan: 3
SI 1.00/1.00 mm
Slice: 10/32
pancreas37_2
pancr37
Time: 18:31
Scan: 3
SI 1.00/1.00 mm
Slice: 11/32
pancreas37_2
pancr37
Time: 18:31
Scan: 3
SI 1.00/1.00 mm
Slice: 12/32

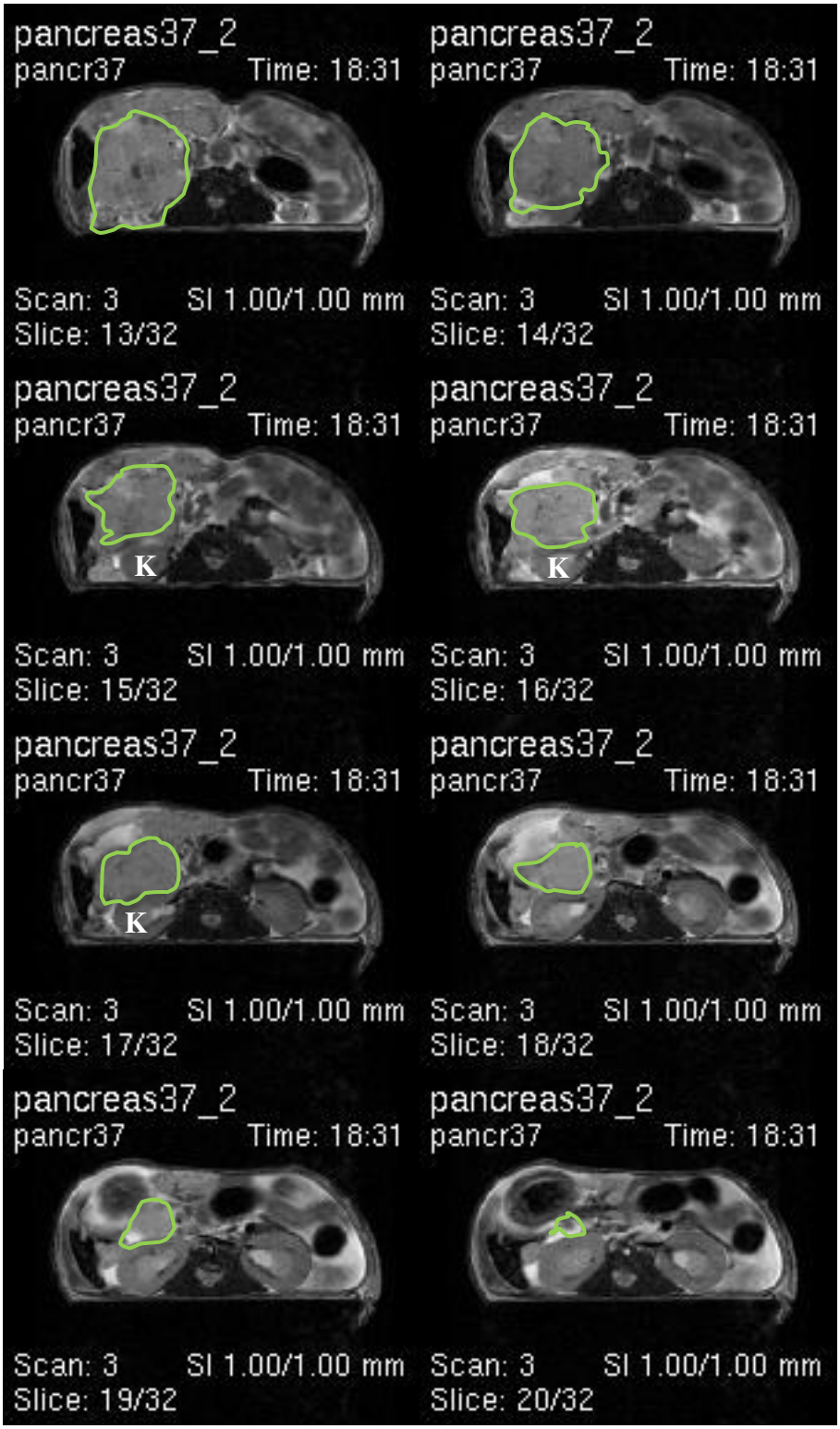

Figure 22. *MRI T2-weight sequences (see slice from 1 to 20) of a mouse orthotopically injected with spheres growing Panc-1 cells, 1week before necropsy. Animal is in supine position, so the tumor mass is detected on the left of the image. No putative metastasis or minor tumor masses can be seen in other anatomical compartment, contrary to what we found at the end of the experiments during necropsy. (K= left kidney; ST= stomach).Green rings dyeline the primary tumor.*

4.4 Morphological analysis of the Panc-1 spheres vs adherent cells in the orthotopic mouse model.

The morphology of tumors derived from Panc-1 spheres and adherent cells was investigated in all orthotopic tumor masses obtained after necropsies from both the two experiments (see section 4.3). Therefore, $5*10^5$ cells of each cell type were injected in the pancreas of athymic female mice.

After more or less 3 month from surgery, before first signals of suffering appeared because of the big size of tumors, mice were sacrificed; tumors were processed using formalin-embedded paraffin technology.

Tumor derived from adherent cells showed different areas of organization, probably due to the eterogeneity of the starting population (Fig. 23). Instead, tumors derived from spheres growing cells were more homogeneous (Fig. 24) and have dense tissue organization, because of their derivation from a selected subset of cells starting from adherent the Panc-1 cell line. H&E staining demonstrated that sphere growing tumors established in nude mice showed more irregular mitotic than adherent cell-derived tumors.

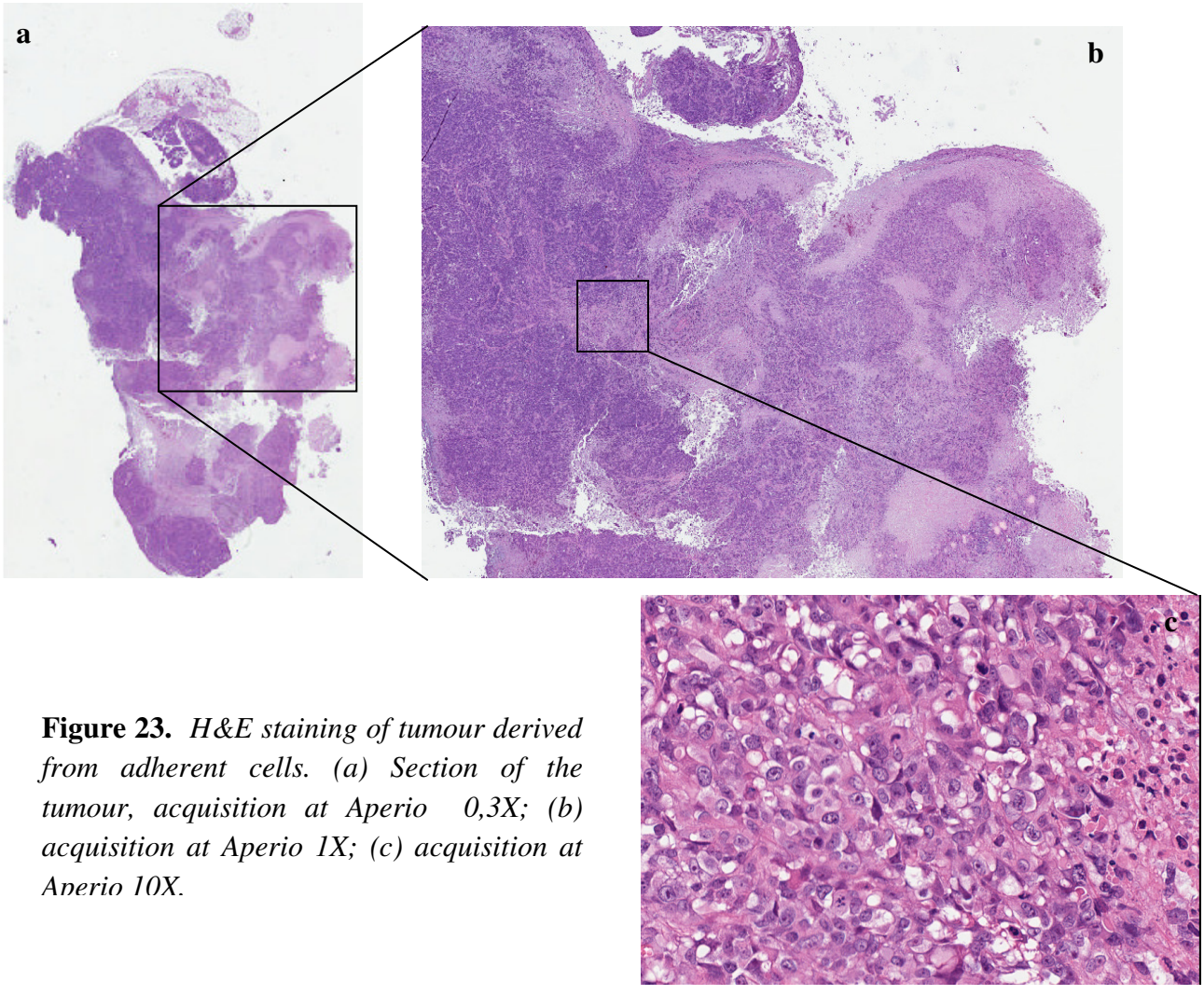

Figure 23. *H&E staining of tumour derived from adherent cells. (a) Section of the tumour, acquisition at Aperio 0,3X; (b) acquisition at Aperio 1X; (c) acquisition at Aperio 10X.*

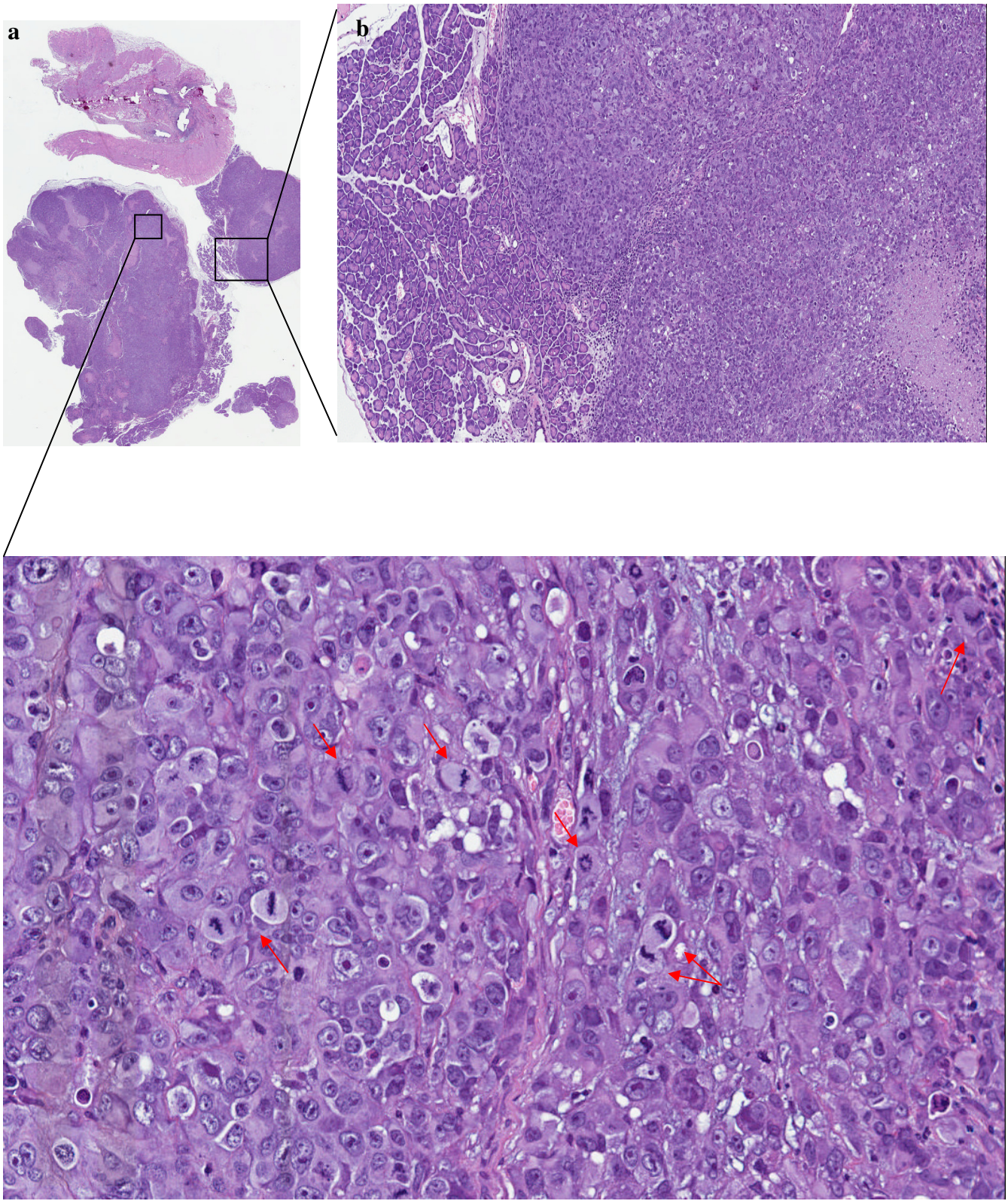

Figure 24. *H&E staining of orthotopic tumors derived from spheres growing cells. (a) Section of the tumor, acquisition at Aperio 0,3 X; (b) acquisition at Aperio 1 X, residues of normal pancreas on the left; (c) acquisition at Aperio 10 X, arrows indicate evident mitotic cells.*

4.5 Epithelial-mesenchymal transition (EMT) in adherent Panc-1 and spheres growing cells Panc-1 cell lines.

The epithelial-mesenchymal transition (EMT) is an orchestrated series of events in which cell-cell and cell-extracellular matrix (ECM) interactions are altered, the cytoskeleton is reorganized to confer the ability to move, and a new transcriptional program, typically resembling mesenchymal phenotype is induced. Even if it's essential for embryonic development, EMT during tumor progression allows noninvasive and non metastatic tumor cells to acquire the capacity to infiltrate in the surrounding tissue and to ultimately metastasize to distant sites. We examined the expression of the most important EMT markers such as E-Cadherin, Vimentin, S100A4, Twist and Slug, in cytospinned adherent Panc-1 and spheres growing Panc-1, then in subcutaneous tumors derived from both cell lines and, finally, in tumors derived from each kind of cells orthotopically injected into the pancreas of nude mice.

➢ *4.5.1 EMT in cytospinnd adherent and spheres growing Panc-1 cell lines*

We performed immunohistochemical assay on adherent Panc-1cells culture and spheres growing Panc-1 cells in order to analyze the expression of EMT markers before they grow *in vivo* (subcutaneous and orthotopic sites). the two cell lines shows a little difference in term of E-Cadherin expression, slightly more weak in spheres cells respect to adherent cells. Both adherent and spheres Panc-1 cells resulted strongly positive for the expression of Vimentin marker. We found an important different in the expression of S100A4 both in adherent and spheres cells: it was strong in spheres, and absent in adherent cells (Fig. 25). No considerable differences in the expression of Slug were found comparing the two cell lines, which results weakly positive in the cytoplasm of cells in few tumor areas. By nature, Twist was absent in adherent and spheres cells, even if the latter showed some atypical granule cells positive to Twist antibody (Fig. 26).

➢ *4.5.2 EMT in adherent and spheres growing Panc-1 from Subcutaneous Pancreatic Cancer Xenograft*

Tumors grown in subcutaneous xenografts showed very faint expression of E-Cadherin both in tumors derived from adherent than tumors derived from spheres cells; no important differences were found in Vimentin expression such as Twist expression markers. S100A4 probably displayed a slightly stronger expression in spheres derived tumors (Fig. 27). A strong difference of expression was found for Slug marker, resulting in a negative pattern for adherent derived tumors and a evident positivity in tumors derived from spheres, especially in tumor border (Fig. 28).

Adherent Panc-1 | ***IN VITRO*** | **Spheres- growing Panc-1**

1. E-cadherin expression

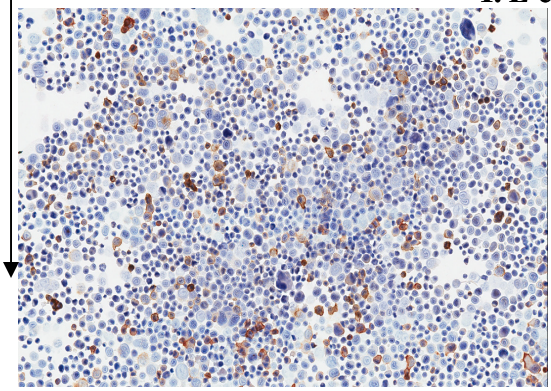
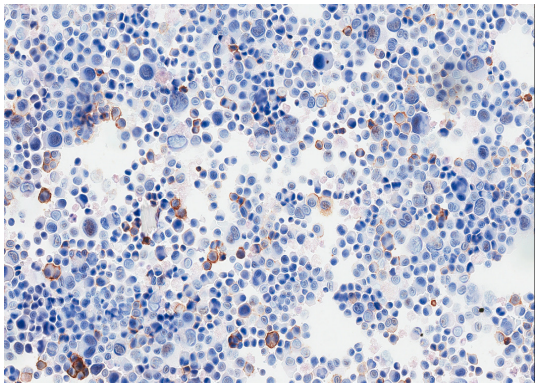

2. Vimentin expression

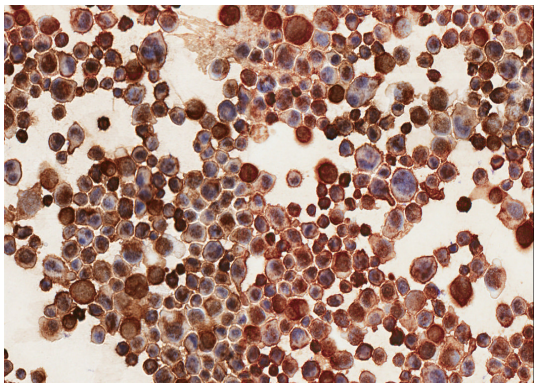
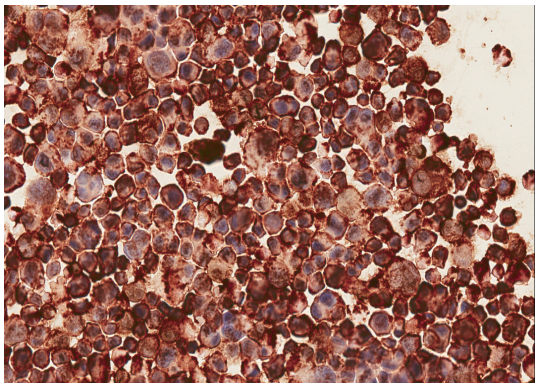

3. S100A4 expression

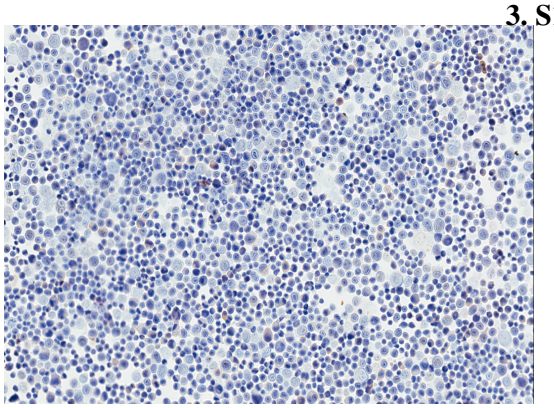
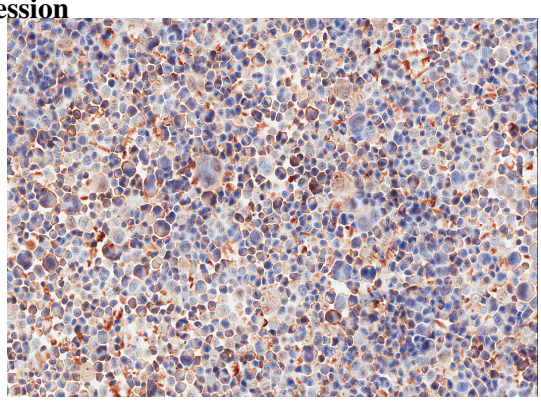

4.Twist expression

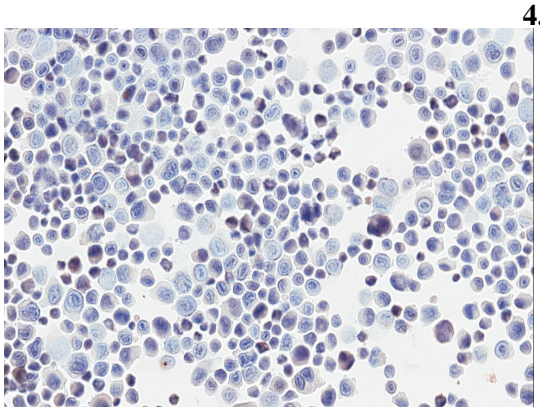
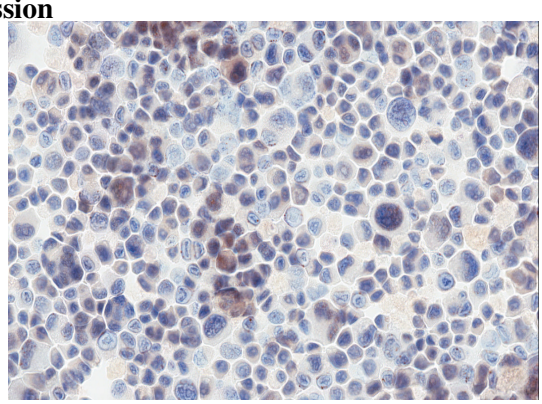

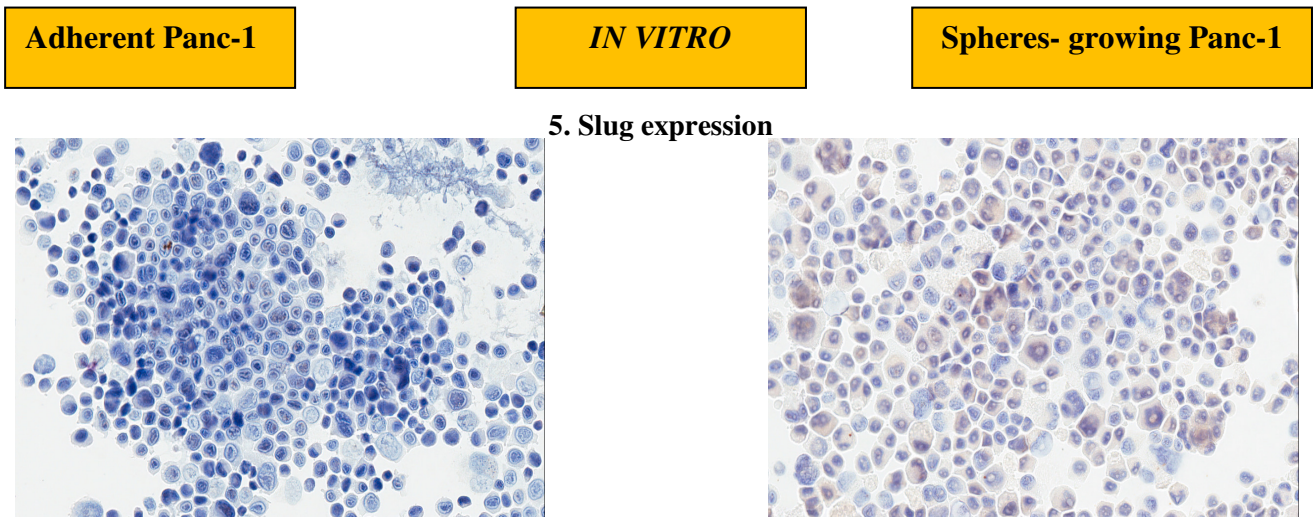

Figure 25. *EMT markers expression in cytospinned Panc-1 adherent cells (left column) and spheres-growing Panc-1 cell (right column). Acquisition at Aperio 10 X (couples 1-3) and 20 X (couples 2-4-5).*

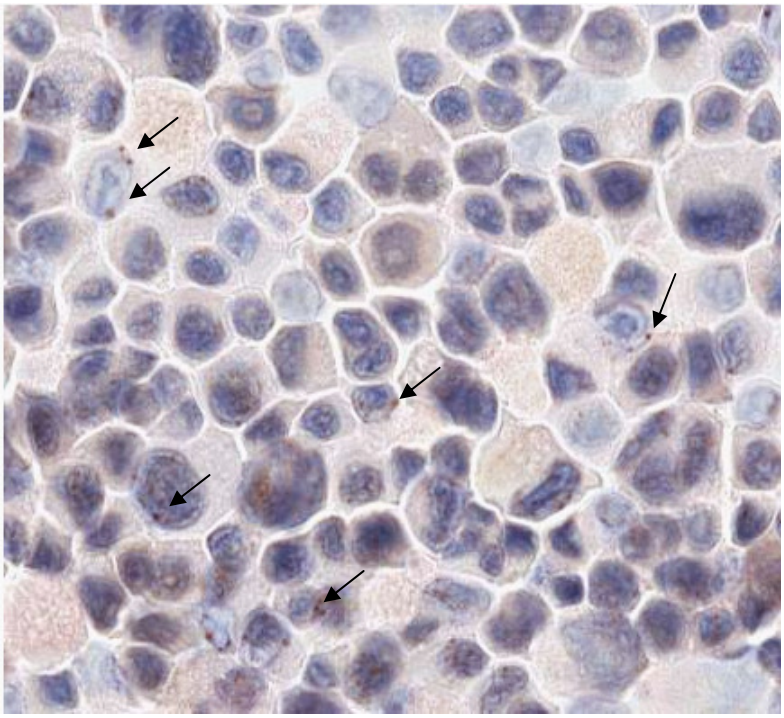

Figure 26. *Detail of Twist expression in spheres cells. Arrows show granules inside nucleus and cytoplasm.*

Adherent Panc-1

IN VIVO **Subcutaneous** Pancreatic Cancer Xenografts

Spheres- growing Panc-1

1. E-cadherin expression

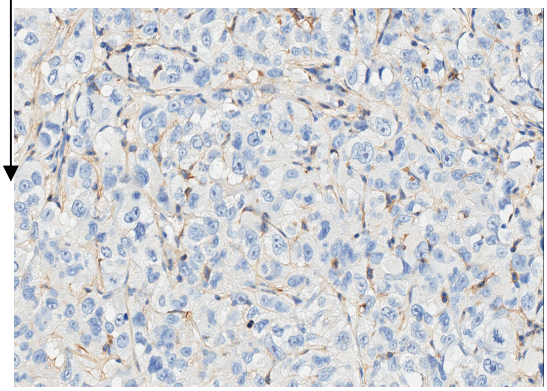

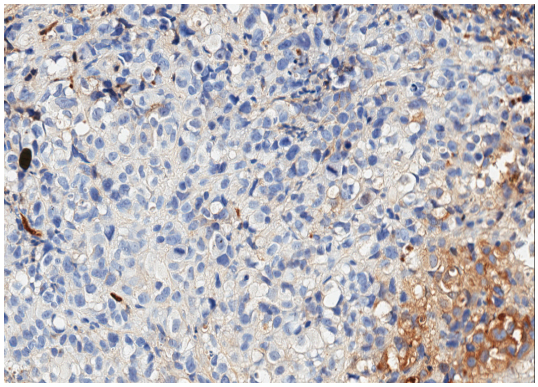

2. Vimentin expression

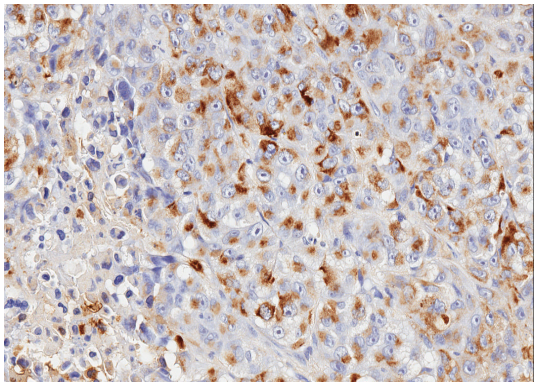

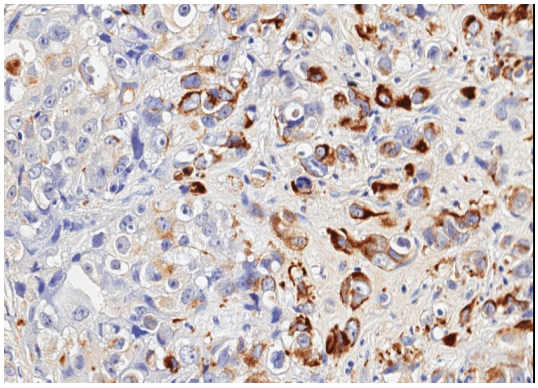

3. S100A4 expression

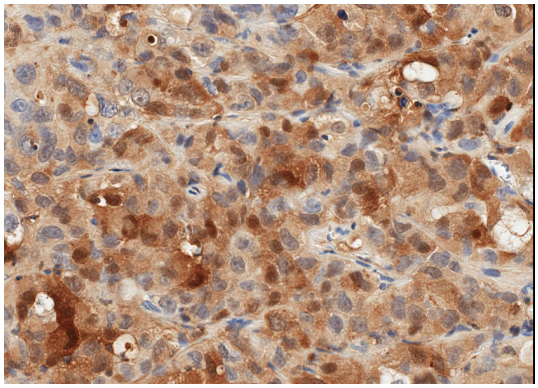

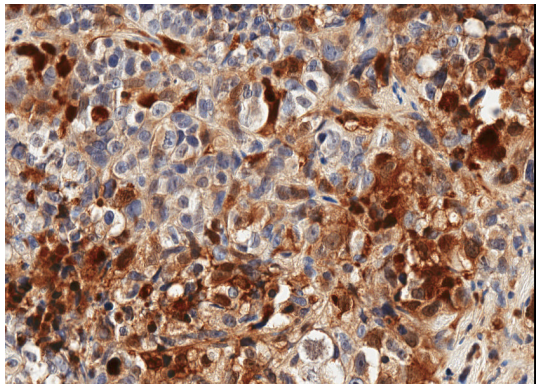

4. Twist expression

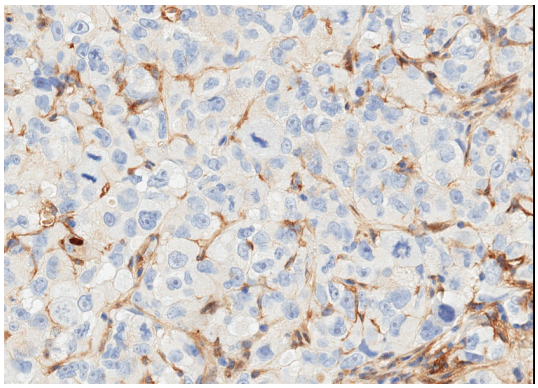

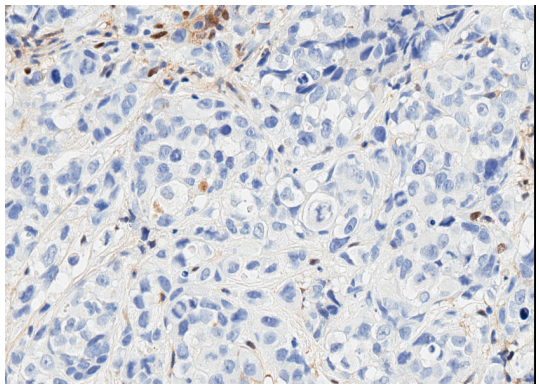

Adherent Panc-1

IN VIVO **Subcutaneous** Pancreatic Cancer Xenografts

Spheres- growing Panc-1

5. Slug expression

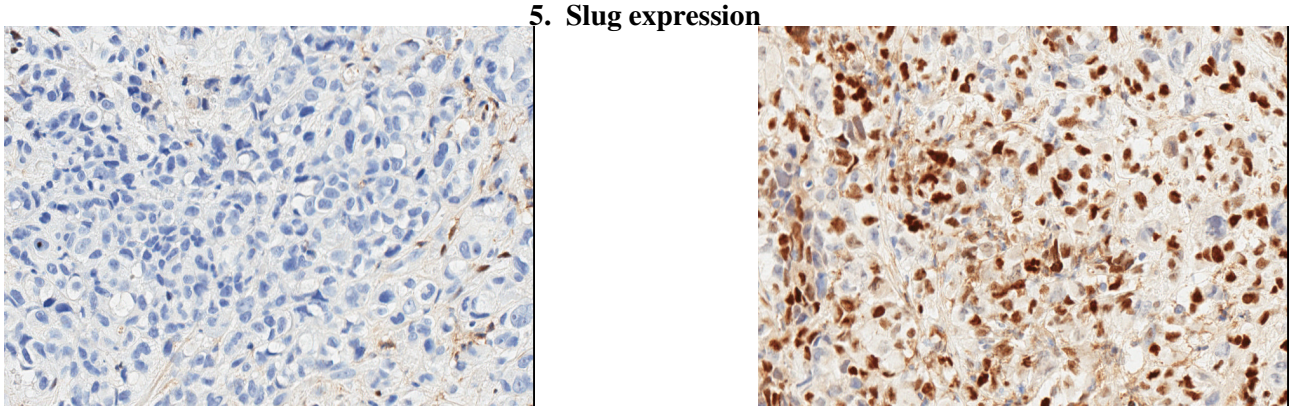

Figure 27. *EMT markers expression in subcutaneous tumors derived from Panc-1 adherent cells (left column) and tumors derived from spheres-growing Panc-1 cell (right column; it's a detail of Fig.ure 27). All acquisition were performed at Aperio 20 X.*

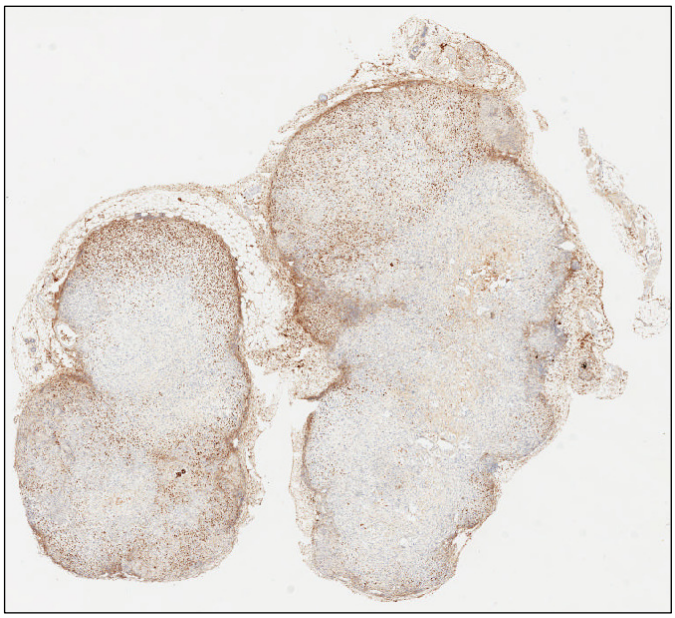

Figure 28. *Expression of Slug in a section of subcutaneous tumor derived from adherent Panc-1 determinate by immunohistochemistry. Picture shows that Slug localizes mainly in the tumor border.*

➢ ***4.5.3 <u>EMT in the Orthotopic Pancreatic Cancer model.</u>***

We analyzed the expression of EMT markers in primary tumors derived adherent cells and spheres-growing Panc-1 cells. All orthotopic tumor masses were characterized by a strong lymphocyte infiltration.

Adherent Panc-1

IN VIVO **Orthotopic** Pancreatic Cancer Xenografts

Spheres- growing Panc-1

1. E-cadherin expression

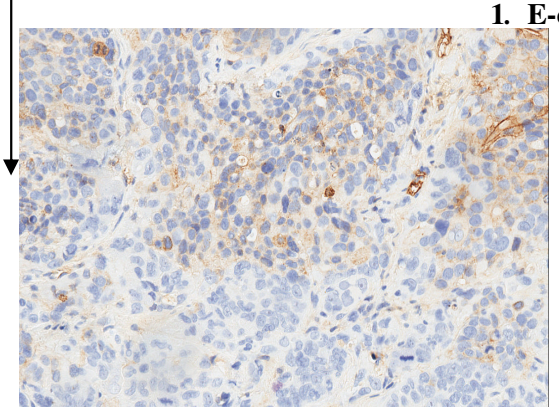

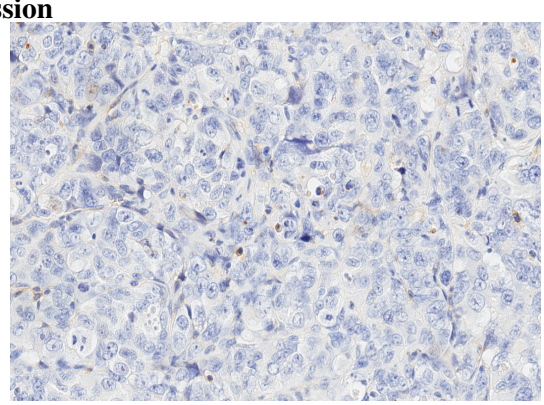

2. Vimentin expression

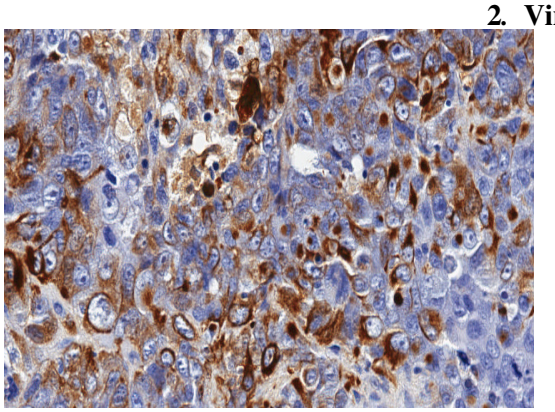

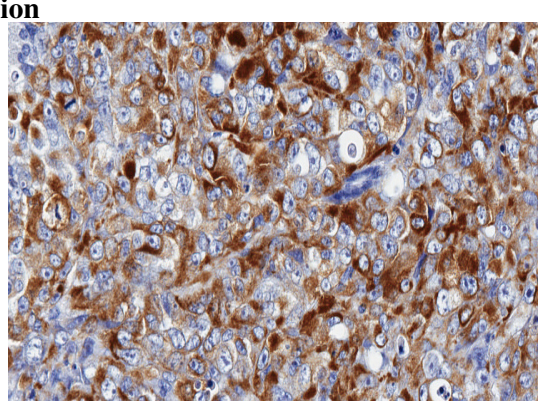

3. S100A4 expression

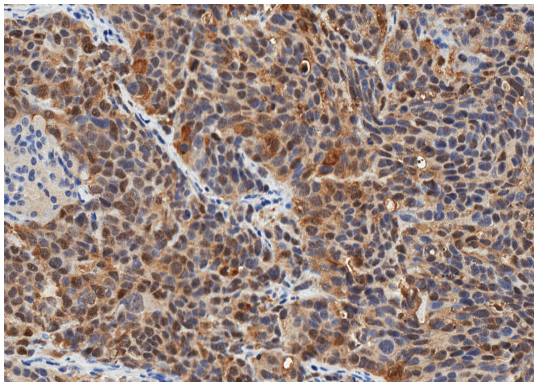

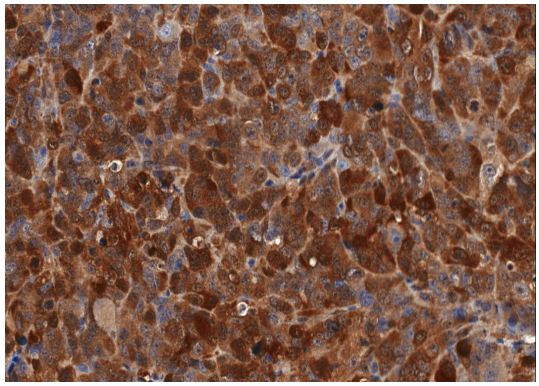

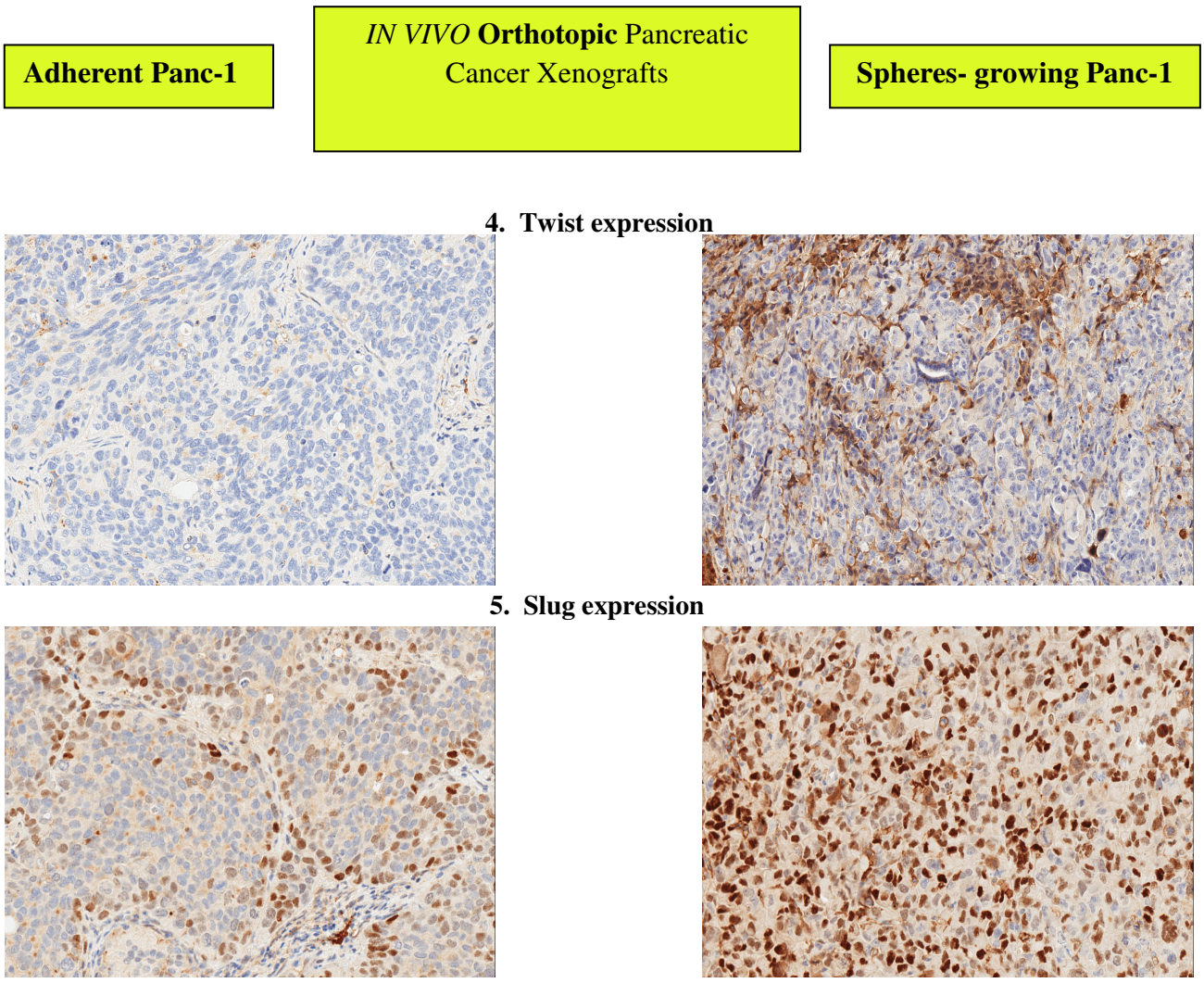

Figure 29. *EMT markers expression in orthotopic primary tumors derived from Panc-1 adherent cells (left column) and tumors derived from spheres-growing Panc-1 cell (right column). All acquisition were performed at Aperio 20 X.*

As shown in Fig. 29, differences in EMT markers expression in orthotopic primary tumors immunohistochemistry are more evident than in the subcutaneous growing tumors derived from both cell lines. Except of E-Cadherin expression, that displays starting low intensity in the adherent-derived Panc-1 tumors and completely disappears becoming negative in spheres-derived tumors, in all the other cases, the expression of Vimentin and S100A4 markers increase appreciably. In particular, similarly to how shown in Fig. 26 regarding the subcutaneous mouse model, an increase expression of Slug can clearly be appreciate; moreover, in the case of the orthotopic growth of tumor cells, we observed an increase expression of Twist in sphere-derived primary tumors if compared with what happens in adherent-derived primary tumors. Twist expression resulted positive in tumors derived from spheres, even if only in a few cells, in particular for those closed to necrotic areas of the tumor mass.

➢ *4.5.4 EMT in the Orthotopic Pancreatic Cancer model: analysis of putative metastasis*

As said before in section 4.3, putative metastasis were found in 9/10 animals injected with spheres, in which we identified the presence of small masses in the gut and tumor spots on the liver (as shown in the Fig. 19 and Fig. 20).

IN VIVO ***Putative Metastasis***

in

Orthotopic Pancreatic Cancer model

Spheres- growing Panc-1 cells

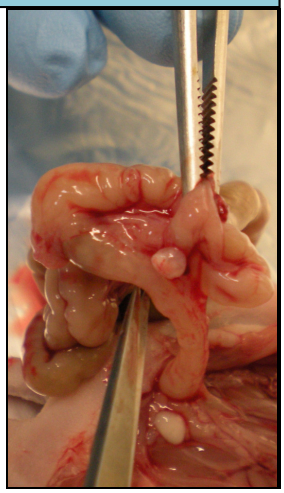

1. E-cadherin expression

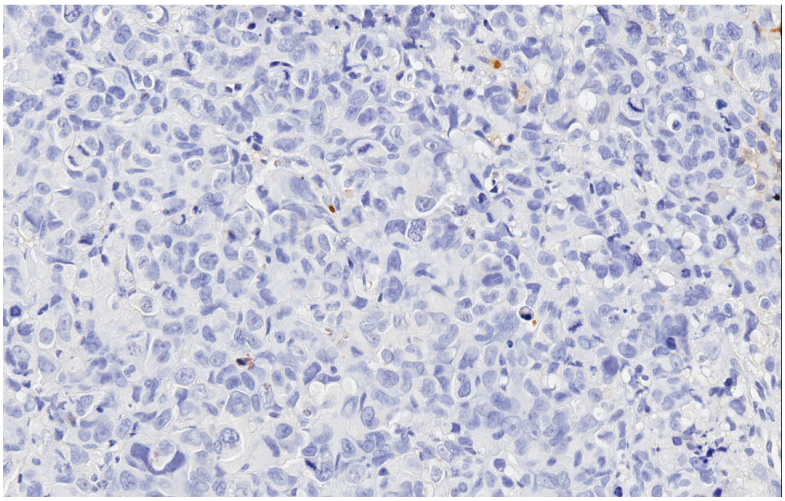

2. Vimentin expression

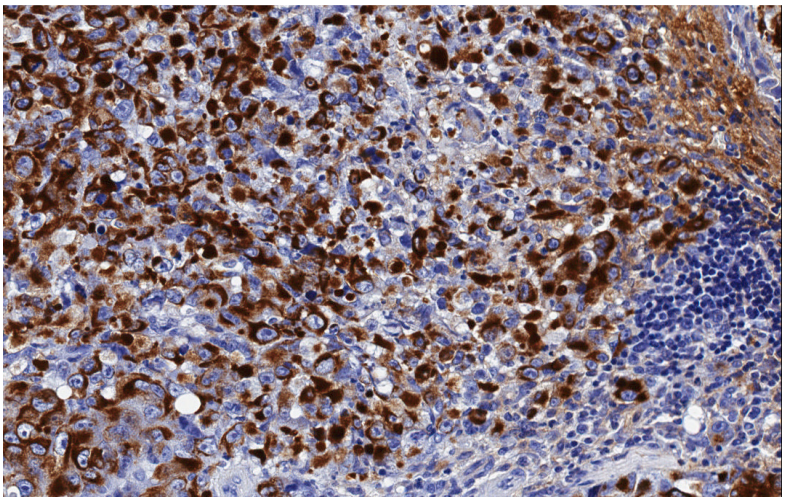

3. S100A4 expression

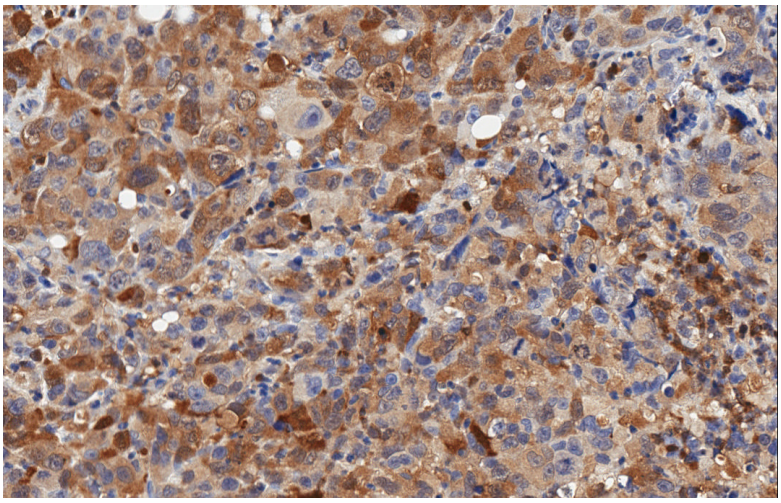

4.Twist expression

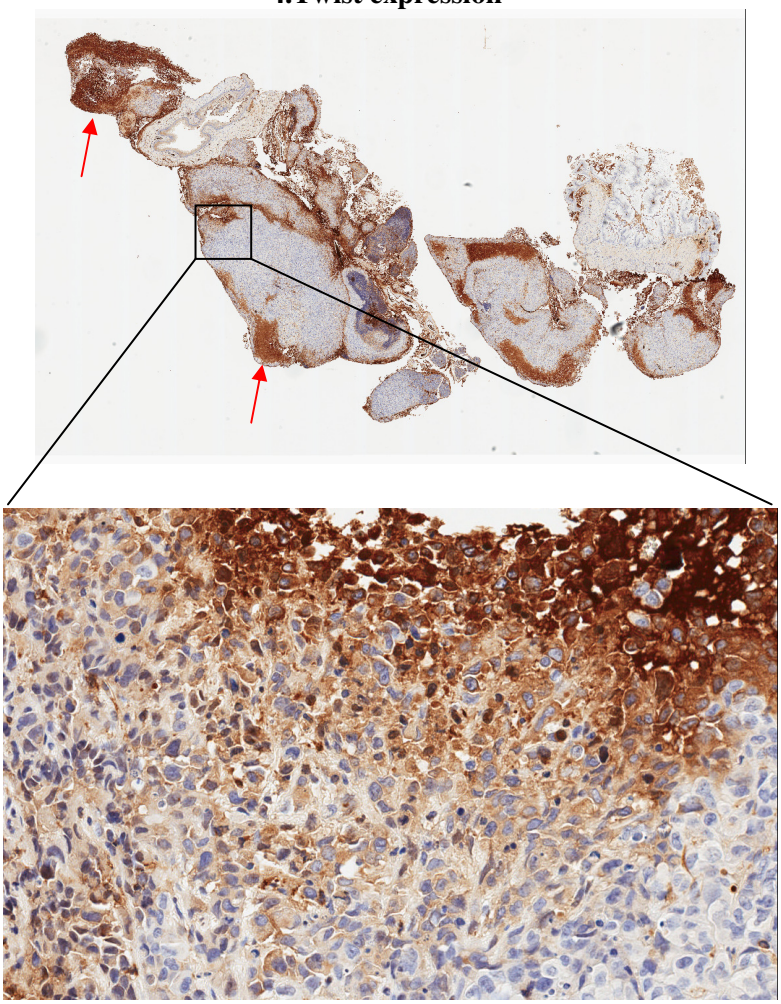

5. Slug expression

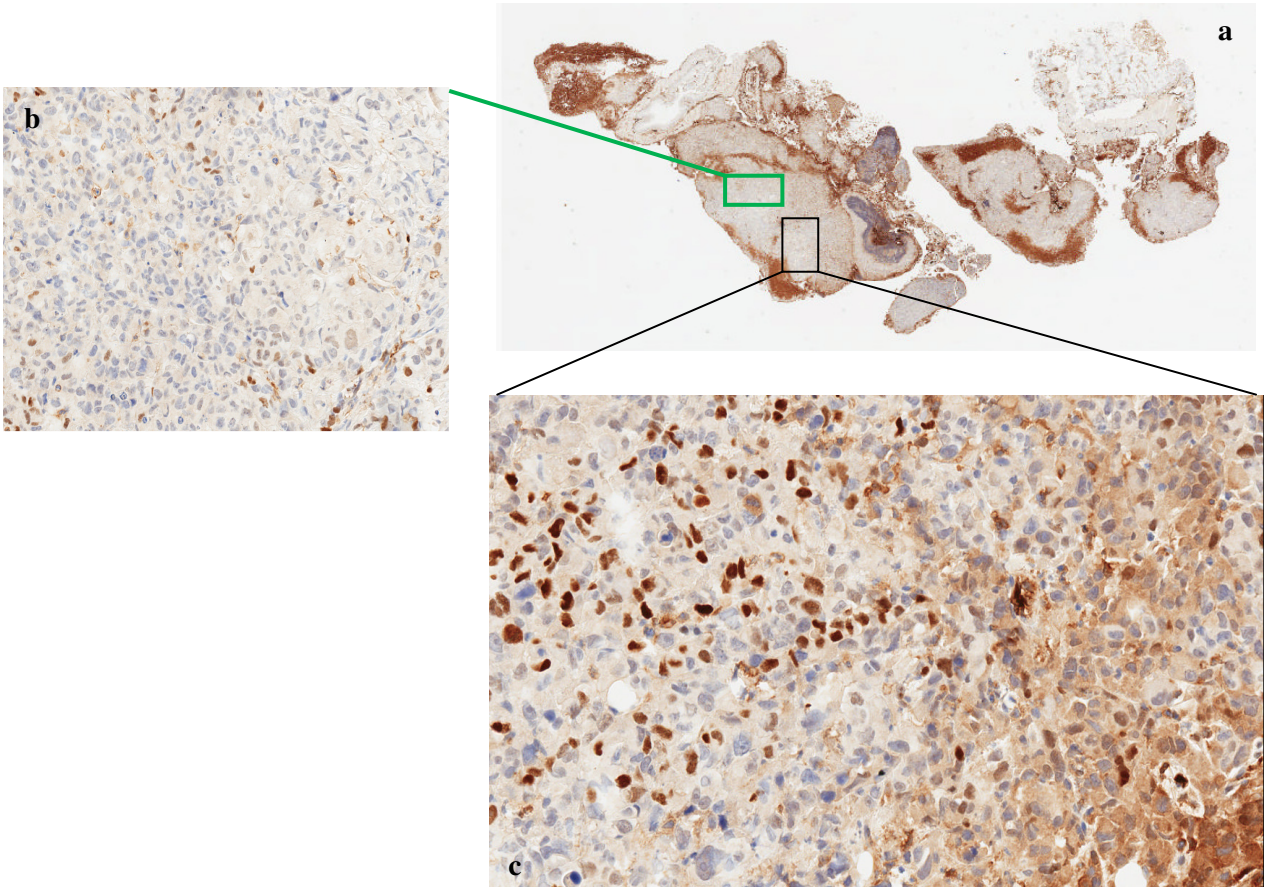

Figure 30. *EMT markers expression in putative metastasis derived from spheres-growing Panc-1 cell. All acquisition were performed at Aperio 20 X. Arrows in section for Twist staining (point 4) reports an example of necrotic area, that appears strongly colored because of aspecific DAB accumulation. Points 5(b) and 5(c) indicate differences in Slug expression in the same section.*

Immunostaining for EMT markers shows that E-Cadherin was not expressed in secondary masses found in the intestine. Vimentin displays a strong positivity such as S100A4 especially localizing in the cytoplasm (more than 50% cells are positive), where the staining was more intense. Similarly to what happens in primary orthotopic tumor, from which these masses may derive, both Twist and Slug are expressed in an irregular way, both in nuclei and in cytoplasm, in a non homogeneous way, but closed to necrotic regions (with regard to Twist, in the pictures necrotic areas are strongly colored in brown because of the aspecific DAB accumulation; positive cells are detectable closed to these areas) or rather along tumor border, but not in the center of the tumor, in the case of Slug (Fig.30).

4.6 Staining for CK7 in adherent and spheres-derived orthotopic tumors

We studied reactivity to cytokeratin 7 (CK7) in both adherent and spheres cells-derived orthotopic tumor. Cytokeratins are intermediate filament proteins present in epithelial cells. They are expressed in a tissue-specific manner in normal organs and the tumors that arise from them. Monoclonal antibodies have been established against several of the cytokeratin polypeptides and are used to evaluate the pattern of cytokeratin expression in cells of epithelial origin. CK7 is as marker that indicates the grade of differentiation of a tissue. In Panc-1 adherent-derived orthotopic tumors, CK7 expression is characterized by patterns with variable degrees of cytoplasmatic staining (Fig. 31).

Adherent-derived orthotopic tumor

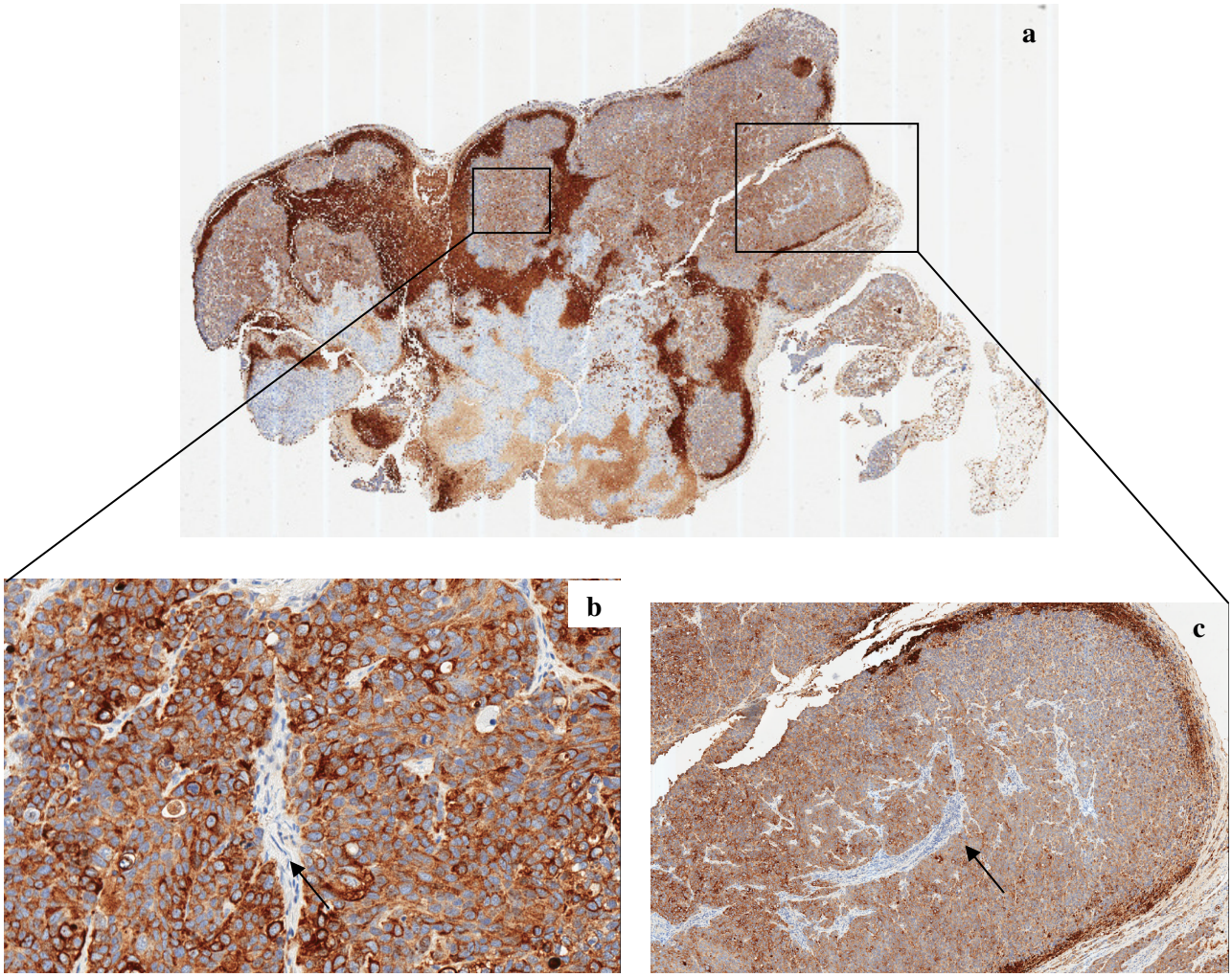

Figure 31. *(a), Expression of CK7 in Panc-1 adherent-derived orthotopic tumor. Staining for CK7 is more intense only in a part of the tumor, whereas the others are completely negative. CK7 expression is characterized by patterns with variable degrees of cytoplasmatic staining. Lymphocytes infiltration is strong (arrow). Acquisition at Aperio 20X (b) and 4X (c).*

The tumor mass is divided in a very clear way in areas in which staining of CK7 is positive, such as others one in which CK 7 expression is totally absent.

Infiltrating CK7-negative tumors cells are clearly detectable within CK7-positive tumor areas, creating zones in which the contrast between positivity and negativity to CK7 staining is strong (Fig. 32). Necrosis delimitate these positive and negative areas among them. Lymphoid component is strong (arrow in Fig.32,d).

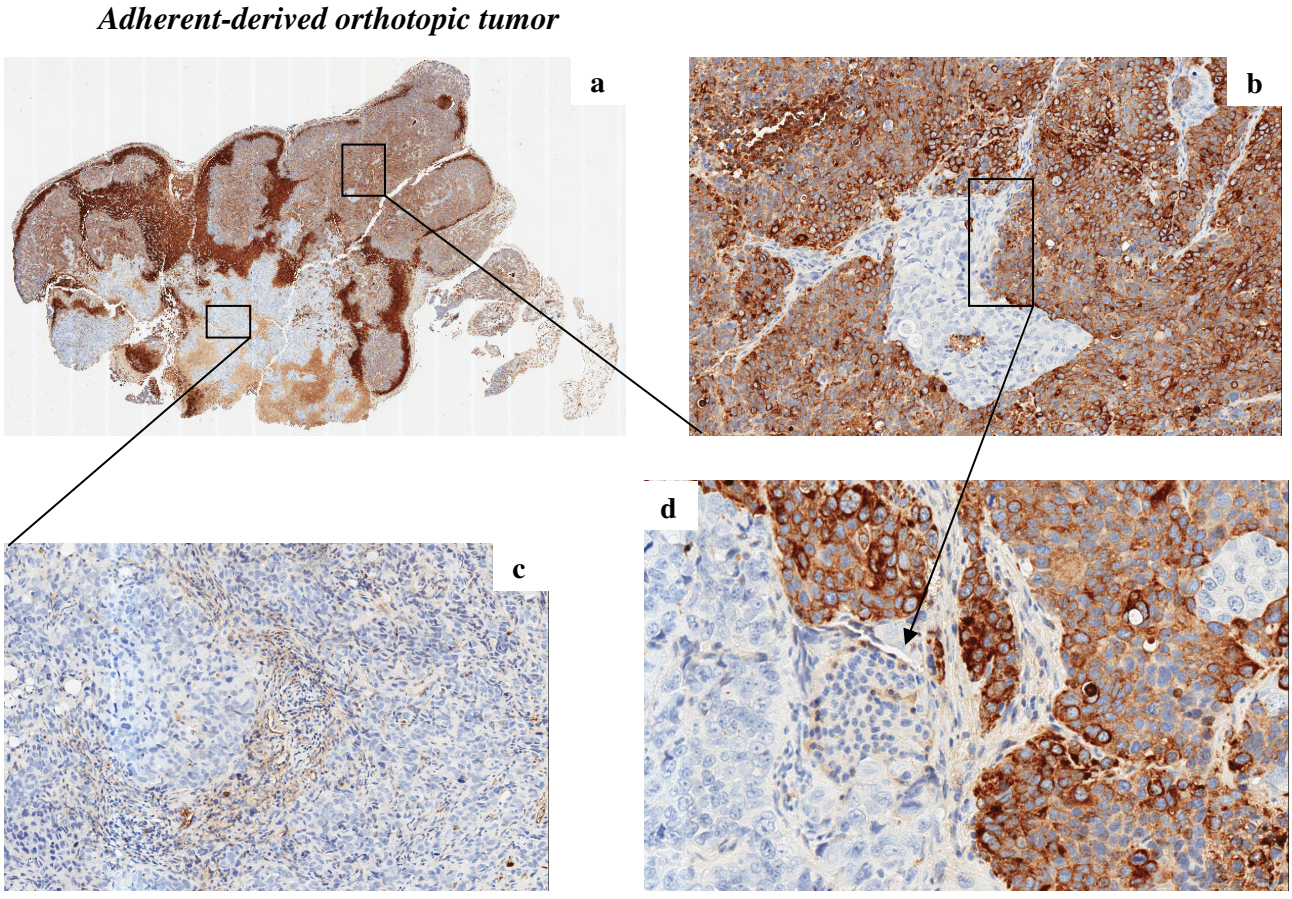

Figure 32. *Details of negative CK7 tumor area in Panc-1 adherent-derived tumor and of a small negative CK7 area in a region in which the expression of CK7 is strong.*

Immunohistochemistry for CK7 for spheres-derived orthotopic tumors displays a more homogeneous sight than that in adherent-derived tumors. A part of necrotic regions in which aspecific DAB accumulation is strong, creating a non-specific reaction, these tumors showed no CK7 expression. The organization of the tumor masses appear regular if compared with the

adherent-derived tumor; mitotic activity is stronger, as already shown previously, and also lymphoid invasion seems to be less important than in the adherent-derived tumor (Fig.33).

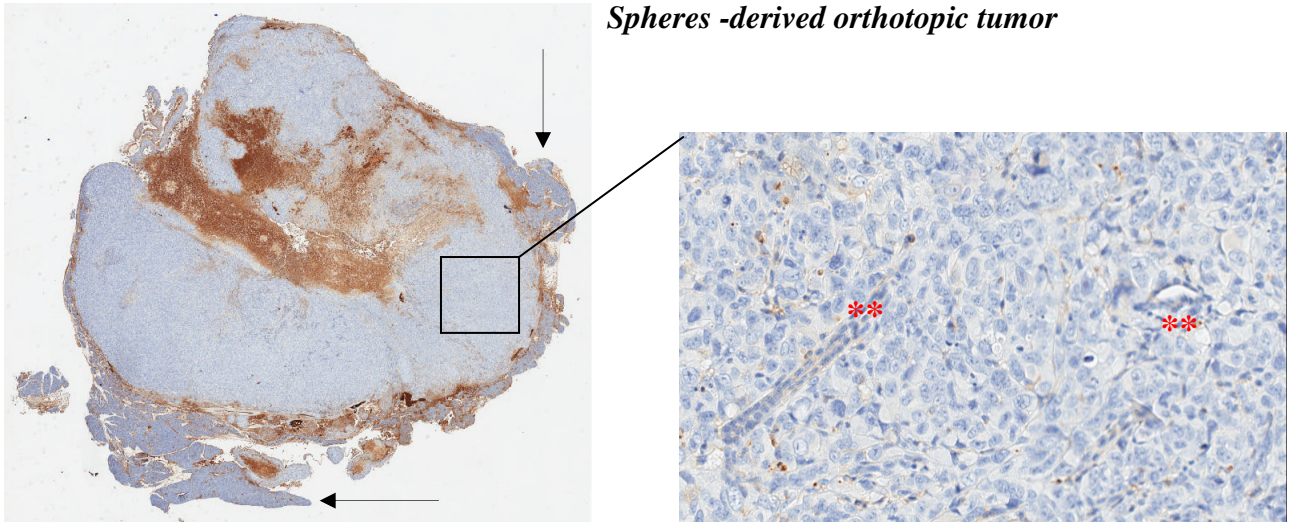

Figure 33. *Details of negative CK7 area in Panc-1 spheres-derived tumor. Red asterisks indicate residual pancreatic ducts within the tumor mass. Arrows show residual normal murine pancreas.*

4.7 Ki67 labeling index

The proliferation index of both adherent cell and sphere-derived orthotopic tumors was determined by Ki67 immunostaining on paraffin-embedded tumor sections, as done for subcutaneous tumors. As depicted in Figure 34, sphere-derived tumors demonstrate a significantly higher proliferation rate (80% positivity) when compared to adherent cell-derived tumors (30% positivity) (Fig.34).

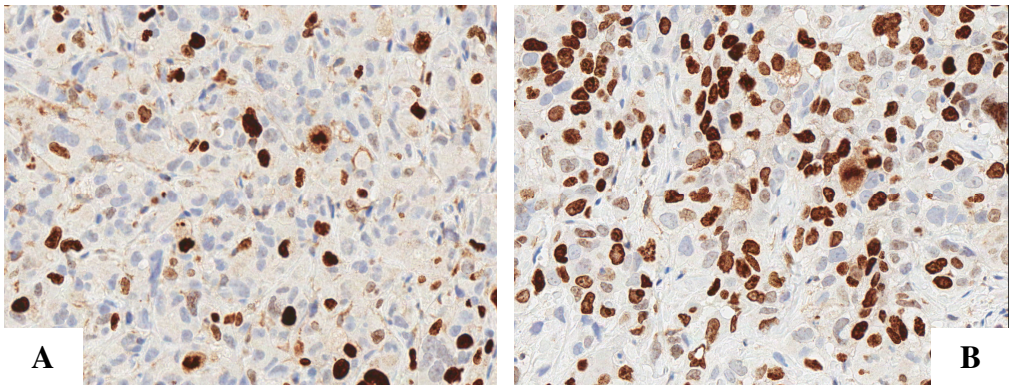

Figure 34. *Representative images of the Ki-67 staining of Tumor derived from Panc-1 adherent cells (A) and tumor from Panc-1 spheres cells (B). Images acquired at Aperio 40X.*

4.8 In vivo imaging: advantages and limits of MRI

As mentioned before in paragraph 4.3, tumors growth after orthotopic injections in mice was followed by MRI, starting from one month after surgery. This technique allowed to detect the primary tumors and to follow their growths during the time but it was not able to detect putative metastasis adhering to the surface of small intestine or to the liver, even if they were founded during necropsy (for a total of 9/10 mice injected with spheres growing cell). Actually, pancreas imaging in mice is particularly difficult because this organ is not a solid retroperitoneal organ like in humans and artefacts due to breathing and peristaltic movements, or the presence of gas into the intestines, may seriously affect the image quality. On the other hand, the tail of pancreas in mice is closely adjacent to spleen and stomach, which are easily detectable in MRI, driving pancreas identification. We performed all MRI acquisition using parameters such as fat suppression filters, in order to minimize the interference of abdominal fat that is brilliant in MRI. Moreover, slices thickness was maintained fixed on 1 mm without any distance factors, so that pancreas tissue could be differentiated from other tissues. All primary tumors were well detectable for sizes no less than 2 mm; this size corresponds to a time interval from the surgery no shorter than one month from orthotopic injection. For this reason, earlier tumor development can't be followed in our orthotopic models by MRI. At the same time, putative metastasis we found in small intestine and adhere on the liver surface of 9 mice injected with spheres; however, because of their small sizes and their location in the abdomen, they have been never individuated by MRI (Fig. 21; Fig. 35-36).

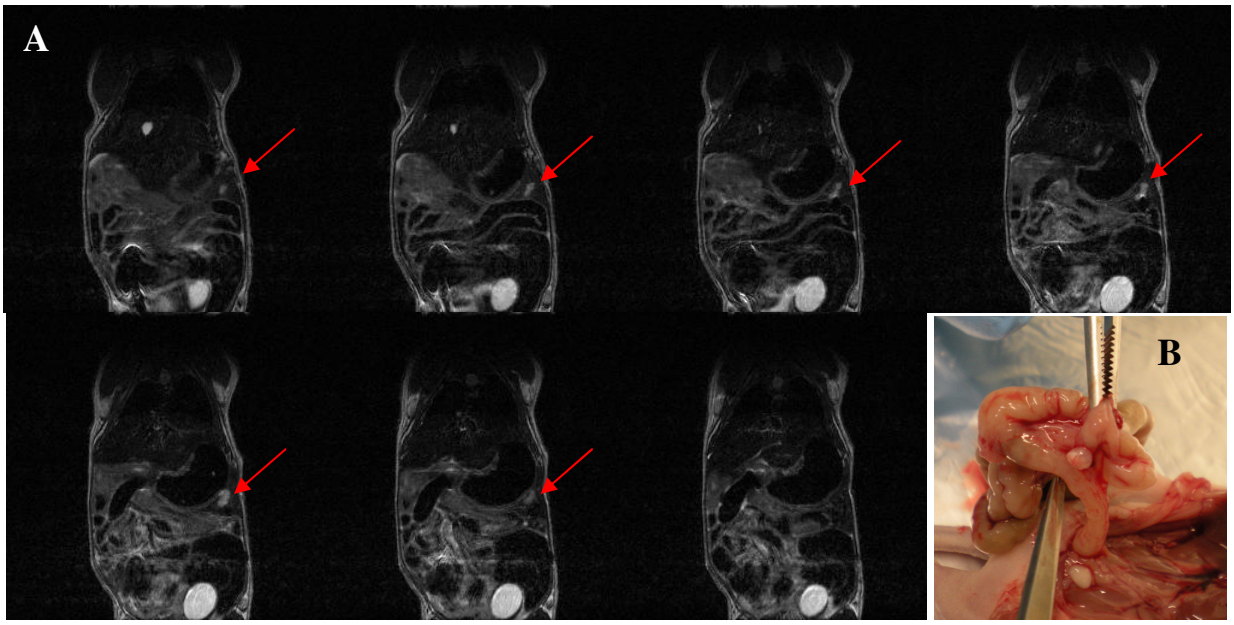

Figure 35. *MRI T1-weight of a orthotopic mouse model 30 days after injected with spheres growing cells; arrows indicate primary tumors. Picture (B): Putative metastasis in small intestine have been not identified in MRI sequence (Panel A).*

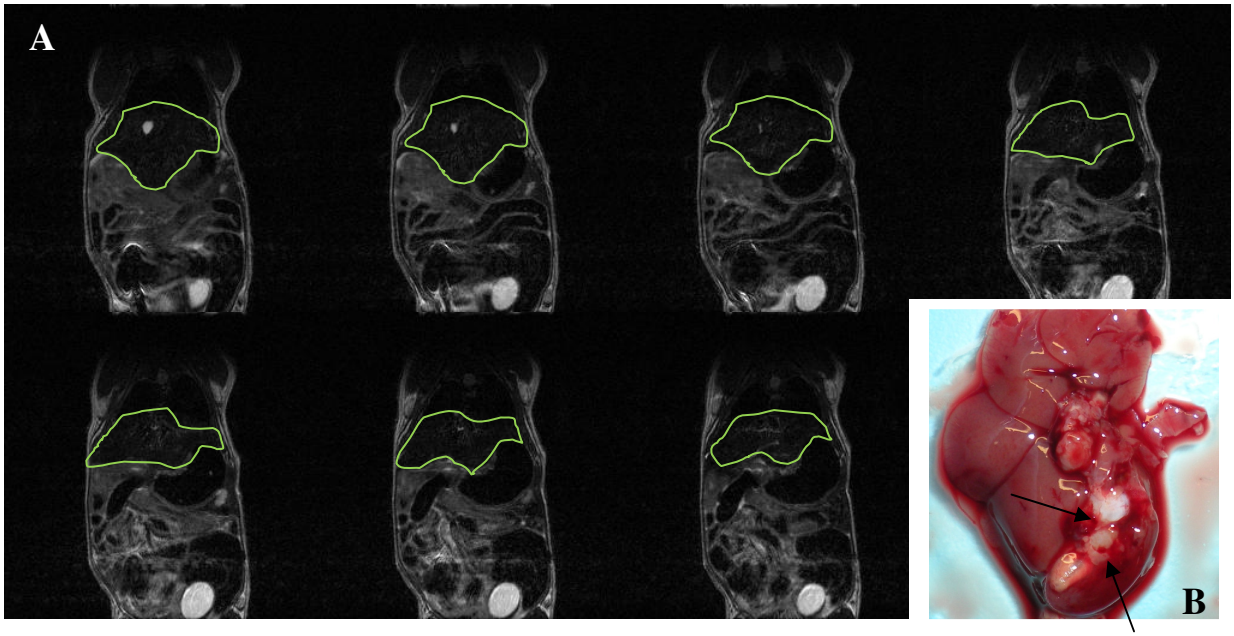

Figure 36. *MRI T1-weight of a orthotopic mouse model 30 days after injected with spheres growing cells; liver is highlighted in green. Picture (B): Putative metastasis in liver have been not identified in MRI sequence (Panel A).*

MRI is necessary to identify the anatomical location of primary tumors, to follow growths and to measure sizes showing at the same time the shape of the developed mass. It's a crucial technique in small-animal imaging but is not sufficient, if used alone, for detection of small masses above all in difficult anatomical region such as abdomen cavity.

4.9 Bioluminescence Imaging for the detection of small masses.

Since MRI resulted useful but not sufficient for the follow up of the tumor development in our orthotopic models, we decided to focus the attention on a combined imaging system in order to individualize positively both primary tumors and putative metastasis. We chose to study the complementary roles of MRI, Bioluminescence imaging and Micro-US performing new orthotopic injections using Panc-1 cells transfected with the reporter gene Luciferase (Panc-1-Luc+ cells). The latter were injected in the pancreas of twenty-three nude female mice according to the protocol described in section 3.3. Animals were divided in two groups: thirteen were inoculated with $5*10^6$ Panc-1-Luc+ cells (Group one) and the other ten with $2*10^6$ Panc-1-Luc+ cells (Group two). Cells were suspended in 60 µl in PBS containing 1% serum-free Matrigel (vol/vol). The negative control group was constituted by five mice which received only Matrigel (60 µl). Five mice belonging to the Group one received cells suspended in RMPI serum-free instead of sterile PBS because we also wanted to evaluate the effect in term of tumor size progression of colture medium respect to PBS.

Before performing orthotopic injections using Panc-1-Luc+ cells, we tested *in vitro* their bioluminescence activity in presence of the substrate Luciferin. Since bioluminescence test *in vitro* had to be performed screening cells in their flask, in order to avoid interferences with the cell signals, emissions by flask plastic was analyze alone. Flasks used for cells cultures didn't show auto-bioluminescence proprieties; moreover, Panc-1-Luc+ cells showed a strong bioluminescence activity (Fig. 37).

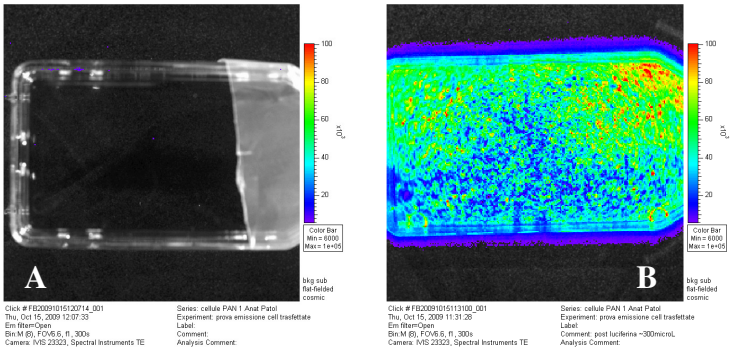

Figure 37. *Panc-1-Luc+ cells Bioluminescence test activity in vitro: Flask plastic doesn't emit light (A), so positivity shows in B is due to activity of firefly Luciferase (Luc) present in Panc-1 transfected cells.*

Before beginning, we decided to inoculated $2*10^6$ Panc-1-Luc+ cells in the flank of five nude mice in order to control their capability to grow *in vivo* and evaluated the emission of photons thought overlying tissue. Bioluminescence emission from tumors grown in the subcutaneous models were high and ground noise was very low (Fig. 38).

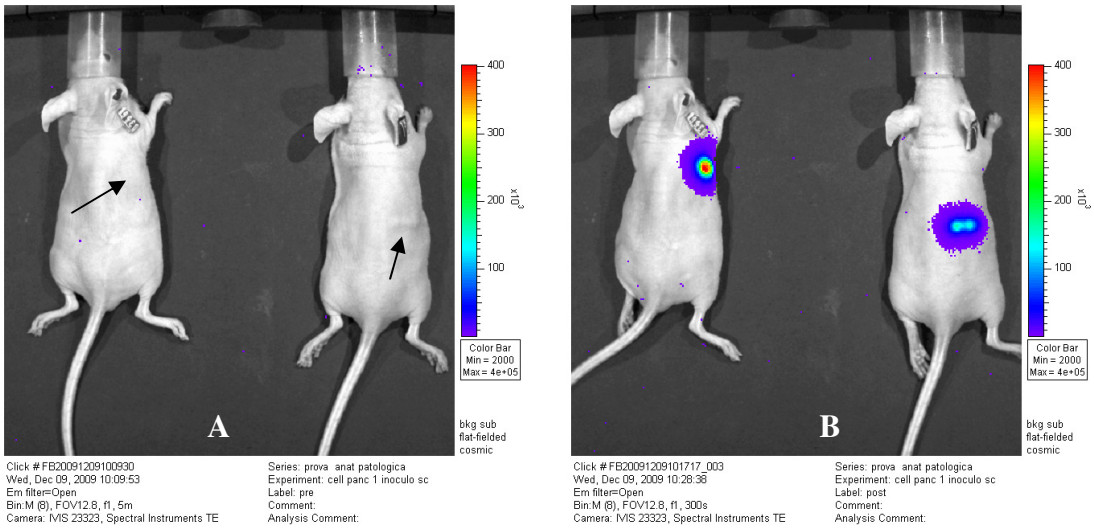

Figure 38. *Subcutaneous injection of Panc-1-Luc+ cells. In picture (A), subcutaneous mice model before Luciferin injection (acquisition "pre"); in (B), light emission from subcutaneous tumors (acquisition "post"). Arrows indicate subcutaneous tumors.*

For all animals, we measured the Region of interest (ROI) which corresponds to measures the signal intensity in a specified area of the Optical image. In that way, it is possible to estimate total photon flux from the point source coming from the selected area. We calculate for each mouse two ROIs: one comprised whole abdominal area (ROI 1, the bigger one) and one drew also around light emission corresponding to the primary tumor (ROI 2, the smaller one). In this way, we obtained, from time to time, information about the total emission in that mouse, due to primary tumor alone or in association with eventual supplementary masses, and information about the specific contribution to developing primary tumor in the total intensity of the emission signal (Fig. 39).
Using a small selected ROI within the total abdominal area (smaller ROI), we made a correlation of whole tumors bioluminescence imaging and MRI for assessment of tumor size in mice.

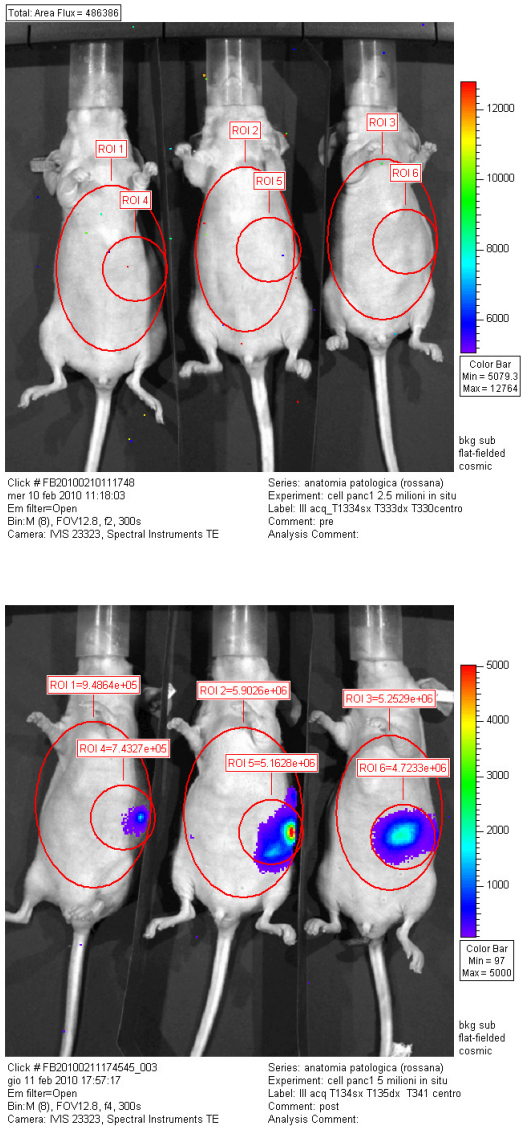

Figure 39. *Two examples of selected ROI in an acquisition before (up) and after (down) the Luciferin injection, both in whole abdominal region and in the site of tumor growth.*

4.10 Correlation of MRI, Ultrasound and Optical Imaging for monitoring tumor growth over time

➢ *4.10.1 First time-point, 30 days after surgery*

When Panc-1-Luc+ orthotopic injections were performed in each animal according the scheme described before, we decided to investigate tumors development and growth using MRI, Bioluminescence imaging and Ultrasound (US) fixing the first control 30 days after surgery. Then, we chose to repeat acquisitions for all mice every 30 days for no less than two times, up to animals showed good health. Imaging analysis were performed in a time-frame of three days for each time-point in order to minimize differences in measured sizes and avoid to administer high doses of anesthetics at the same time.

Findings obtained from the first *in vivo* imaging acquisitions one month after surgery showed clearly that US failed to visualize tumors which were too much smaller to be detect by our US probe (data not shown). Also Micro-MRI and Bioluminescence failed in the detection of such small masses whereas those larger were identified. At the first time-point acquisition, MRI detected 9/13 mice belonging to the Group one, whereas only 1/10 mice of the Group two showed a measurable mass. Bioluminescence imaging resulted more accurate at the same time point: all mice (13/13) belonging to the first group had good light emissions, even if different to each other for intensity. Moreover, in three of them, apart from light emission by primary tumors developed within the pancreas, small light sources were detected in anatomical areas different from the pancreas itself. In the case of mice from the Group two, Optical imaging obtained positive sources from 5/10 mice (1:2), but in this case no little supplementary light emissions were found except to those derived from primary tumors (Fig. 40- 41- 42).

Picture 40 (B) shows two mice belonging to the Group two represented in a sequence acquired during the same session: picture numbers 1, 2 and 3 concern to the three time-frames in which the acquisition is divided (0-5; 5-10; 10-15 minutes). Luciferin reaches its emission peak until 15 minutes after its injection, then the last time-frame corresponds to the maximum in the Luciferin emission spectrum.

Picture 40 (A) shows two of the mice of the Group one. Firstly, having received a high number of cells, it's evident that signals are stronger by comparison with the previous one. Moreover, in line with the Luciferin emission spectrum trend, it's possible to appreciate an increase of spot intensities with the passing of time, especially in mouse on the right. The reverse rainbow color table in both images assigns violet to the lowest number on the array and red to the highest number, and convert

numerical contents of scientific image data (photon flux) into luminescent images acquired with an IVIS Imaging System. Pseudo-color associated-scale of values is increased considerably in mice of group one (B).

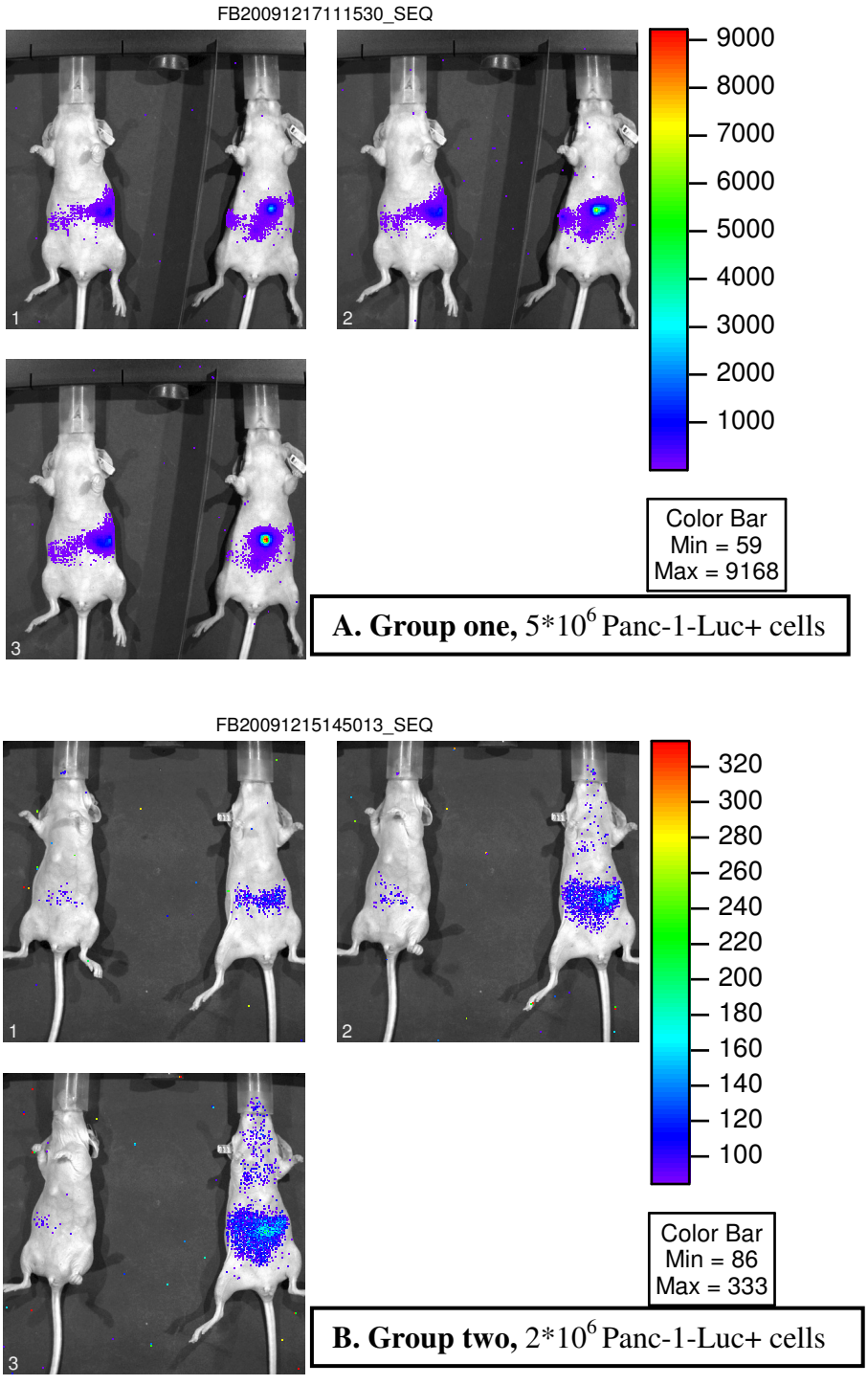

Figure 40. *In picture (A), two mice belonging to Group one; tumors show bright signals already at the first time-point. In (B), no tumor was detected in mouse on the left at the first time-point acquisition, one month after surgery. On contrary, the other one show a good emission.*

Figure 41 and 42 show that there is a correlation between MRI and Optical imaging for the detection of primary tumors. One mouse doesn't show light emission both in MRI and in Optical imaging (Fig 42 B).

A. Group one, $5*10^6$ Panc-1-Luc+ cells

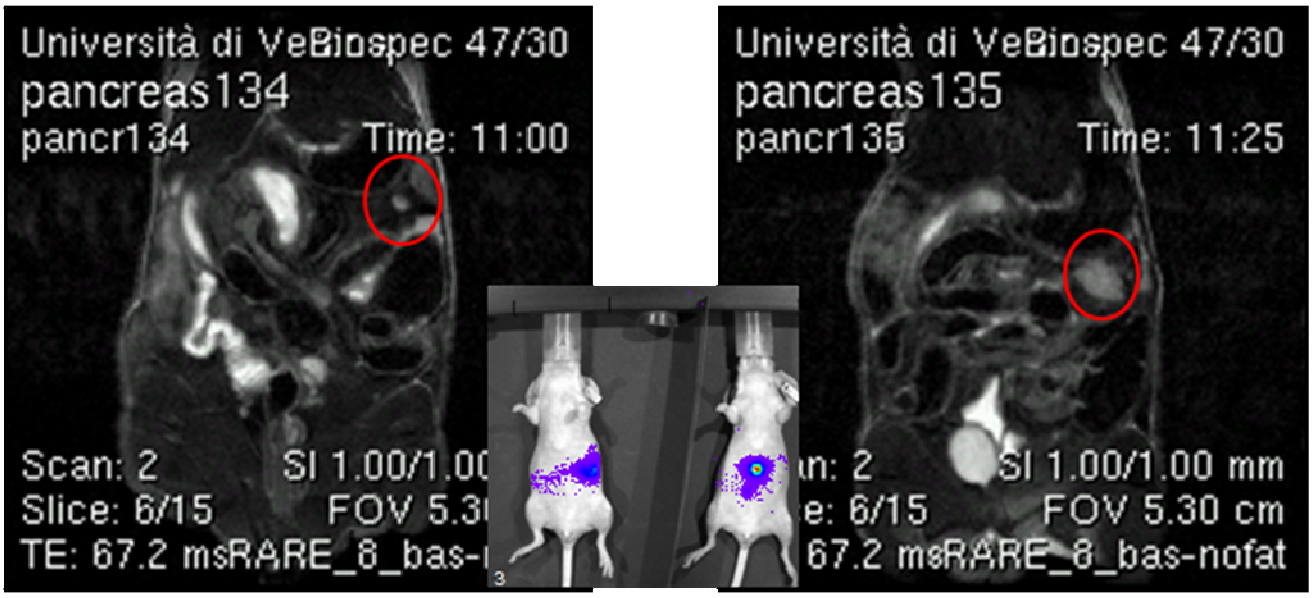

Figure 41. *Two mice belonging to group one; smaller optical imaging picture in the center refers to picture 3 of Figure 40, (A). In both cases, MRI identified the two tumor masses (red rings).*

B. Group two, $2*10^6$ Panc-1-Luc+ cells

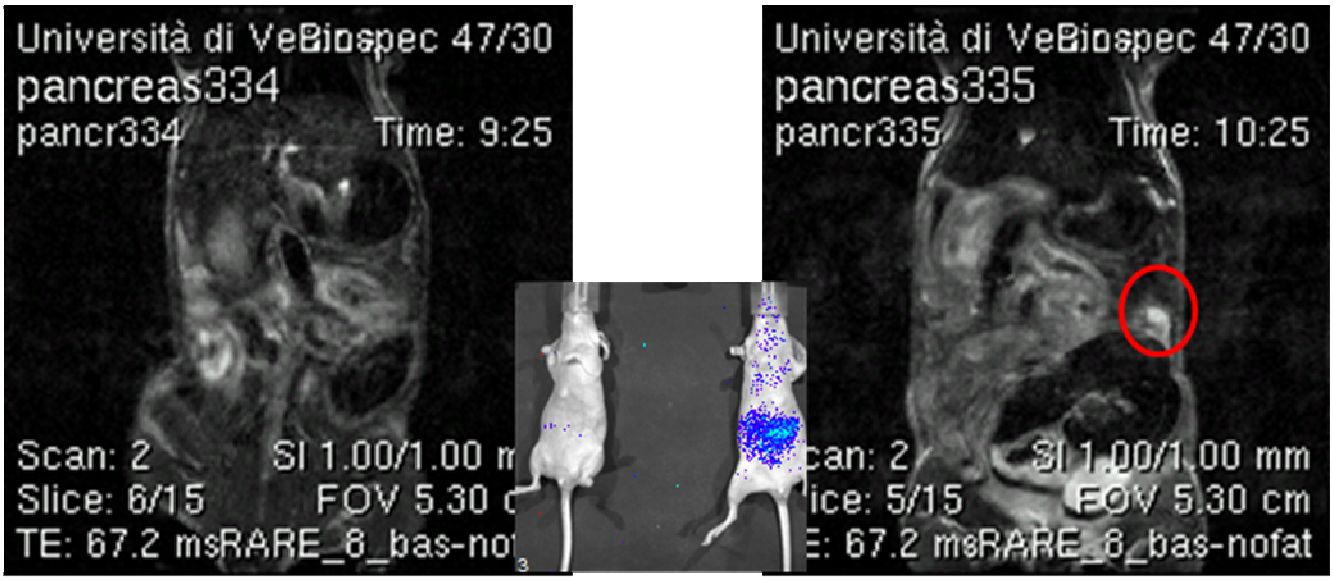

Figure 42. *Two mice belonging to group two; smaller optical imaging picture in the center refers to picture 3 of Figure 40, (B). Only in mouse on the left, MRI identified the tumor masses (red ring).*

- ***4.10.2 Second time-point, 60 days after surgery***

We firstly evaluated the tumors growth in Optical imaging and MRI, with attention to avoid to administer in the same day both anesthetics to the same animal. Increase in size of tumors was clearly visible in MRI, so that we decided to perform also acquisition with US at this time-point. MRI detected 12/13 mice of the Group one at this time-point, three mice in addition respect to previously acquisitions. In Optical imaging acquisitions, we obtained very good emissions from each mouse of the same group (13/13); moreover, supplementary light emissions probably corresponding to smaller tumor masses were detected in three mice, confirming what seen in the first acquisition session. An increase of detected masses was also seen in mice belonging to the Group two: MRI individualized 6/10 tumors, whereas Optical imaging was 8/10 (three in addition respect to the first time-point acquisitions), even if some of them had very low signals, without other light sources except from primary tumor. Once again, in this group, only one animal showed no detectable photons emission in Optical imaging and corresponded to one of the mice of group two never seen before in RMI (Fig. 43B and 45).

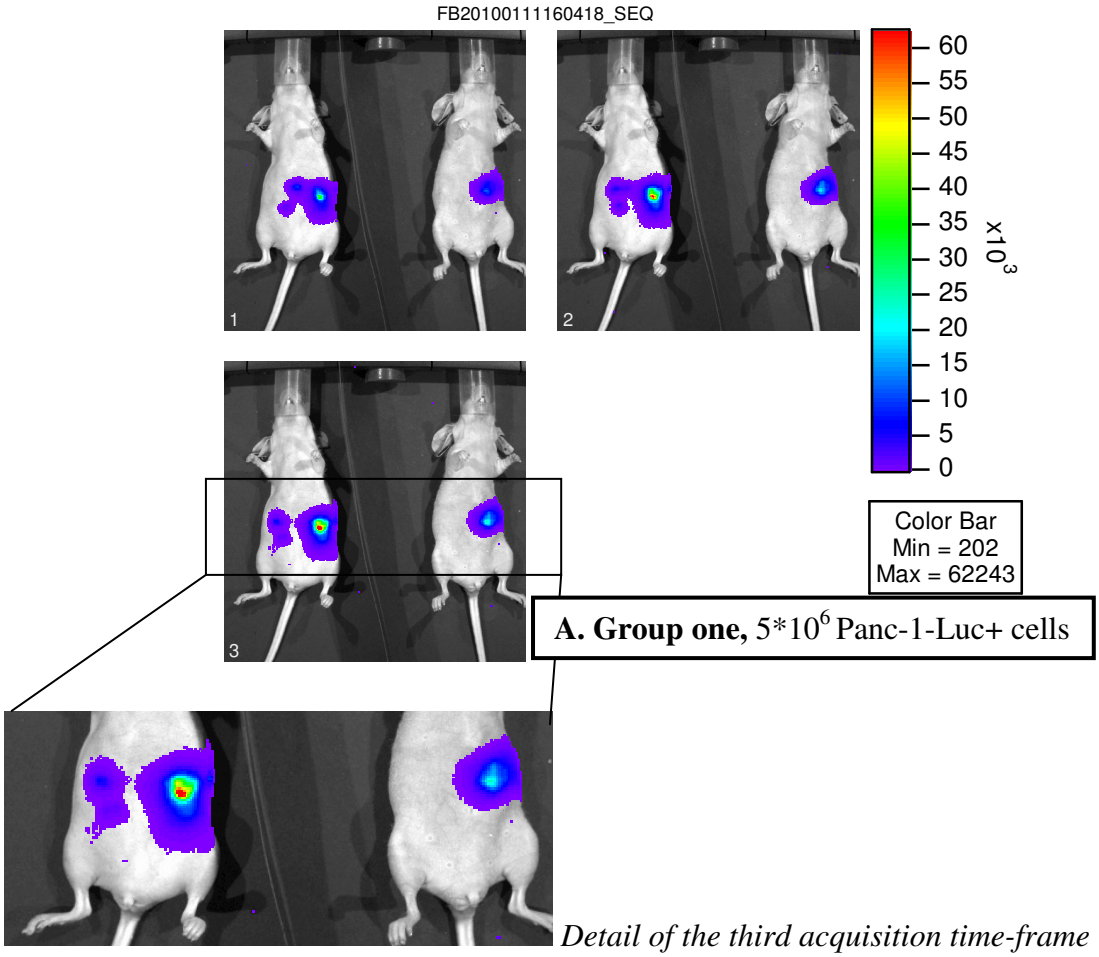

Detail of the third acquisition time-frame

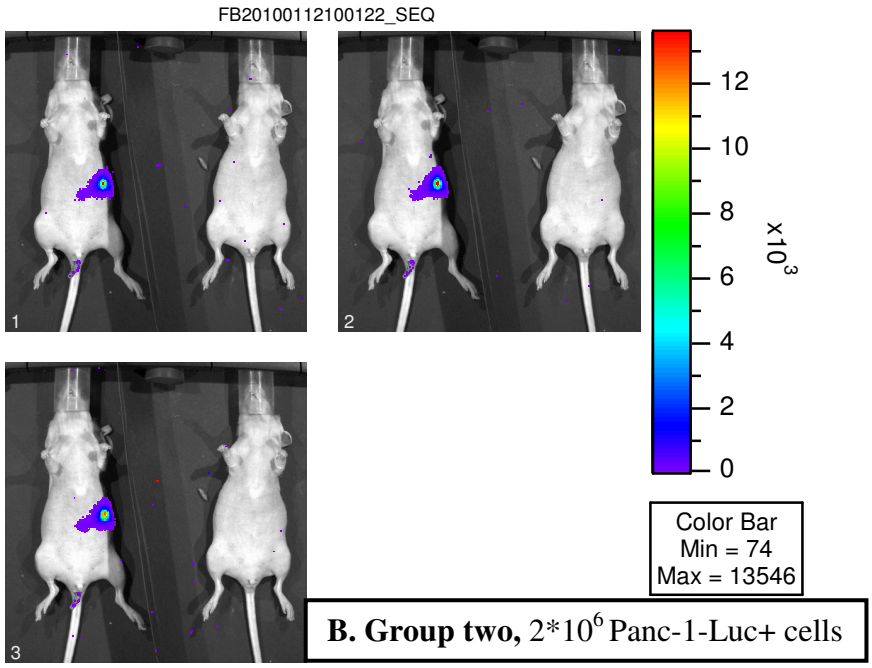

Figure 43. *In picture (A), mice of group one; tumors show very bright signals at the second time-point. A supplementary light emission appears in mouse on the left. In (B), no tumor was detected in mouse on the right, as well in Imaging performed 30 days after surgery. On contrary, the other one shows a good emission.*

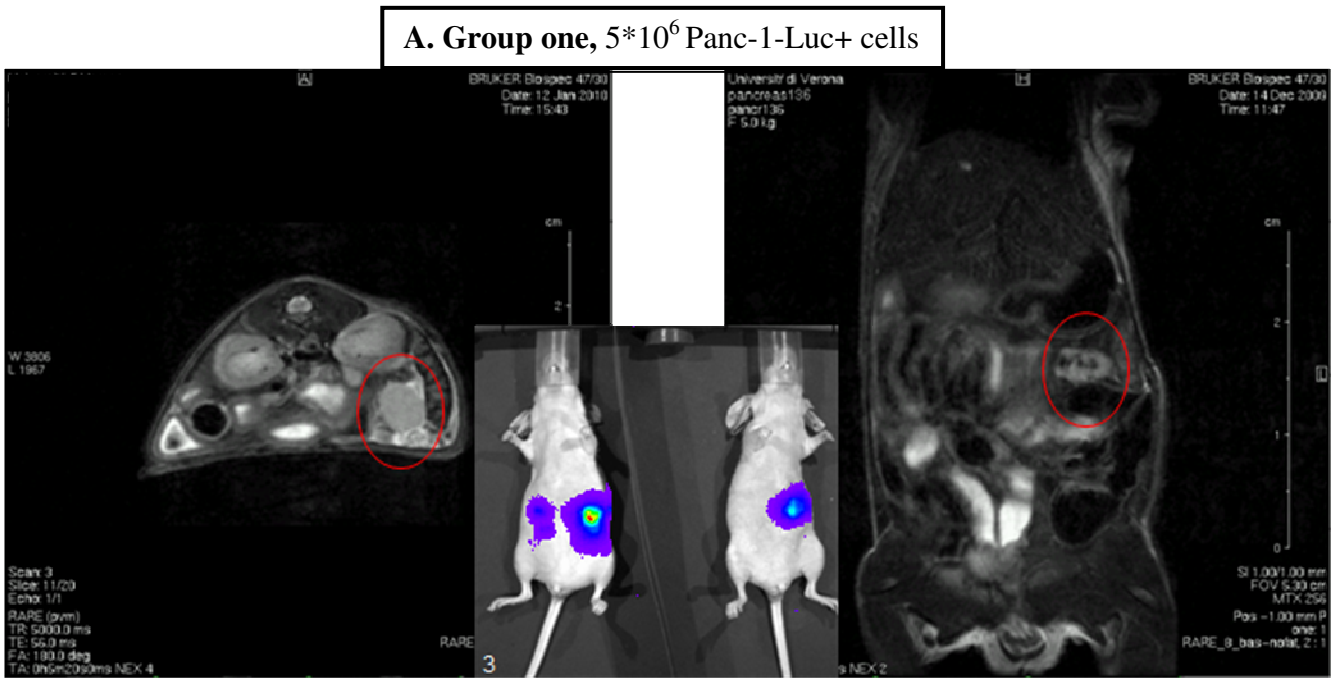

Figure 44. *Two mice belonging to group one; smaller optical imaging picture in the center refers to picture 3 of Figure 43, (A). In both cases, MRI identified the two tumor masses which were bigger than the one identified in the first time-point (red rings).*

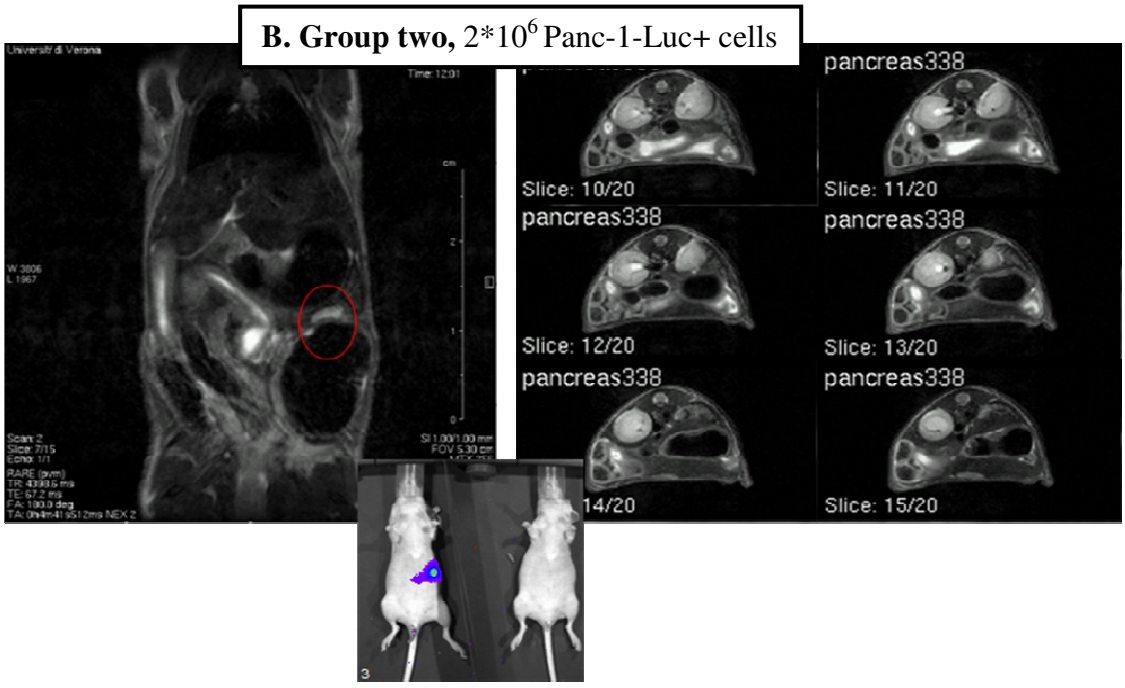

Figure 45. *Two mice belonging to group two; smaller optical imaging picture in the center refers to picture 3 of Figure 43B. MRI identified the tumor masses in mouse on the left (red ring). No tumor was detected, for the second time, in mouse on the left (the same one than in Figures 38 and 41).*

Ultrasound acquisitions were performed without anesthetized mice. Since tumors began to be sizable in MRI, we expected to can see them also in US. Even if quickly and very convenient, detection of tumors was complicate by presence of gas in the intestine of mice. 10/13 tumors in mice belonging to the first group were individuated, and only 4/10 tumors in mice of the Group two were clearly visualized in US (Fig. 46).

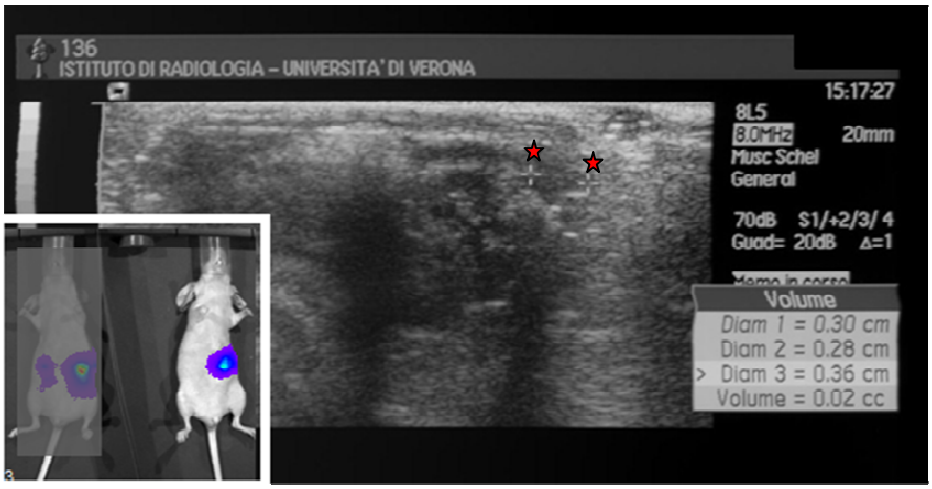

Figure 46. *US images of the mouse already shown in Fig.ure 42A, on the right. Tumor mass is located between the two stars.*

➢ ***A particular case in Group two***

As described before, MRI individualized 6/10 tumors from Group two, whereas Optical imaging was 8/10. However, one of two "negative" mice corresponded to a mouse that showed light emission at the first time-point. This particular case observed during the second acquisition of Optical imaging is described below in details. Summarizing, in this mouse we didn't find visible masses in MRI at the first imaging session, but a good light emission was detected in Optical imaging at the same time (Fig. 47). The situation was reversed during the second imaging acquisition: in fact, MRI and US indicated the presence of a tumor mass, even if small, but photons emission, already seen 30 days before, disappeared (Fig. 48).

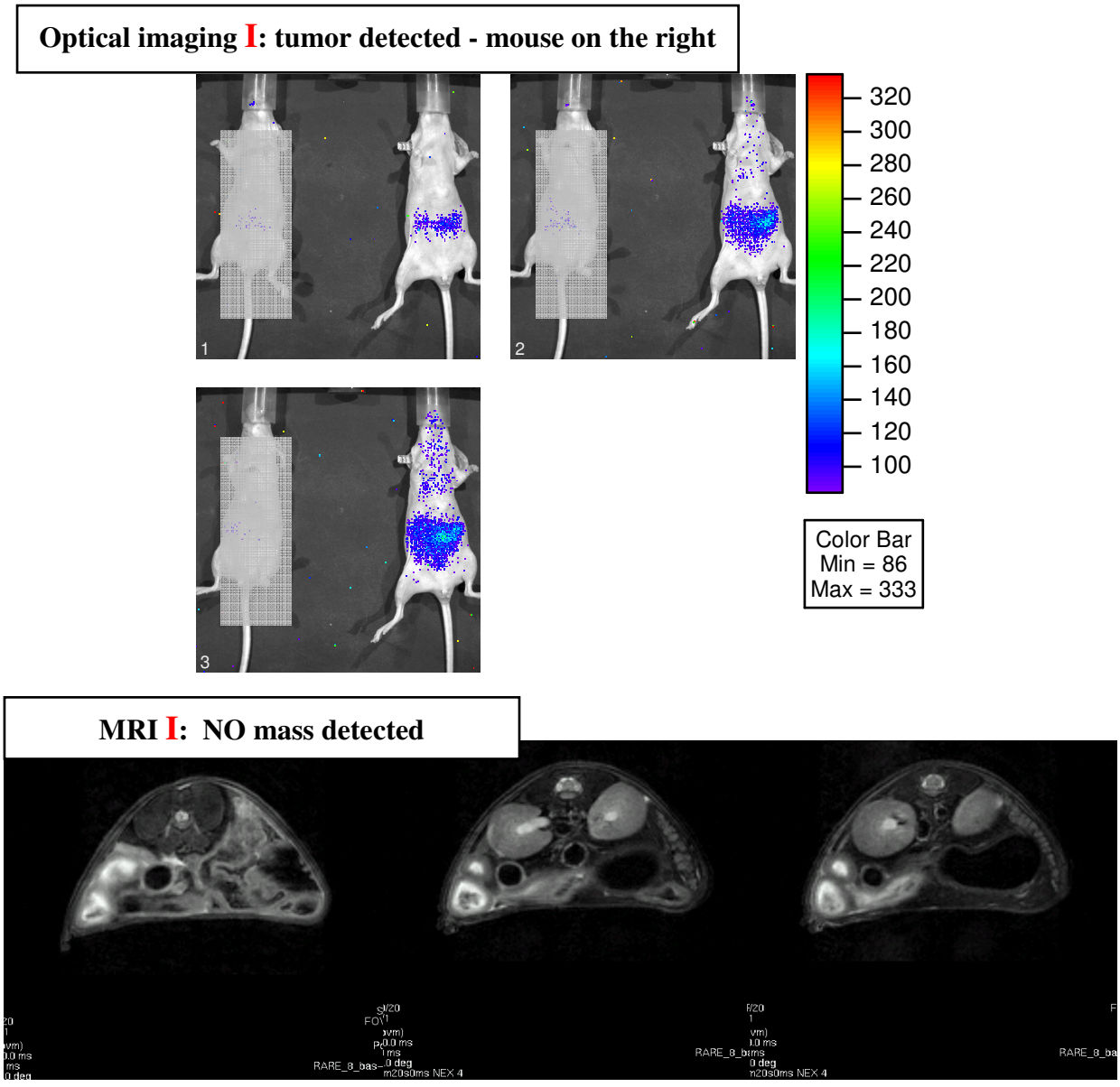

Figure 47. *Optical imaging and MRI, acquisition at time point one, 30 days after surgery: only Optical imaging detected tumor mass.*

Optical imaging II: NO tumor detected - mouse on the right

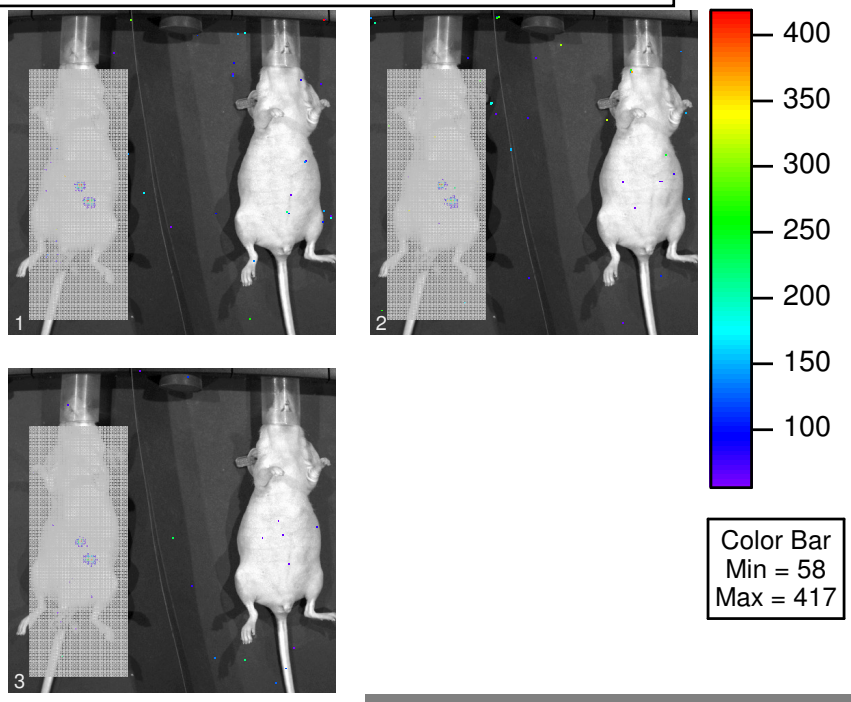

US II: tumor mass was detected

MRI II: tumor mass was detected

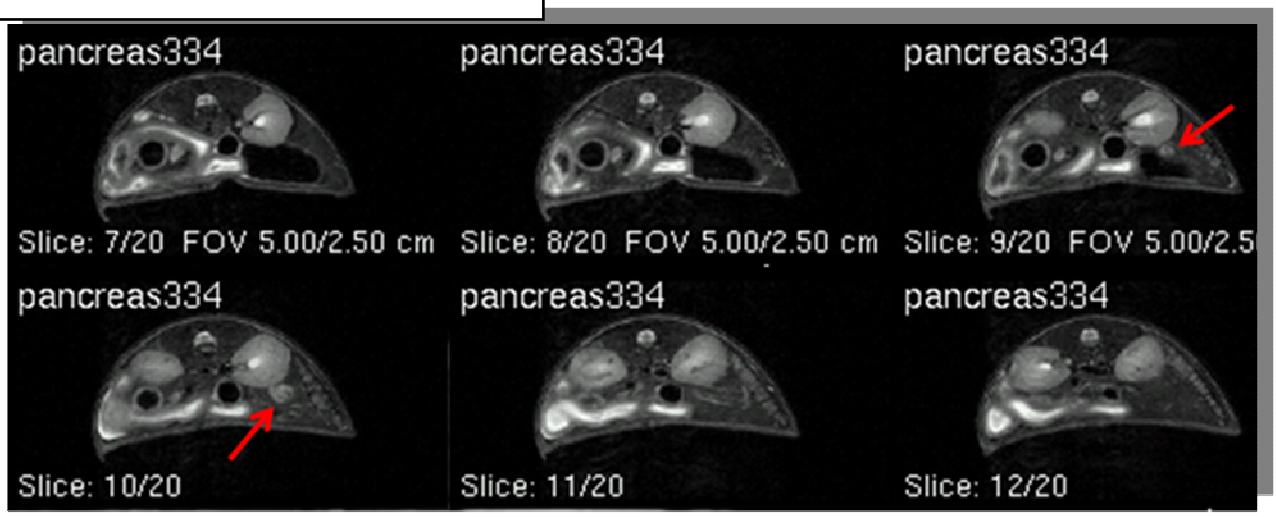

Figure 48. *Optical imaging , US and MRI, acquisition at time point two, 60 days after surgery: only MRI and US detected tumor mass.*

Knowing differences in sensibility between Optical imaging and MRI respect to the detection of small masses, findings resulting from the second time-point appeared immediately strange; in fact, since we had already seen emission light in the first session, we expected certainly to detect bioluminescence signals in the second optical imaging session too, and perhaps, in MRI, but not the contrary. In order to better understand what happened about this animal, we decided to repeat bioluminescence acquisition the day after, avoiding in this way to administer double dose of anesthetic during the same day. Luciferin is not toxic, so repeated administrations in short time don't make negative effects on the animal.

Figure 49 shows findings we obtained thanks to the repetition of optical imaging acquisition for that mouse. Bioluminescence signal was evident now. In conclusion, the number of tumor detected by bioluminescence imaging, for the Group two, was confirmed to be 9/10 mice.

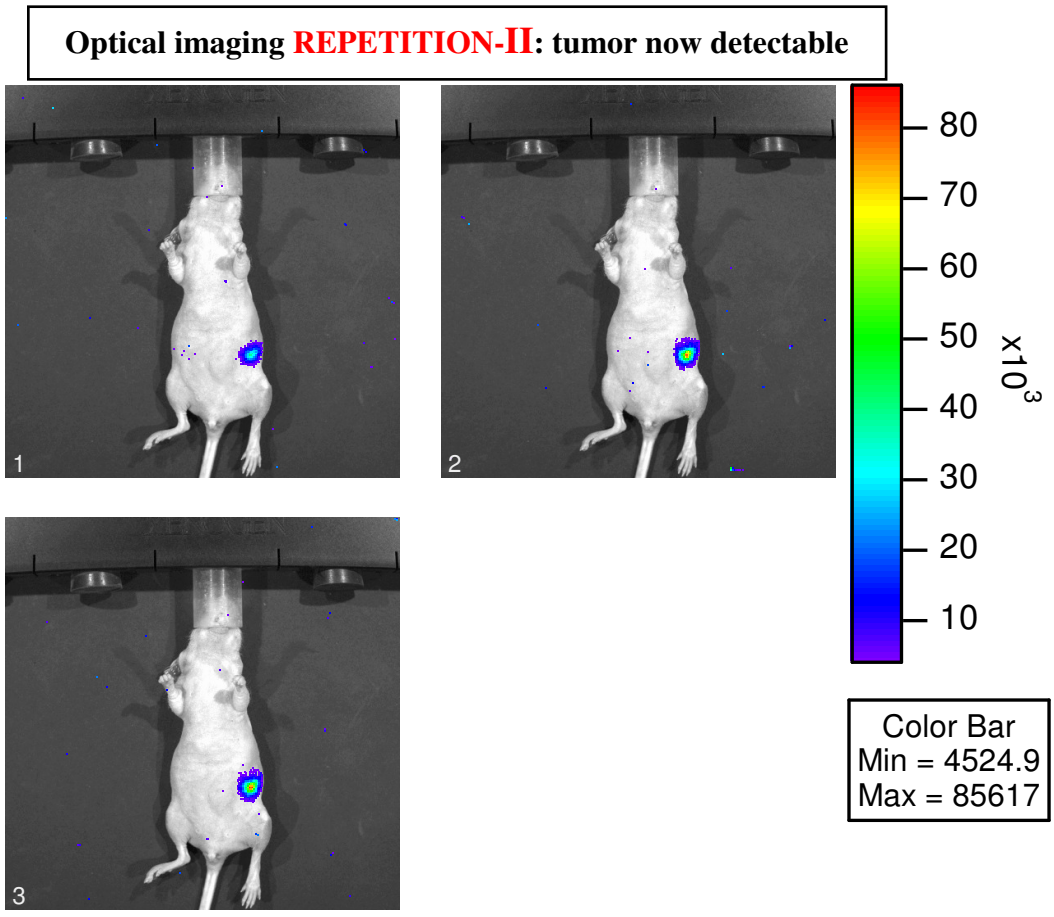

Figure 49. *Repetition of optical imaging acquisition for one mouse belonging to Group two: the tumor, already detected by MRI, is evident now.*

➢ ***4.10.3 Third time-point, 90 days after surgery and necropsies***.

Three months after orthotopic injection of Panc-1-Luc+ cells, animals were imaged by each technique for the last time because first signs of suffering occurred. Then, they were sacrificed and tumors processed for histological analysis. Tumors became very large so MRI individuated easily masses in all 13 mice belonging to group one (13/13); for the same reason, very high level of photons emission were detected during Optical imaging acquisition (Fig. 50), so much that we had to repeat some acquisitions because such images contained saturated pixels. Moreover, an increase intensity of photons flux coming from supplementary sources was observed, even if they seem to come from different anatomical region respect to what observed in the previous finding. With regard to Group two, MRI detected 7/10 tumors, only one in addition respect to the second acquisition; with the regards to Optical imaging technique, results of the second time-point were confirmed (9/10, because one mouse never showed emission light).

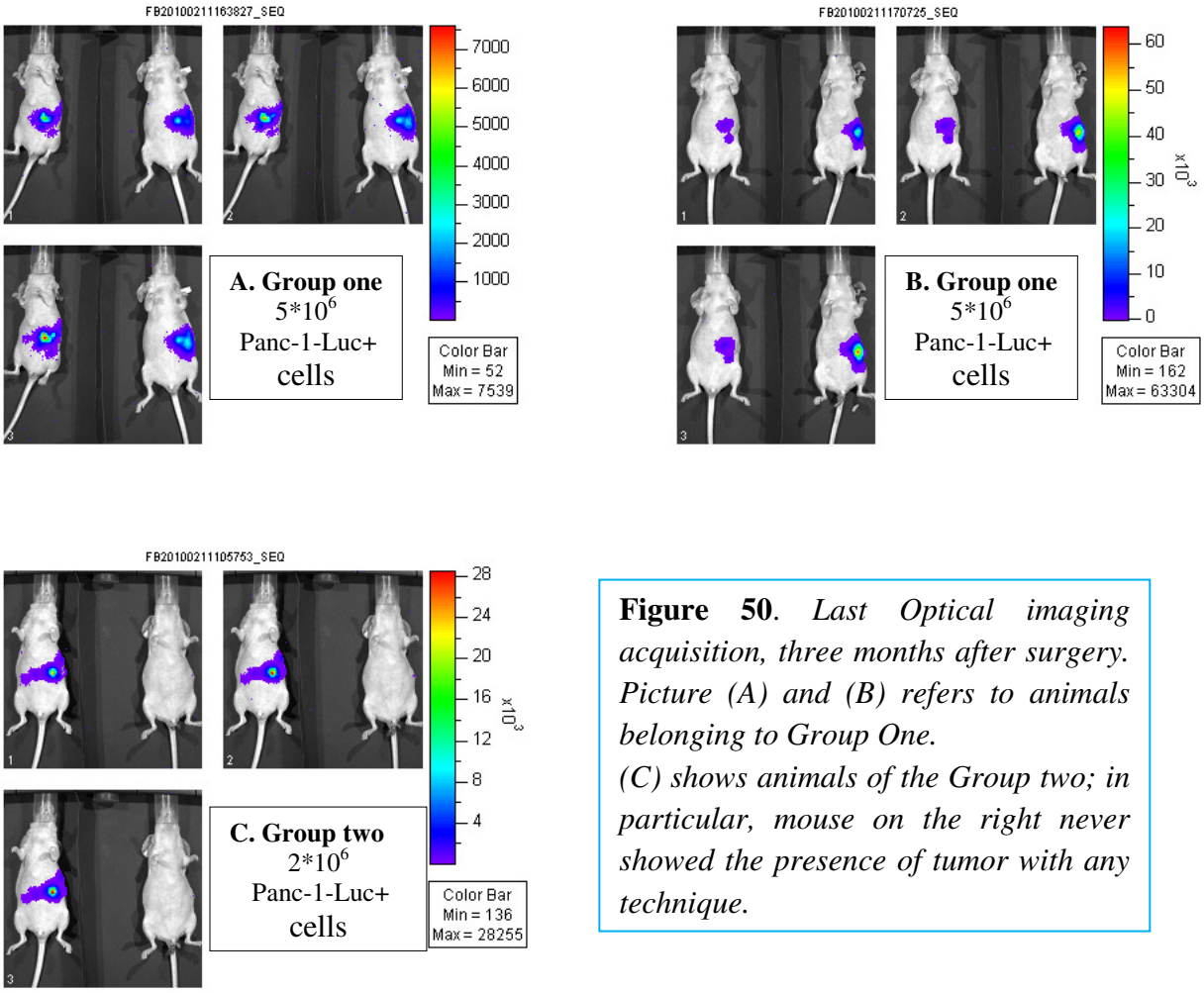

Figure 50. *Last Optical imaging acquisition, three months after surgery. Picture (A) and (B) refers to animals belonging to Group One.*
(C) shows animals of the Group two; in particular, mouse on the right never showed the presence of tumor with any technique.

Tumors in mice belonging to the Group one grew dramatically in the last month; their size and shape could be observed perfectly in the last MRI acquisitions. On the contrary, Ultrasound was not able to individualize all the tumors of the Group one (8/13), in general because of the presence of acoustic impedance in the abdominal activity and because the low frequencies of US probe produces an insufficient resolution.

Thanks to high-quality MRI images, especially of those of Group one, and to the easy application for measuring tumors, we noticed that a sub-group within the Group one existed. In fact, five animals in the group one showed tumors evidently bigger than the others (Fig. 51). They corresponded to animals which received Pan-1-Luc+ cells suspended in RPMI-serum free instead of sterile PBS. Probably, the presence of culture medium together with the Matrigel is able to assure major cell survival both before injection and once inoculated in the pancreas. Moreover, in spite of their sizes, these tumors seem not to have necrotic regions inside.

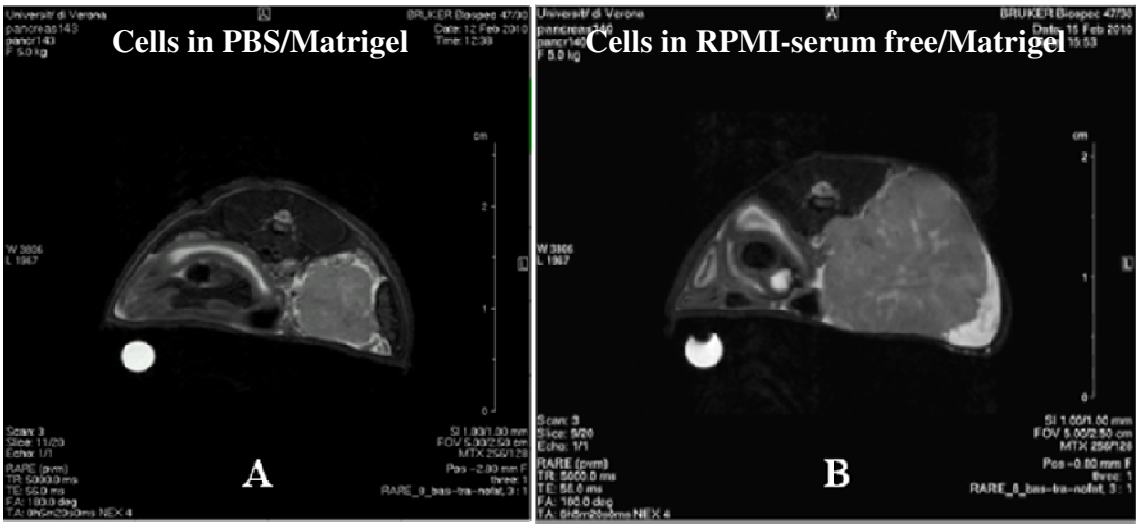

Figure 51. *Differences in sizes between tumor derived from Panc-1-Luc+ suspended in PBS (A) and suspended in RPMI serum-free (B). Images refer to last MRI few days before necropsies.*

All mice were sacrificed by cervical dislocation at the end of the last images data capture. After the first macroscopic analysis, we took tumors, spleen, residual normal pancreas, small intestine. During necropsies, we often noticed the presence of small and with projections adhering to the small intestine, so we collected also some of them. In Figure 52, we report a comparison between last acquisition of MRI, Optical imaging, US and necropsy relative to one the mice belonging to the Group one. We report also the same comparison but relative to the only mouse that never showed both bioluminescence activity and sizable masses in MRI and US. Histological analysis confirmed in this case that no tumors were present inside the pancreas, that appear normal closed to the spleen (Fig. 53); probably, in this case the problem was linked to surgery or cells survival rate, but surely not to *in vivo* imaging techniques.

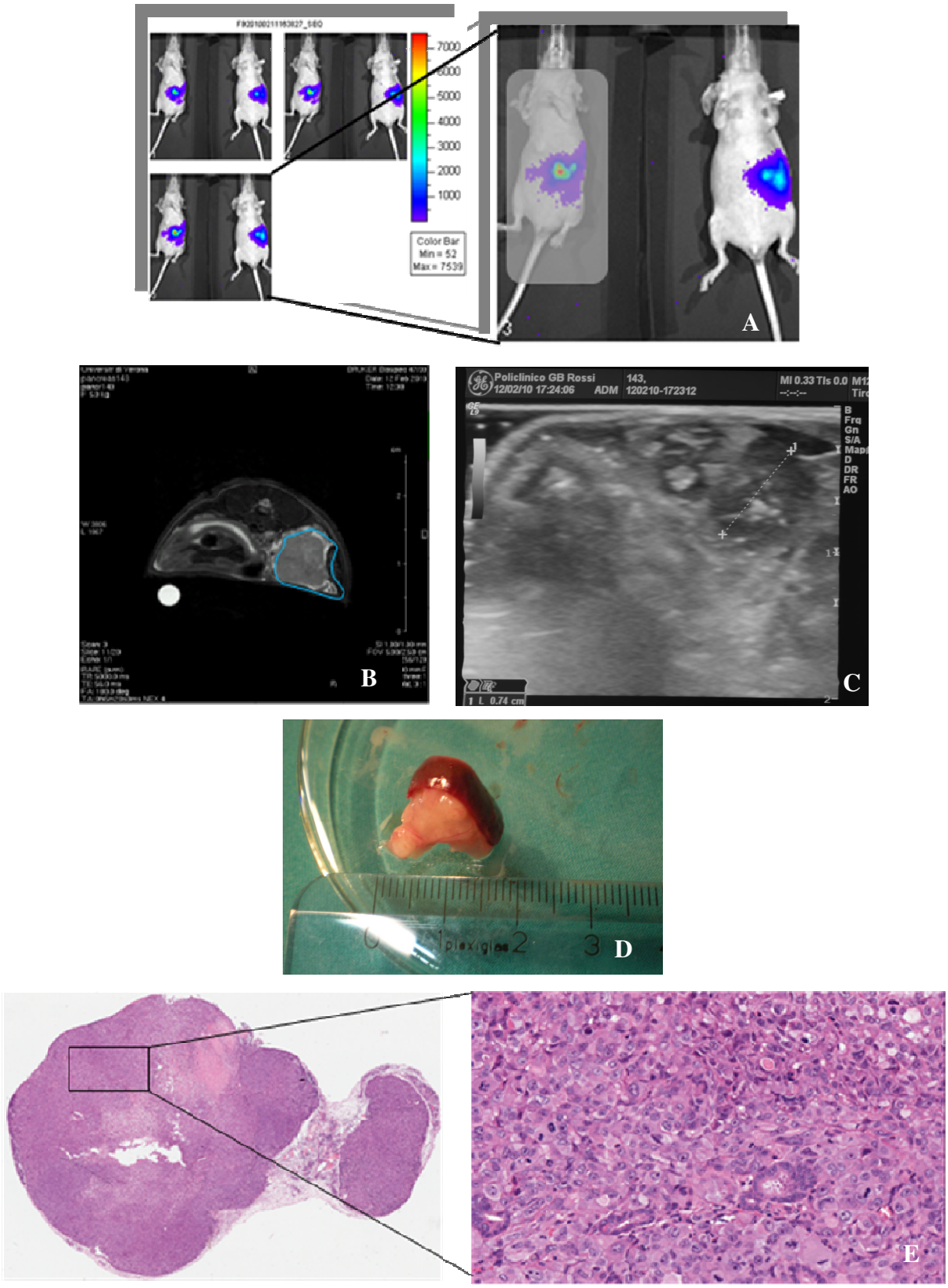

Figure 52. *Optical imaging (A), MRI (B), US (C), tumor sample (D) and H&E staining of a mouse belonging from the Group one. All imaging techniques detected the tumor. Images refer to the third time-point acquisition.*

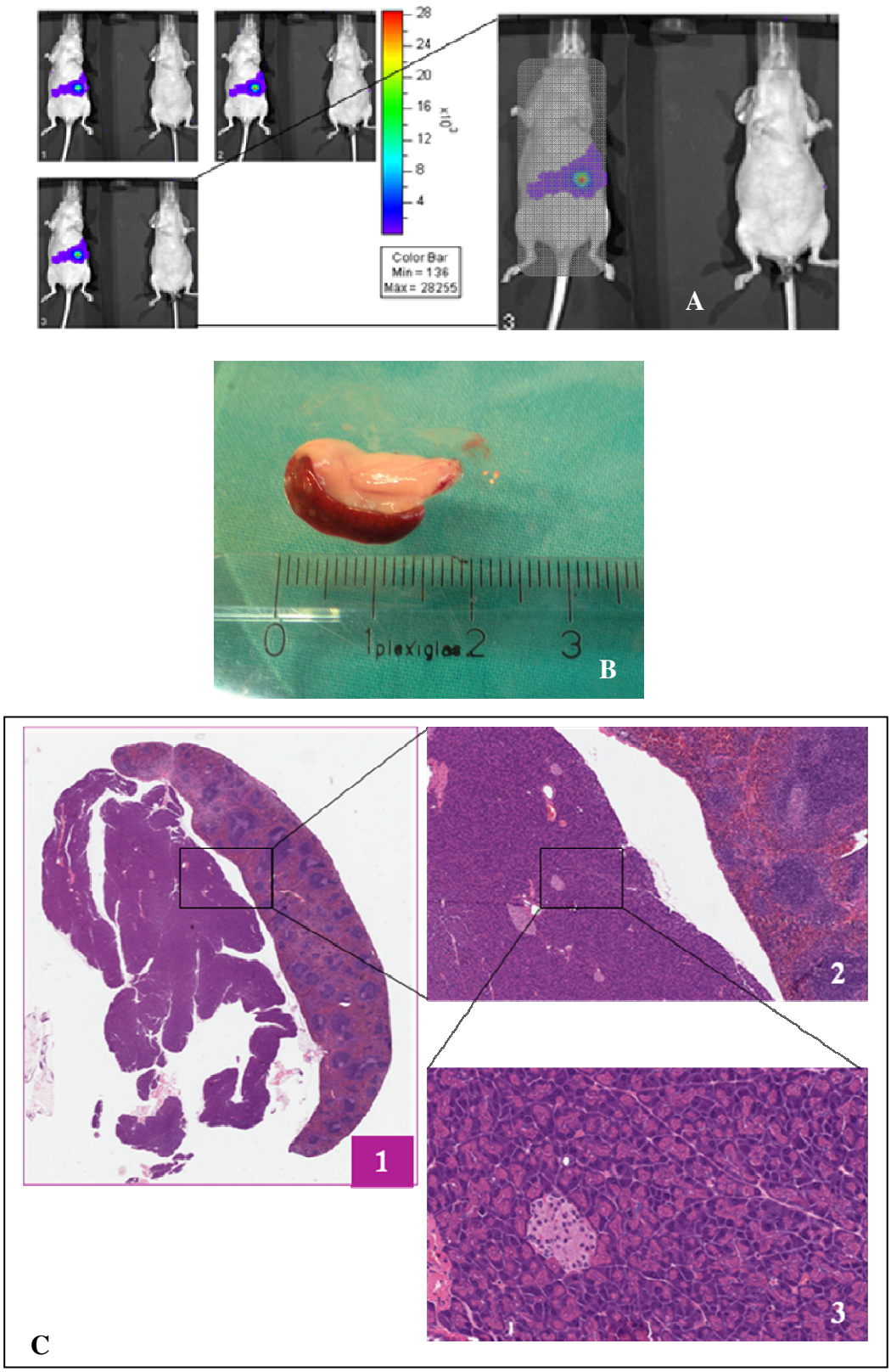

Figure 53. *Optical imaging (A), pancreas and spleen (B) and H&E staining relative to the mouse in which imaging technology have never found tumor. The histological analysis shows normal pancreas closed to the spleen. Details 2-3: Langerhans isle.*

In few cases such as the one reported below regarding a mouse of the Group one, we observed a strict correspondence between Optical imaging and MRI in regard to the fact that primary tumor was divided into two parts; also US distinguished the two components thanks to the low depth of the smaller one. These findings were confirmed at the moment of necropsy (Fig.54).

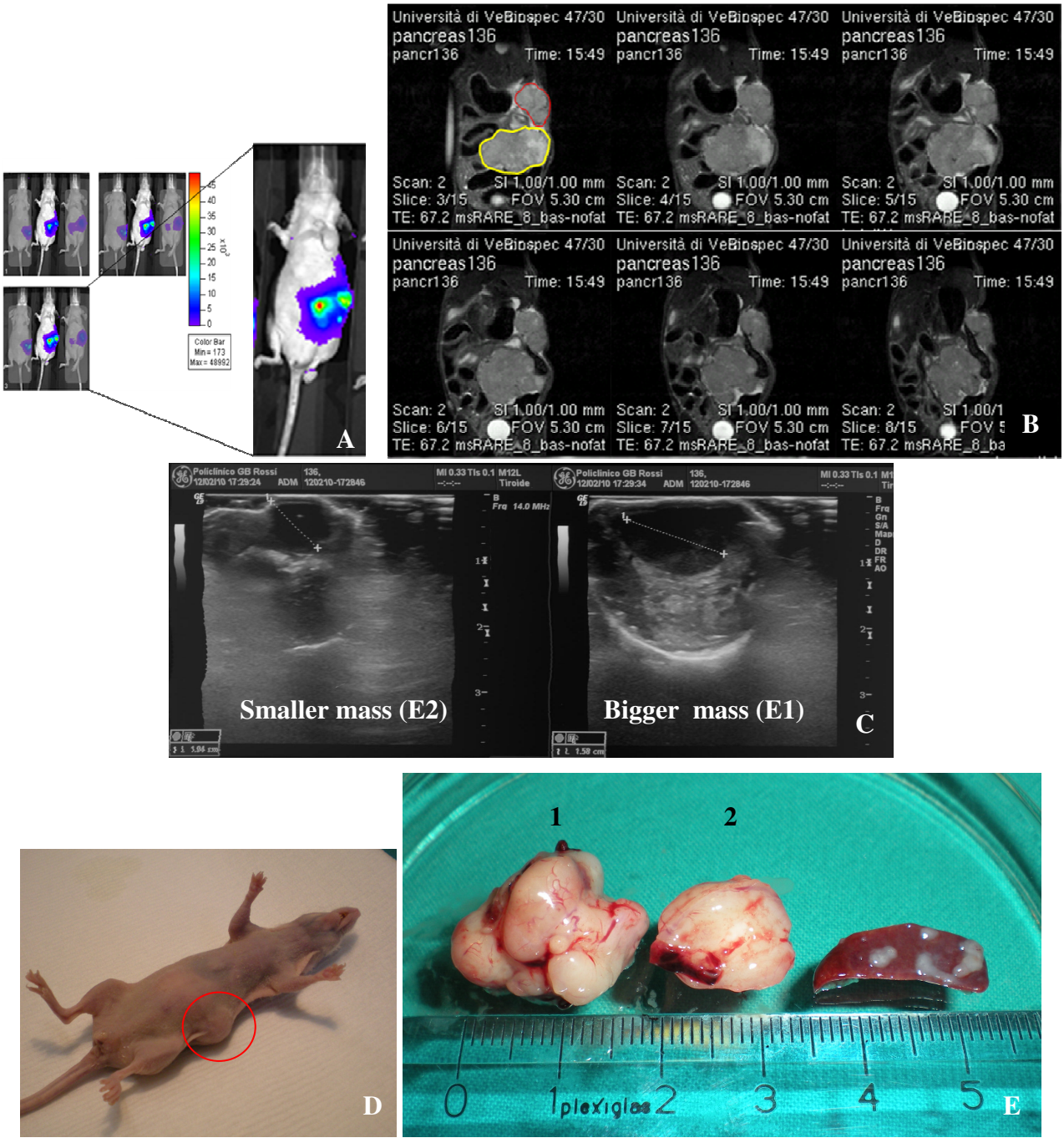

Figure 54. *Correspondences between all techniques and final necropsy for a mouse of the Group one.*

4.11 Analysis of Supplementary masses

In three cases belonging to the Group one we founded, already in the first Optical imaging acquisitions, 30 days after surgery, supplementary small light spots coming from anatomical regions different from the pancreas, and far to the primary tumor emissions. Because of Luciferin is the substrate of Luciferase, present only in the tumor cells we inoculated, and doesn't emit light by itself, we supposed these light spots could be putative small metastasis. These supplementary light spots were founded also in the second and the third Optical imaging acquisition, but never by the other two imaging techniques we used. Moreover, supplementary emissions are localized in different regions moving from the first , the second and the third acquisitions. However, at the time of necropsy, we found evident small tumor masses only in one of the three mice involved in these supplementary study (Fig. 54). On the other hand, checking through the small intestine of these latter, we noticed the presence of small white protuberances adhering to the intestine of all the mice (Fig. 55). We collected that intestine portions to perform H&E.

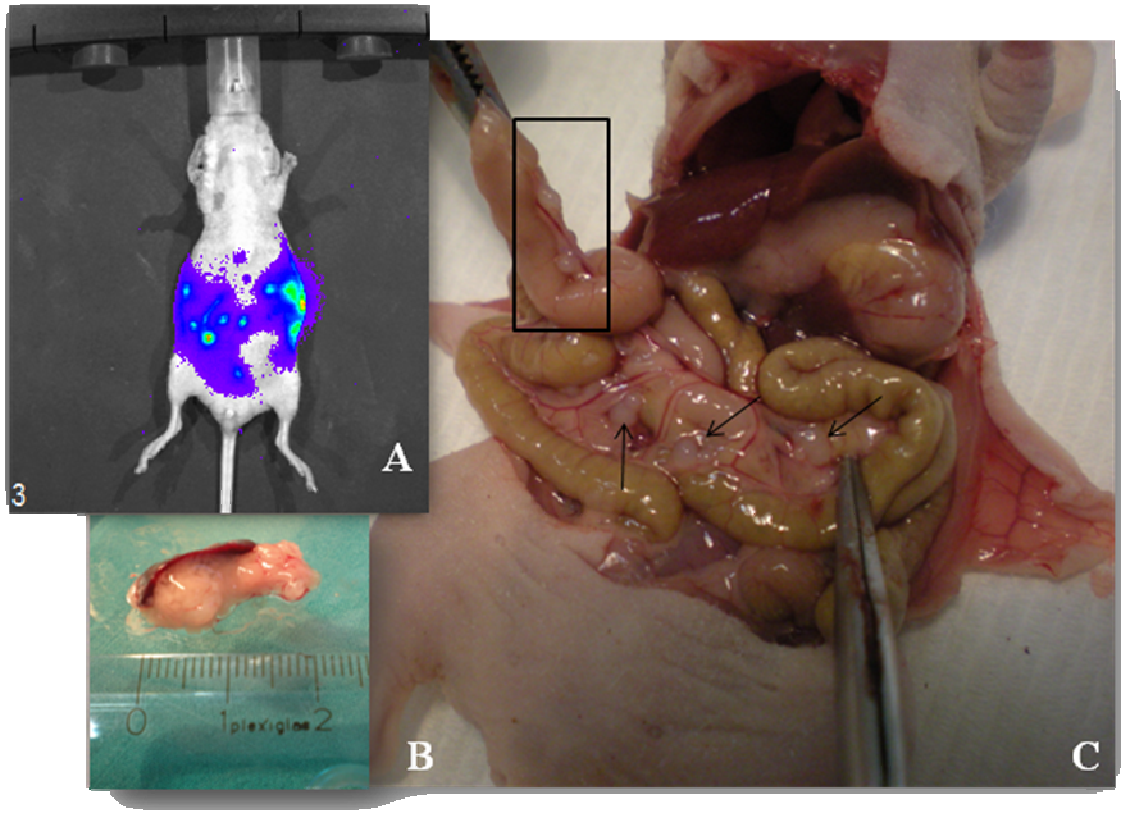

Figure 54. *Small tumor masses found in the abdominal cavity of one of the three mice which presented supplementary light spots (A: acquisition at third time-point). Arrows in C show them, whereas black rectangular indicates the masses we collected for H&E staining.*

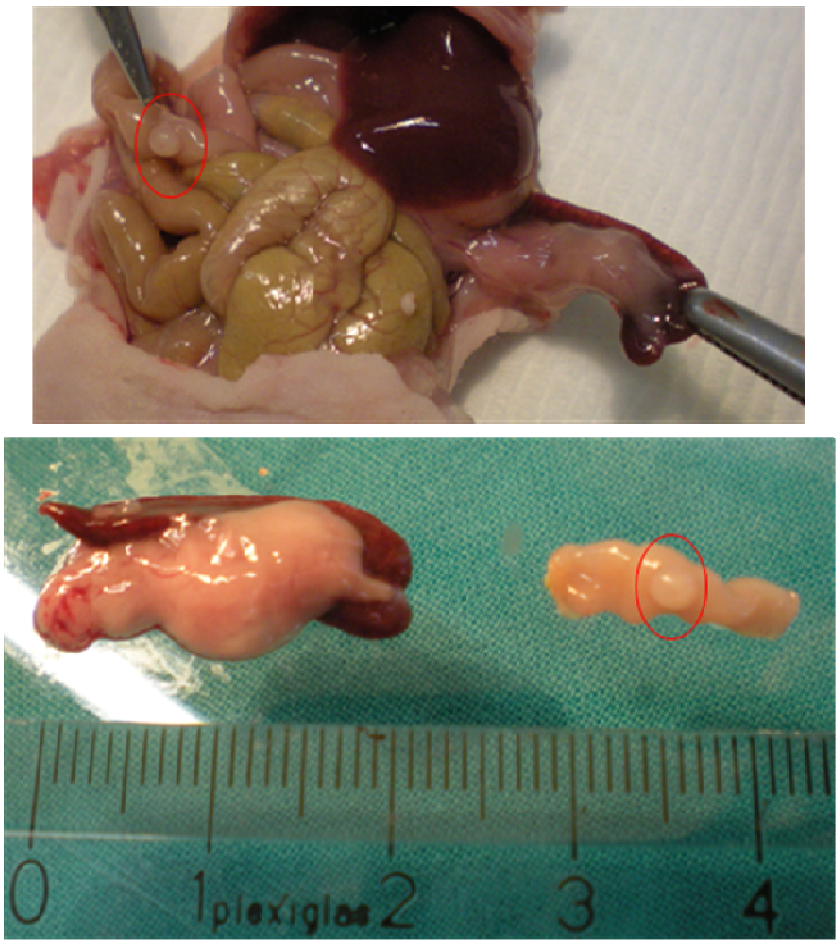

Figure 55. *A part of the primary tumor, no evident supplementary masses were found. We noticed the presence of small white protuberances adhering to the intestine (red rings).*

H&E staining confirmed that small masses collected from mouse showed in Figure 54 were composed by tumor cells (Fig. 56), whereas no tumor cells were found in the other two mice. Protuberances present in the intestine of the latter were identified as small intestinal intraepithelial lymphocytes (Fig. 57-58), lymphoid nodules normally present in the intestine of mice. Probably they became bigger following to general inflammation stimuli, showing foreign body granuloma characteristics, clearly distinguishable from the surrounding normal tissue. Histologically, it is composed of macrophages that have differentiated into large cells with indistinct cell boundaries called cells epitheloid.

Some of these may fuse with each other to give rise to the multinucleate cells called "foreign body giant cells" in which typically nuclei are distributed randomly all over its cytoplasm. No tumor cells can be detected inside these nodules. Finally, we found putative metastasis in only one animal, even if emission spots were detected in other two animals since the first Optical imaging acquisition. In all other mice, in spite of very big sizes of the developed tumour, light signals corresponded always to the presence of the primary tumors.

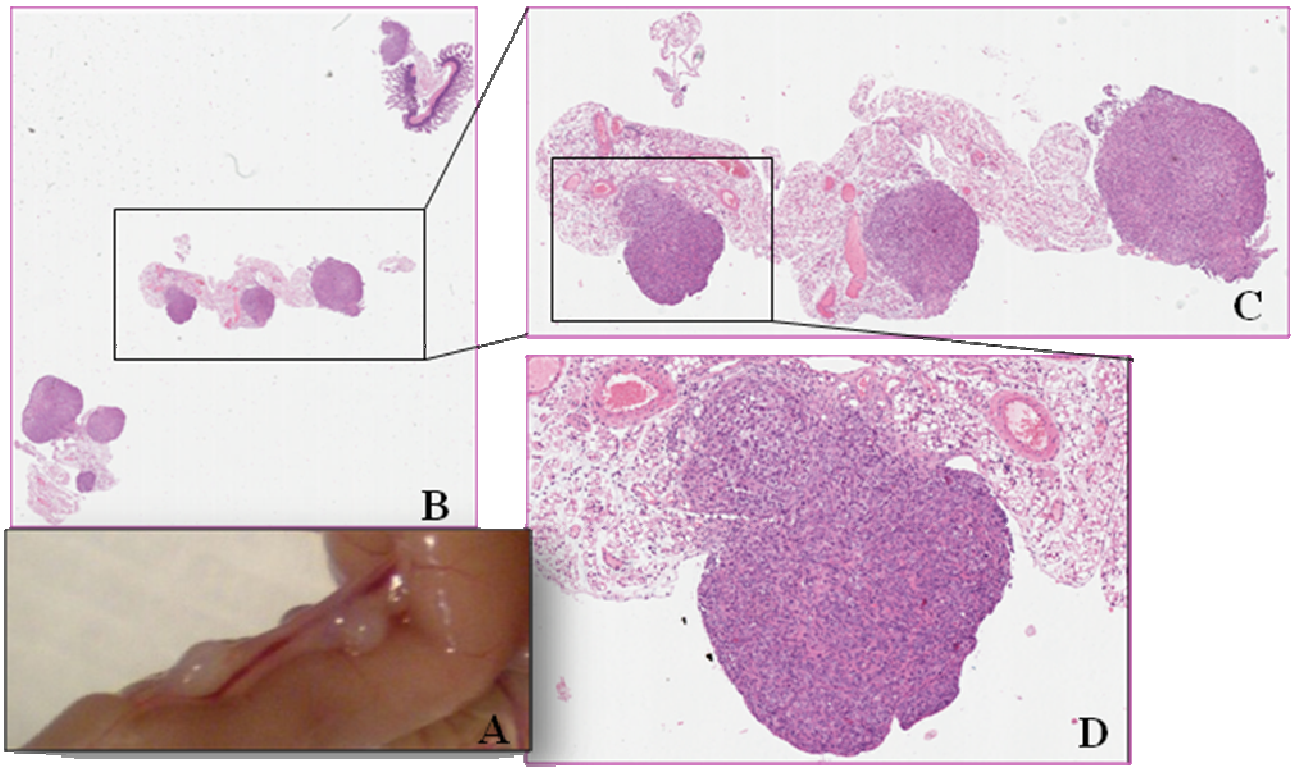

Figure 56. *In (A), a detail of Fig.ure 54: small masses collected from the small intestine of the animal. H&E staining (B, C and D, images Aperio 1X, 4X and 20X respectively) confirmed that they were tumors.*

.....

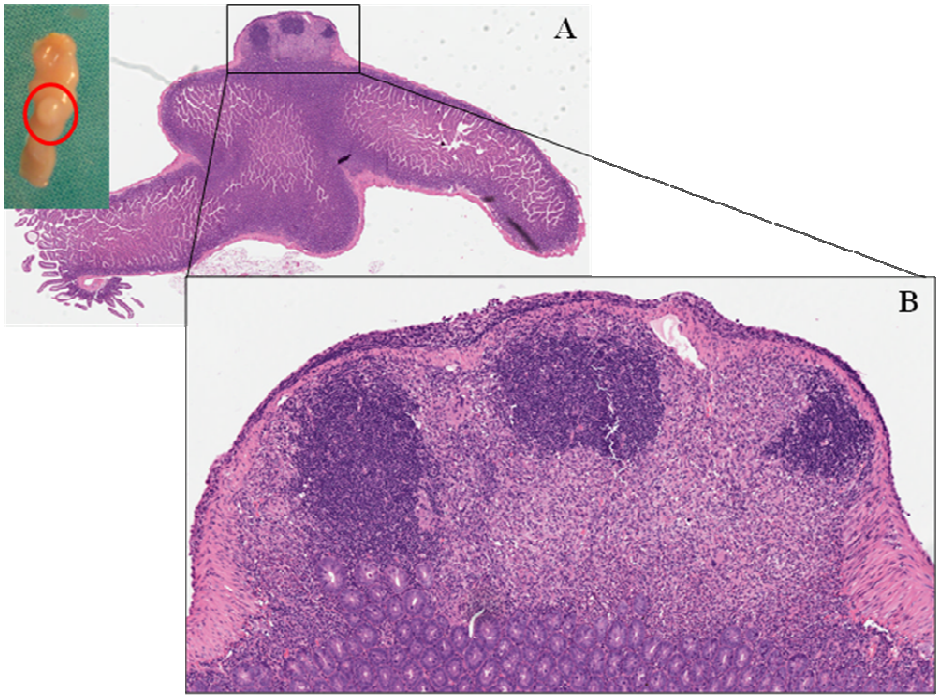

Figure 57. *Small intestinal intraepithelial lymphocytes found in one of the two mice that showed light emission but not supplementary visible small masses (A, Aperio 1X; B, Aperio 5X).*

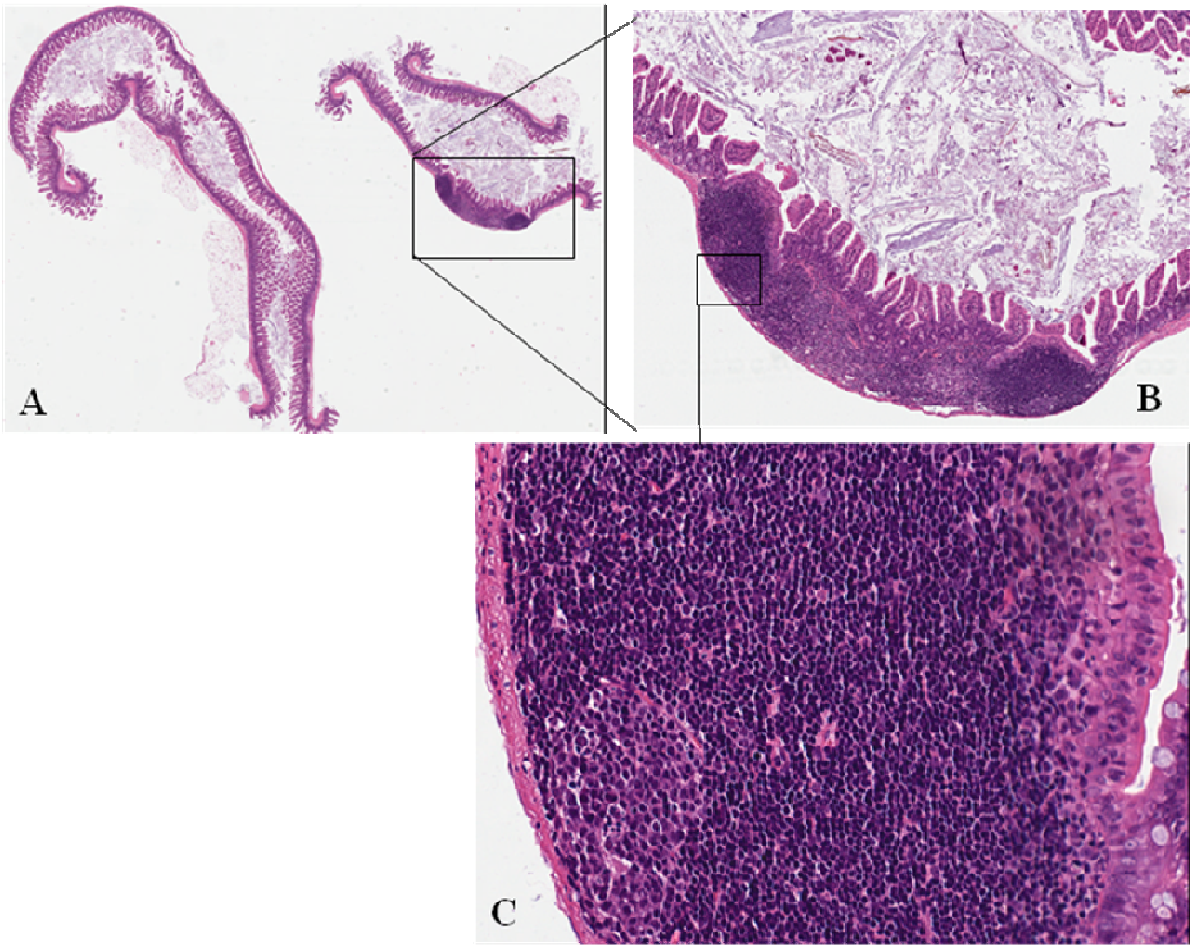

Figure 58. *Small intestinal intraepithelial lymphocytes found in the other mouse that showed light emission but not supplementary visible small masses (A, Aperio 1X; B, Aperio 5X;C, Aperio 20X).*

Summarizing, even if light signals from supplementary masses were detected in three mice, we found small tumor masses in the intestine of only one of them. Trying to get the fact, we studied the emission light trend relative to the two mice with intraepithelial lymphocytes stations. We considered both total emission coming from all the abdominal area (*e.g.*, see bigger ROI in figure 39) and the emission relative to only primary tumor (*e.g.*, see smaller ROI in figure 39), in order to appreciate the differences and understand what was the contribution of photons emission of small masses considered alone. Looking to the flux values calculated considering primary tumors alone (corresponding to the smaller ROI) and the total flux values corresponding to the total abdominal emission (bigger ROI), we observed that there are not significative differences between them. These findings suggests that there is not contribution in light emission coming from supplementary small masses. Probably, some very little tumor cells aggregations were present in the abdominal cavity of those two mice, so small that it was hard to see them at the moment of necropsies, but their number was sufficient to emit a light signal detectable by our Optical imaging devise. However, a little but significative difference was found analyzing the flux values relative to the

smaller and the bigger ROI acquired from the mouse in which visible putative metastasis were found.

4.12 More information from MRI and Bioluminescence imaging

Other information could be extracted comparing MRI and Optical Imaging results in a very easy way. Looking to the photon flux values from the first to the last acquisition, we expected to see that they increase, due to the presence of more tumor cells which oxidize the Luciferin substrate. In the majority of the cases, especially in mice belonging from the Group one, the bioluminescence activity increased in a considerable way. If necrotic regions were present within the expanding tumor mass, bioluminescence activity should decrease because only vital cells can oxidize the Luciferin. It was not our case, as shown in Figure 59. MRI can supports this analysis *in vivo*, thanks to the fact that necrotic regions appear like more "brilliant" focal areas, and prevent the diffusion of the contrast agents. In fact, the homogeneous diffusion of the contrast agent Gadolinium in the tumor mass, as shown in the MRI sequence in Fig. 59, confirmed this finding. Tumors in our models were characterized by very low necrotic parts, in spite of their big sizes (Fig. 59).

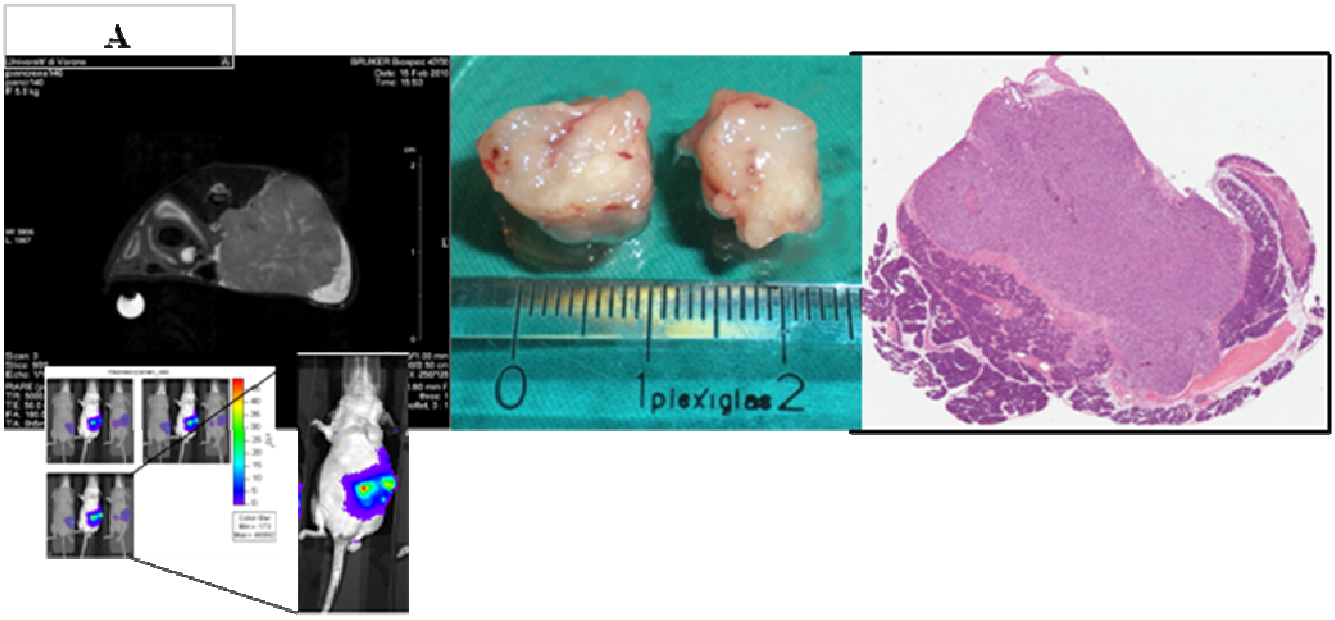

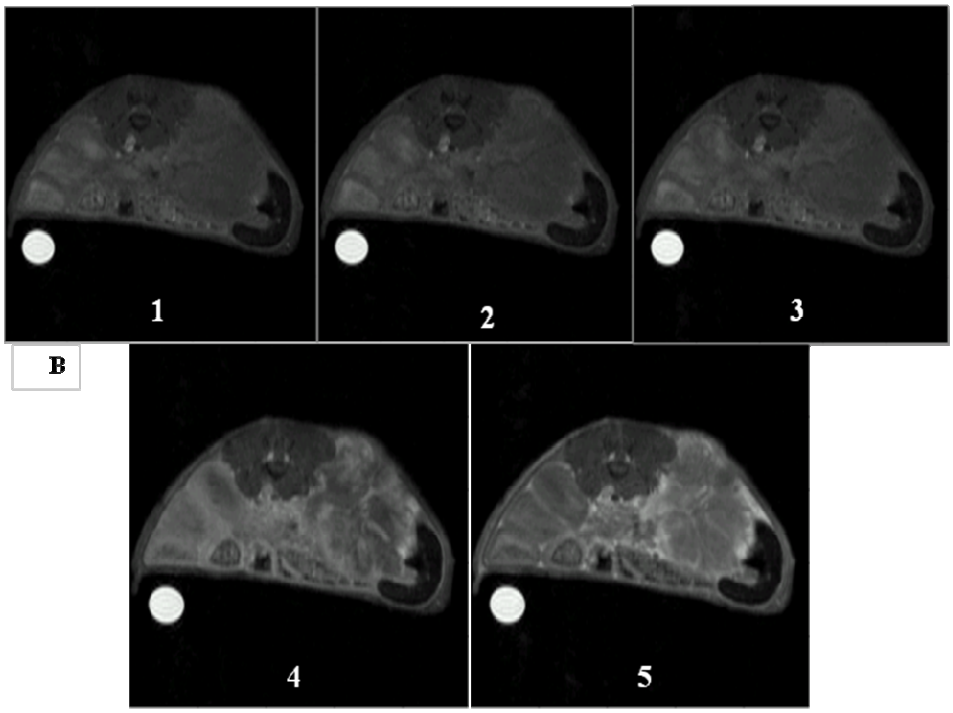

Figure 59. *In Panel A, correspondences between an MRI image and Bioluminescence activity of a mouse belonging to the Group One. Histology confirmed what the tumor didn't contain necrotic regions. In Panel B, the same mouse was imaged in MRI using contrast agent Gadolinium (sequence from 1 to 5):pictures 1,2,3 showed tumor before diffusion of contrast agent, whereas pictures 4 and 5 indicate that the complete diffusion of Gadolinium in the tumor mass.*

4.13 3D Reconstruction individualizes location of putative metastasis

We performed 3D reconstruction on one of the animal showed in figure 55, in which we didn't found putative metastasis even if supplementary light emissions were detected. Thanks to the Living Image 3D Analysis Package (an image analysis application for viewing and analyzing image data acquired by the IVIS® Imaging System Series), we was able to collocate the supplementary light sources, as shown in figure 60.

The photograph of our mouse is visualized as a tridimensional subject. T his application consents to choose which organs have to be introduced in the transparent body of our mouse. We chose to visualize liver, small intestine, and the pancreas. Brain was inserted in order to orientate the mouse body in the space. Looking to the reconstructions, two light sources are clearly visible and are located distant far from the primary tumor. They are shown as two voxels (tridimensional pixels) collocated in correspondence of the small intestine.

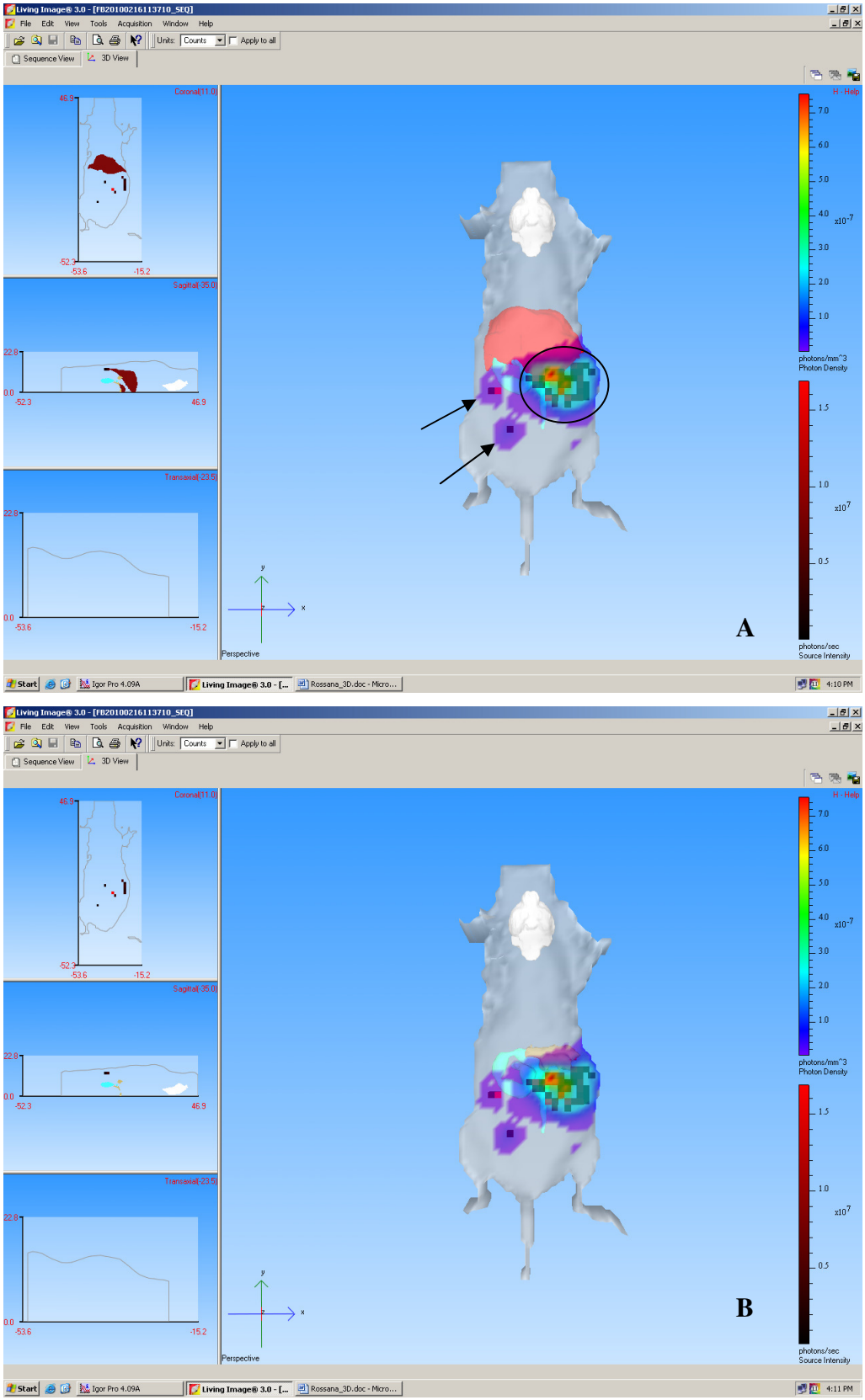

Figure 60. *3D Reconstruction of the mouse showed in showed in Fig. 55. In (A), arrows indicate the two voxel corresponding to the supplementary light sources. Ring indicate the primary tumor emission. Brain in colored in white, pancreas is yellow, small intestine is pale blue and the liver is red. In (B), the same image but without the liver.*

Moving the body in the 3D spaces (fig.61), it is possible to see better that emission of these two light sources come from the small intestine. So, it is believable that some tumor cells, in a sufficient number to emit a detectable light signal, are organized in small intestine, even if they cannot be seen to a naked eye.

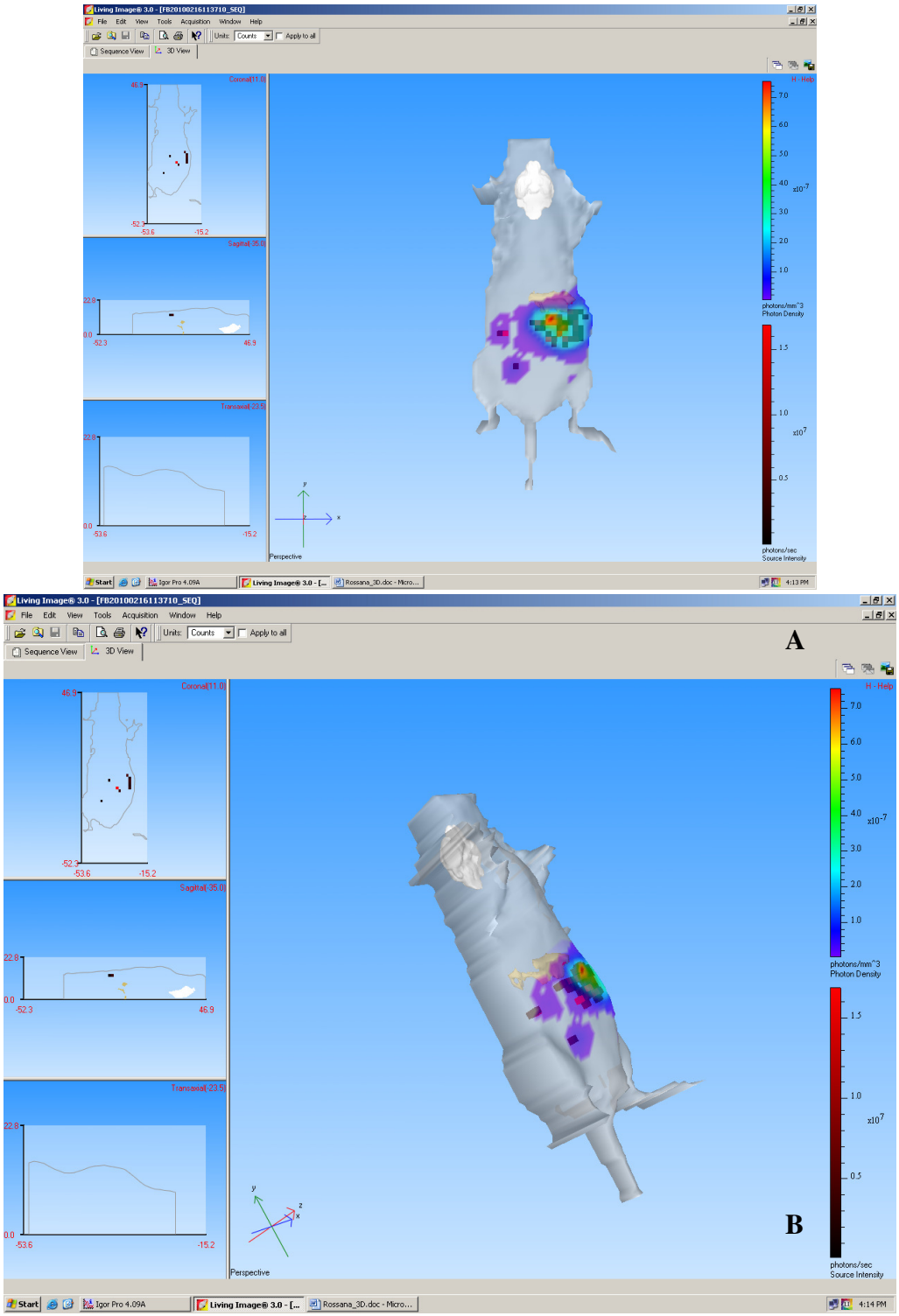

Figure 61. *In (A), only the pancreas have been inserted. Closed to it, light emission coming from the primary tumor. In (B), rotation of the 3D model shows the depth of supplementary light sources.*

5. Discussion

Pancreatic cancer remains one of the most lethal malignancies and metastatic pancreatic carcinoma represents a bleak prognosis for the patient. Late diagnosis together with the rapid disease progression and poor responses to available therapies are the causes of the high mortality linked to this disease. Even if, in recent years, many efforts have been made to better understand the genetic mutations involved, the reasons of the inefficient drug delivery, the cellular signaling and novel biomarkers specific of pancreatic cancer, the final resolution doesn't seems imminent yet.

The cancer stem cells (CSC) hypothesis, identifying these cells as the key of tumor development, progression and metastasis, offers the opportunities to develop therapies which actually enhance survival rate and life quality. However, the *in vitro* studies of cultured tumor cells have some limitations because they will never resemble what happens in the development and progression of the tumor within living organisms. So, the better way to intersect together the need of increase our pancreatic cancer stem cells knowledge without moving away from all the mechanisms of a living organism is to establish a pancreatic mouse model in which behavior of pancreatic CSC can be study directly and on which novel therapies can be test.

Stem-like proprieties of sphere growing Panc-1 cells, selected starting from Panc-1 adherent cell line, was already demonstrated in our laboratory. Briefly, Panc-1 adherent cells were cultured under specific stem cell promoting culture conditions. The use of a serum-free medium, supplemented with growth factors, which are also present in the pancreatic microenvironment, resulted in sphere-growing cells. The presence of membrane markers expression CD24, CD44 and ESA, multipotentiality and stem functionalities, together with an increased expression of markers of active Hedgehog signaling, confirmed the typical stem features of spheres growing cells. The chemoresistance of the Panc-1 sphere-growing vs adherent cells was assessed by incubating the cells with increasing concentrations of Gemcitabine (GEM). 10% of the sphere population survived to Gemcitabine at high doses, confirming the observation of Gou et al. who reported that Panc- 1 spheres contain a chemoresistant side population of 15%.

These preliminary results suggested that Panc-1 spheres might be a clinically more reliable model system to study the stem-like cell population than Panc-1 adherent cells.

On the basis of these findings, in the current study, we focused on the behavior of spheres growing cells when injected in the pancreas of nude mice; for this goal, we decided to follow tumor growth in MRI. Moreover, following some troubles linked to difficulties to see clearly small masses in abdomen cavity by MRI, we decided to take an interest also to other small-animal imaging modalities capable of following tumor development and progression *in vivo* in a rapid, fast and above all safely way.

Firstly, we demonstrated that spheres grow faster, when injected in the pancreas of nude mice, than the adherent counterpart, and tumor they generated were bigger than those obtained in the latter. From the histological point of view, H&E staining demonstrated that sphere growing tumors established in nude mice showed more irregular mitotic figures than adherent cell derived tumors. Moreover, adherent cells demonstrated a more organized architecture, whereas the spheres generated a more dysplastic tumour structure. Moreover, immunostaining for CK7, a marker of differentiation commonly used in diagnostic of epithelial tumors, showed a great difference between the two kind of tumors: we observed a strong positivity of adherent derived tumor for CK marker, whereas spheres resulted totally negative.

Taken together these findings demonstrated that, starting from the total pool of adherent Panc-1 cells, we selected the less differentiated subset of cells, CK negative, characterized also by elevated mitotic activities that could explain the fact that tumor derived from spheres grow faster than those derived from adherent cells.

Putative metastasis were found in 9/10 mice inoculated with spheres growing Panc-1 cells, in particular in the liver and within small intestine, and in 1/10 inoculated with adherent Panc-1 cells. These findings suggested that spheres cells are more aggressive than adherent cells when inoculated in the orthotopic site.

Because of numerous observations support the idea that Epithelial to Mesenchymal transition (EMT) has a central role in tumor progression, we studied the EMT markers (E-Cadherin, Vimentin, S100A4, Twist and Slug) expression in spheres Panc-1 cells and adherent Panc-1 cells *in vitro* and then in tumors derived from spheres growing Panc-1 and adherent Panc-1 cells, after subcutaneous and orthotopic injections. In these EMT immunohistochemical study, we also included putative metastasis we found in 5 animals inoculated with spheres growing cells.

Our findings demonstrated that EMT markers expression was higher in spheres derived tumors developed in the orthotopic site compared with all the other cases we considered. Expression of the EMT markers in primary spheres derived tumors and putative metastasis was almost comparable, but anyway higher respect to expression the same cells *in vitro* or in subcutaneous tumors.

The acquisition of Mesenchymal markers from spheres cells, particularly stronger when they grow *in vivo* in the orthotopic site, may be the key that could explain the aggressiveness of spheres compared to adherent cells. During EMT, invasion epithelial tumor cell degrade their basement membrane and migrate by alternating phases of adhesion and detachment from extracellular matrix (ECM) and Integrins are the main receptors involved in binding and in response to ECM. For this reason, as a future development of EMT study in spheres growing Panc-1 cells, we will study the

role of Integrins both in spheres growing cells *in vitro* and in tumors derived from them after orthotopic injection.

The generation of a pancreatic mouse model in which only spheres growing cells are used to induce tumor formation acquired considerable importance especially in the contest of *in vivo* testing of novel drugs. Therapies available today, such as Gemcitabine, are not able to kill this "stem-like" subset of cells which may coincide with the chemoresistant subpopulation within the heterogeneous total pool of tumor cells; for this reason, survival cells can reestablish the tumor.

As already said, only thanks to necropsies, we found putative metastasis in 9/10 mice inoculated with spheres growing cells but these small masses were never identified during MRI acquisitions. MRI pancreas imaging in mice is particularly difficult because this organ, extremely soft, is immediately adjacent to the gut; moreover, artifacts due to the presence of gas within the intestine, such as breathing movements of the mouse, really may compromise the images quality. However, MRI is useful when tumors achieve considerable sizes, because it gives us the possibility to measure the tumor widths, identifying shape and anatomical location of the mass. So, the identifications of small imaging techniques capable to detect precisely possible decreases in primary tumor sizes and, at the same time, able to identify metastasis, following their "destiny" during drugs therapies, is a need that cannot be neglected. Considering difficulties we encountered using MRI, before the beginning of any novel test compounds *in vivo* on our spheres-derived mice models, we decided to actuate in parallel the study of other two imaging techniques for overcoming limits of MRI : Optical imaging based on Bioluminescence and Ultrasound (US).

We used Panc-1 cells transfected with the gene reporter Luciferase (Luc), performing novel orthotopic injections in 23 nude mice. In particular, mice were divided into two groups: the first one included mice (13, Group one) injected with $5*10^6$ Panc-1- Luc+ cells; the second one comprised mice (10, Group two) injected with $2*10^6$ Panc-1- Luc+ cells. We performed the *in vivo* imaging acquisitions, with all three techniques, 30, 60 and 90 days after surgeries.

The first time acquisition showed that MRI detected 9/13 tumors in the Group one and 1/10 in the Group two; Optical Imaging was 13/13 for the first and 5/5 for the second group. No tumors were detected using US. These first finding are in line with we expected: tumors in Group one were bigger than those in Group two, simply because they derived from a different starting number of inoculated cells. Since Optical imaging has higher sensibility respect to MRI, all tumors were individuated, whereas 4 tumors were too smaller to be seen in MRI. US probe we used (16 MHz) probably was not sufficient for detecting tumors at this time point. Measures at the second time point, 60 days after surgery, the number of tumors detected in MRI rose to 12/13 for the Group one and to 6/10 for the Group two. US individualized 10/13 and 4/10 for the first and the second group

respectively. Tumors of the Group one seen in Optical imaging remained fixed to 13/13, whereas the number of emissions light detected from the Group two increased from 5 to 8. However, curiously, one of the two mice resulting "negative" at this time point corresponded to one of those in which light emission for clearly detectable at the first Optical imaging acquisition. Because of this technique may show false negative results but not false positive one, we believed in the light spot seen at the first time. Moreover, at the second time point, tumor was clearly visible both in MRI and in US.

Light emission appears only if Luciferin is oxidized by Luciferase which is present only in transfected tumor cells we inoculated. So, light emission corresponded to the fact that Luciferase-Luciferin reaction is happened. Since Luciferin has not bioluminescence activity by itself, we excluded that the light source seen at the first acquisition was due to substrate accumulation in such tissues different from the tumor mass. We repeated the acquisition the day after, in order to avoid side effects for excess of inhaled isofluorane. Interestly, after this repetition, the light signals coming from primary tumor was detectable now. Thinking to the reason why emission disappeared at the second time point in this animal, we concluded that probably a mistake in the Luciferin injection occurred. Protocols of Optical Imaging suggest intraperitoneally injection of Luciferin; moreover, it well know that the emission peak is reached more or less 15 minutes after Luciferin is inoculated in the abdominal cavity; this is the reason why programmed acquisitions time of Bioluminescence signals is divided into three time-point (0-5, 5-10, 10-15 minutes, after Luciferin injection), a time-frame that corresponds to the maximum Luciferin emission time. If injection is performed in the wrong way, involving for example an intestinal handle, the diffusion of Luciferin may be compromised and slowed down, Luciferase cannot oxidize its substrate in time, because not available, and when programmed acquisition time is completed, no light emission can be detected.

At the third and last time-point, 60 days after surgery, 13/13 animals belonging to the Group one were detectable using both Optical Imaging and MRI because tumors became too big (till 13 mm). However, these big sizes became a limit for US sensibility: US failed in detecting such big tumors, in general because of the presence of acoustic impedance in the abdominal activity and also because the low frequencies of US probe of our devise produced an insufficient resolution. With regard to the Group two, MRI detected 7/10 tumor masses against 9/10 seen in Optical imaging. One mouse belonging to the Group two never display the tumor mass.

In addition to these finding, the comparison between all three imaging techniques gives as other important results. In fact, since from the first acquisition session, 30 days after surgery, three animals belonging to the first group displayed more than one light sources in Optical imaging. These supplementary small masses were not visualized in MRI or US. We focused our attention on

these small masses, just because difficulties in detection of putative metastasis in MRI was the reason why we decided to deepen the imaging issue in the current study. From the first to the second time-frame, the number of mice presenting supplementary masses was the same (3); however, we immediately noticed that the location of the light spots was changed. Since one of the disadvantages of Optical imaging is that light sources cannot by collocated precisely in the anatomical regions from which they come from, it was not possible to speak about liver or intestinal masses. The fact that their positions changed from an acquisition to the next one suggested that probably emitting small masses may move following the intestinal movements. However, as in the case of the mouse on which Optical imaging acquisition was performed twice, the fact that an emission was detected meant that such tumoral Luciferase+ cells emitted. Surprisingly, at the time of necropsies, evident small tumor masses were found only in one of these three mice, contrary to what we expected: these masses, scattered within the abdominal cavity, were collected for histological analysis. In the other 2 mice, small white protuberances were detected on the surface of small intestine; we collected them believing they may coincide to small tumor cells aggregations, but histological analysis identified those protuberances as small intestinal intraepithelial lymphocytes stations, and no tumors cells were found within them. Intestinal intraepithelial lymphocytes stations are natural lymphocytes aggregations present in the gut of mice: probably, they became bigger following general inflammatory reaction, resembling small tumor masses to the naked eye.

We noticed that there is not contributions in light emission coming from supplementary small masses in the two mice with small intraephitelial lymphocytes aggregations. Probably, some very little tumor cells aggregations were present in the abdominal cavity of those two mice, so small that it was hard to see them at the moment of necropsies, but their number was sufficient to emit a light signal detectable by our Optical imaging devise. A possible solution to overcome this troubles may be to let small masses become bigger, but this solution implicates that primary tumor reaches sizes incompatible with the life of the animal.

Another possible solution contemplate the use of Fluorescence instead of Bioluminescence if we want to perform a guided necropsy. Fluorescence imaging uses external dyes or fluorescent markers which are either molecules that absorb electromagnetic energy in the near-infrared region or the new emerging class know as quantum dots. Even if fluorescence imaging requires the addition of an external light source to obtain a spectrum of the light emitted, it has the advantage to be detectable in non living animals. It is possible to perform an optical imaging acquisition before the animal is sacrificed; then, once the abdominal cavity is open, we can repeat the acquisition using the same fluorescent emission, but seeing directly from which organs the emission comes to. Also

combination of both optical imaging techniques, in the same animal, is possible. In fact, we are going to perform a double stable transfected pancreatic CSCs, expressing both Luciferase and the Red fluorescence protein (RFP).

Finally, our finding demonstrated the need of using both MRI and Optical imaging for the detection of tumor masses in small animals. The use of US may be very practice and economic because no anesthetics and particular preparations of animals are required; however, it is necessary to have at our disposal high frequencies US probes, otherwise imaging in small animal, especially in the abdomen cavity, is very complicate. MRI and Optical imaging are complementary techniques of monitoring tumor progression and, used together, they acquire much more importance for monitoring tumor and metastasis response to treatments.

We suggest an "Imaging protocol" in which MRI, US and Optical imaging are combined together in order to follow the orthotopic tumor growth in each moment of its development. In the earlier faces of tumor developments, during the first month after the surgery, Bioluminescence Imaging may be used in combination with high frequencies-US, since the latter is faster and relative economic if compared with MRI. When tumor are detectable in high-frequencies US, the following imaging time-frame may include MRI instead of US, in order to better appreciate tumors shape and size. Then, when tumors reach big sizes, and putative metastasis may be present, MRI should be use in combination with bioluminescence and fluorescence imaging, adding the latter optical imaging modality for the detection of micrometastasis.

In order to putting into action all findings of this study , selection of spheres growing cells starting from adherent Panc-1 Luc+ cells is ongoing. So, as a future development of this work, we want to repeat the orthotopic injections in a bigger number of mice but using spheres Luc+ cells. In this way, we hope to obtain a mouse model of pancreatic cancer in which tumor and putative metastasis, enriched in tumor stem-like cells, are easily detectable thanks to the combined imaging approach. Moreover, we want to delve the study of metastatic mechanisms in our model. Another very interest evolution of the present research required the study of tumors interstitial fluid pressure (IFP). Tumors develop elevated IFP during growth above all because of increased fluid permeability of the microvascular network and lack of functioning lymphatic vessels [34]. Elevated IFP may lead to poor tumor uptake of chemotherapeutic agents, and so resistance to treatment. Novel techniques in small imaging animal, such as Dynamic contrast-enhanced magnetic resonance imaging, are a powerful tool for investigating this important biological aspect. Linking together, thanks to the use of our mouse model, the study of IFP with the investigation of the crucial role of CSCs in cancer development, we hope to clarify many obscure aspects of pancreatic cancer development and progression.

Our findings have demonstrated that the pancreatic cancer spheres are more than just cancer stem-like cells. In addition, as these sphere-growing cells can be maintained relatively easily we have also generated a cell line-derived pancreatic cancer model that demonstrates characteristics of the clinically-relevant tumour. This cell system might be very useful to further the understanding of certain aspects of pancreatic cancer and could also be employed to screen compounds for therapeutic intervention, both *in vitro* and *in vivo*. When our models will be establish, they may be used for the testing of novel compounds specifically designed to target this stem-like compartment, resistant to standard chemotherapies. A combined imaging approach in this contest become extremely important, in order to follow decrease in primary tumor sizes, using MRI and US, and metastasis progression, using Optical imaging devises.

Reference List

1.Li, D. et al., Pancreatic cancer. Lancet, 2004. **363** (9414): p. 1049-57.
2.Hezel A. F et al., Genetics and biology of the pancreas ductal adenocarcinoma. Genes and Development , 2006. 20: 1218-1249.
3. Jaster R. Et al., Molecular regulation of pancreatic stellate cell function. Mol. Cancer, 2004 3:26.
4. Maitra A.,et al., Precursors to invasive pancreatic cancer. (2005),Adv. Anat. Pathol. 12:81–91.
5.Serrano M, et al. Oncogenic ras provokes premature cell senescence associated with accumulation of p53 and p16INK4a. Cell. 1997; 88:593-602.
6.Serrano M, et al. Role of the INK4a locus in tumor suppression and cell mortality. Cell. 1996; 85:27-37.
7.Plath et al., Over-expression of pRB in human pancreatic carcinoma cells: function in chemotepapy-induced apoptosis. 2002. J Natl Cancer Inst. 94: 129-42
8.Wilentz RE, et al. Loss of expression of Dpc4 in pancreatic intraepithelial neoplasia: evidence that DPC4 inactivation occurs late in neoplastic progression. Cancer Res. 2000; 60:2002-2006.
9.Ingham P.W, et al., Hedgehog signaling in animal development: Paradigms and principles. *(*2001*)* Genes & Dev. 15*:*3059–3087.
10. Pasca Magliano M., et al., Hedgehog signalling in cancer formation and maintenance. (2003) Nat. Rev. Cancer 3:903–911.
11.Bonnet D. and Dick JE. Human acute myeloid leukemia is organized as a hierarchy that originates from a primitive hematopoietic cell. (1997), Nat Med 3 (7):730-737
12. Li, C., et al., Identification of pancreatic cancer stem cells. Cancer Res, 2007. 67(3): p. 1030-7.
13. Farnie G, Clarke RB. Breast stem cells and cancer. (2006) Ernst Schering Found Symp Proc.;(5):141-53.
14.Shimizu K et al., CD133 expression pattern distinguishes intraductal papillary mucinous neoplasms from ductal adenocarcinomas of the pancreas (2009) Pancreas. Nov; 38(8):e207-14.
15. Hermann PC, et al., Distinct populations of cancer stem cells determine tumor growth and metastatic activity in human pancreatic cancer. (2007) Cell Stem Cell 1(3):313–323
16.Mueller MT, et al., Combined targeted treatment to eliminate tumorigenic cancer stem cells in human pancreatic cancer. (2009) Gastroenterology. Sep;137(3):1102-13.
17. Feldmann G, et al. An orally bioavailable small-molecule inhibitor of Hedgehog signaling inhibits tumor initiation and metastasis in pancreatic cancer. (2008) Mol Cancer Ther. Sep;7(9):2725-35.
18.Feldmann G et al., Blockade of hedgehog signaling inhibits pancreatic cancer invasion and metastases: a new paradigm for combination therapy in solid cancers. (2007) Cancer Res. Mar 1;67(5):2187-96.
19.Guarino M. et al., The role of the ephitelial-mesenchymal transition in cancer pathology. (2007) Pathology 39(3):305-18
20.Shah et al., Acquisition of Ephitelial-Mesenchymal Transition phenotype of gemcitabine-Rasistent Pancreatic cancer cells is linked with activation of Notch Signaling Pathway, (2007) Ann Surg Oncol. Dec;14(12):3629-37
21.Laudanna C, et al., Motility analysis of pancreatic adenocarcinoma cells reveals a role for the atypical zeta isoform of protein kinase C in cancer cell movement. (2003). Lab Invest, 83(8): p. 1155-63.

22.Gao, R., et al., Characterization of endocrine progenitor cells and critical factors for their differentiation in human adult pancreatic cell culture. (2003) Diabetes,. 52(8): p.2007-15.
23.Kolb, A., et al., Osteopontin influences the invasiveness of pancreatic cancer cells and is increased in neoplastic and inflammatory conditions. (2005) Cancer Biol Ther,. 4(7): p.740-6.
24.Thiery JP et al., Complex networks orchestrate epithelial-mesenchymal transitions. (2006), Nat Rev Mol Cell Biol. Feb;7(2):131-42
25.Grassi et al., Small animal imaging facility: new perspectives for the radiologist. (2009) Radiol Med 114:152-167
26. Sato A et al., In vivo bioluminescence imaging . (2004), Comp Med. Dec;54(6):631-4.
27. Schambach S J. et al., Application of micro-CT in small animal imaging (2010) Methods Vol. 50, 2-13.
28.Hauff P**.** et al., Ultrasound basics (2008) Handb Exp Pharmacol.; (185 Pt 1):91-107.
29.O'Neill K. et al., Bioluminescent imaging: a critical tool in pre-clinical oncology research. (2010) J Pathol, 220: 317-327.
30.Contag et al., Visulaizing gene expression in living mammals using a bioluminescent reporter. (1997) Photochem Photobiol 66:523-531
31.Timmins GS et al., Firefly flashing is controlled by gating oxygen to light-emitting cells. (2001) J E xp Biol, 204:2795-2801.
32.Rutter GA. et al., Real-time imaging of gene expression in single living cells. (1998) Chem Biol 5:R285-R290.
33. Scot Kern, et al., High-throughput drug screening of the DPC4 tumor-suppressor pathway in human pancreatic cancer cells. (2001), Ann Surg. 233(5):696-703.
34. Heldin CH et al., High interstitial fluid pressure-an obstacle in cancer therapy. (2004) Nat Rev Cancer, 4:806-13.